GSBS Dissertations and Theses   Graduate School of Biomedical Sciences

2014-08-05

Approaches and Considerations Towards a Safe and Effective Adeno-Associated Virus Mediated Therapeutic Intervention for GM1-Gangliosidosis: A Dissertation

Cara M. Weismann
University of Massachusetts Medical School

Let us know how access to this document benefits you.

Repository Citation

Approaches And Considerations Towards A Safe And Effective

Adeno-Associated Virus Mediated

Therapeutic Intervention For GM1-Gangliosidosis

A Dissertation Presented

By

CARA M. WEISMANN

Submitted to the Faculty of the

University of Massachusetts Graduate School of Biomedical Sciences, Worcester

in partial fulfillment of the requirements for the degree of

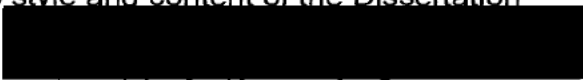DOCTOR OF PHILOSOPHY

AUGUST 5, 2014

INTERDISCIPLINARY GRADUATE PROGRAM

APPROACHES AND CONSIDERATIONS TOWARDS A SAFE AND EFFECTIVE ADENO-ASSOCIATED VIRUS MEDIATED THERAPEUTIC INTERVENTION FOR GM1-GANGLIOSIDOSIS

Dissertation Presented By

Cara M. Weismann

The signatures of the Dissertation Committee signify completion and approval as to style and content of the Dissertation

Miguel Sena-Esteves, Ph.D., Thesis Advisor

Daryl Bosco, Ph.D., Member of Committee

Terence Flotte, M.D., Member of Committee

Casey Maguire, Ph.D., Member of Committee

David Weaver, Ph.D., Member of Committee

The signature of the Chair of the Committee signifies that the written dissertation meets the requirements of the Dissertation Committee

Guangping Gao, Ph.D., Chair of Committee

The signature of the Dean of the Graduate School of Biomedical Sciences signifies that the student has met all graduation requirements of the school

Anthony Carruthers, Ph.D.,
Dean of the Graduate School of Biomedical Sciences

Interdisciplinary Graduate Program
August 5, 2014

DEDICATION

I would like to dedicate this thesis to my father, Kenneth Weismann, my mother Barbara Weismann and my grandmother May Brill. Through my loving and supportive family I was always told that I could become anything I put my mind to, and their belief in me has been my guiding light. My father gave me the gift of acclimating to any situation or assembly through kindness, humor and love. My mother has supported me unconditionally and her tireless work ethic and devotion to her family and friends has been a model for my own. My grandmother's tenacity, leadership and unwavering ethical compass have engrained in me that action with compassion is the only method to accomplishing great things.

ACKNOWLEDGEMENTS

I would like to acknowledge my thesis advisor, Miguel Sena-Esteves who patiently taught me hands on techniques such as cryostat cutting and intracranial injections. I greatly appreciate the many hours spent pondering new experiments and his trust in me to take my own observations and support to develop them into large studies. I will be forever grateful for his faith in my experimental abilities and unwavering guidance towards simplifying the written word.

I would also like to acknowledge the wonderful student and post-doc colleagues I have had the pleasure of working with throughout the GSBS. Most especially my lab mates Lorelei Stoica, Diane Golebiowski, Allison Keeler-Klunk, Sourav Roy Choudhury and Dwijit GuhaSarkar for endless support, commiseration in the tough times, and celebration in success.

A special acknowledgement and thank you to research associate Jennifer Ferreira who came into this work with eagerness, intelligence and an unending quest for knowledge and truth. Without Jenn, the sheer quantity of this work would not have been possible and due to her involvement, the quality of these studies maintained the highest standards. I am forever grateful for her partnership and dedication.

I am also extremely thankful for the opportunities I have had within the University of Massachusetts to work with an amazing support staff, administrators, administration and leadership. Only together, these type of intensive studies are possible and success in any of these arenas are successes for us all.

Finally, I'd like to acknowledge my extended Weismann and Brill family, my great friends Emily Mallick, Shawna Guillemette, and Emma Watson, and my boyfriend Robb Alexander for support, guidance, never-ending scientific curiosity and keeping life happy and fun through it all.

ABSTRACT

GM1 gangliosidosis is a lysosomal storage disorder caused by a deficiency in the catabolizing enzyme β-galactosidase (βgal). This leads to accumulation of GM1-ganglioside (GM1) in the lysosome inducing ER stress and cell death. GM1 gangliosidosis is primarily a disorder of the central nervous system (CNS) with peripheral organ involvement. In this work we report two major findings, 1) systemic treatment of GM1 gangliosidosis with an adeno-associated virus (AAV9) encoding mouse-βgal (mβgal) in a GM1 gangliosidosis mouse model ($\beta Gal^{-/-}$), and 2) an investigation into an intracranial injection of a therapeutic AAVrh8 encoding mβgal. Systemic treatment of GM1 gangliosidosis with AAV9 resulted in a moderate expression of enzyme in the CNS, reduction of GM1 storage, significant retention of motor function and a significant increase in lifespan. Interestingly, the therapeutic effect was more robust in females. Intracranial injections of AAVrh8 vector expressing high levels of βgal resulted in enzyme spread throughout the brain, significant retention of motor function and a significant increase in lifespan. Histological alterations were also found at the injection site in both $\beta Gal^{-/-}$ and normal animals. We constructed a series of vectors with a range of decreasing enzyme expression levels to investigate the cause for the unanticipated result. Microarrays were performed on the injection site and we showed that a lower expressing AAVrh8-mβgal vector mitigated the negative response. Intracranial injection of this newly developed vector was shown to clear lysosomal storage throughout the CNS of $\beta Gal^{-/-}$ mice. Taken together, these studies indicate that a combined systemic and fine-tuned intracranial approach may be the most effective in clearing lysosomal storage completely in the CNS while providing therapeutic benefit to the periphery.

TABLE OF CONTENTS

LIST OF TABLES

LIST OF FIGURES

LIST OF SYMBOLS, ABBREVIATIONS OR NOMENCLATURE

4-methylumbelliferyl (4-MU)
AAV2-brain targeting peptides (AAV2-PFG)
Acid sphingomyelinase (ASM)
Acid sphingomyelinase (ASM)
Adeno-associated viral (AAV)
Adenoviral (Ad)
Amino acid (aa)
Arylsulfatase A (ARSA)
Aspartate aminotransferase (AST)
Assembly-activating protein (AAP)
Bone marrow cells (BMC)
Bone marrow transplant (BMT)
Bovine growth hormone (BGH)
Central nervous system (CNS)
Ceramide (Cer)
Cerebral spinal fluid (CSF)
Cerebral spinal fluid (CSF)
Cytomegalovirus immediate early enhancer/promoter (CMV)
Deep cerebellar nuclei (DCN)
Double stranded (ds)
Elastin binding protein (EBP)
Endoplasmic reticulum (ER)
English Springer Spaniel (ESS)
Enzyme replacement therapy (ERT)
Feline β-galactosidase (fβgal)
Fibroblast growth factor receptor (FGFR)
Firefly luciferase (Fluc)
Galactocerebrosidase (GALC)
Galactosyltransferase I (GalT I)
Galactosyltransferase II (GalT II)
Gene encoding β-galactosidase (*GLB1*)
Glial-derived neurotrophic factor (GDNF)
Globoid cell leukodystrophy (GLD or Krabbe disease)
Glucosylceramide (GlcCer).
Glucosylceramide transferase (GlcT)
GM1 ganglioside (GM1)

GM1 gangliosidosis animals/cells lacking both copies of β-galactosidase gene (βGal$^{-/-}$)
GM1 gangliosidosis animals/cells with one copy of β-galactosidase gene (βGal$^{+/-}$)
GM2 ganglioside (GM2)
GM3 ganglioside (GM3)
Hematopoietic stem and progenitor cells (HSPC)
Hematopoietic stem cells (HSC)
Hematoxylin & Eosin (H&E)
Heparin sulfate proteoglycan (HSPG)
Hepatocyte growth factor receptor (HGFR)
Herpesviral (HSV-1)
High dose (HD)
high performance thin layer chromatography (HPTLC)
Human aromatic $_L$-ammino acid decarboxylase (hAADC)
Humanized green fluorescent protein (hGFP)
Integration site for wild type AAV, human chromosome 19q (AAVS1) locus
Interleukin 1 beta (IL-1β)
intracerebroventricular (ICV)
Intrathecal (IT)
Intravenous (IV)
Inverted terminal repeats (ITR)
Lactate dehydrogenase (LDH)
Lactosylceramide (LacCer)
Late infantile neuronal ceroid lipofuscinosis (LINCL)
LC electrospray ionization mass spectrometry (ESI-MS)
Lentiviral (LV)
liquid chromatography tandem mass spectrometry (LC-MS/MS)
Low dose (LD)
Lower motor neurons (LMN)
Lysosomal storage disorders/diseases (LSD)
Magnetic resonance imaging (MRI)
Major histocompatibility complex class II (MHC class II)
Mannose-6-phospate receptor (M6PR)
Matrix-assisted laser desorption ionization time-of-flight mass spectrometry (MALDI TOF)
Metachromatic leukodystrophy (MLD)
Metachromatic leukodystrophy mice/cells carrying a two copies of a mutation in the arylsulfatase A gene (As2$^{-/-}$)

MicroRNA de-targeting sequence (miRT)

MicroRNA-126 (miR-126)

Mouse β-galactosidase (mβgal)

Mucopolysaccharidosis I (MPS1)

Mucopolysaccharidosis VII (MPS VII)

Multiple reaction monitoring (MRM)

Muscle creatin kinase (MCK)

Myelin basic protein (MBP)

N-acetylgalactosaminyltransferase (GalNAcT)

N-acetylneuraminic acid (Neu5Ac)

N-acetyl-β-D-galactosamine (GalNAc)

Neuraminidase-1 (NEU1)

Neuron specific enolase (NSE)

Nitric oxide (NO)

N-octyl-4-epi-β-valienamine (NOEV)

Non-human primates (NHP)

Open reading frame (ORF)

peripheral blood mononuclear cells (PBMC)

Peripheral nervous system (PNS)

Portuguese Water Dog (PWD)

Promoter composed of CMV enhancer fused to the chicken beta-actin promoter followed by a chimeric chicken beta-actin/rabbit beta globin intron (CBA)

Protective protein/cathepsin A (PPCA)

Recombinant AAV (rAAV)

Retroviral (RV)

Rostral migratory stream (RMS)

Sandhoff disease (SD)

Self complementary (sc)

Sialictransferase (SAT)

single stranded (ss)

Substrate reduction therapy (SRT)

Subventricular zone (SVZ)

Sulfamidase (Sgsh)

Survival motor neuron 1 (SMN1)

Thymidine kinase (*tk*)

Thymidine kinase (TK)

Transforming growth factor beta (TGFβ1)

Tumor necrosis factor alpha (TNF-α)

Unfolded protein response (UPR)

Uridine diphosphate galactose (UDP-galactose)

Uridine diphosphate glucose (UDP-glucose)

Vascular endothelial growth factor (VEGF)

Ventral tegmental area (VTA)

Wild type (WT)

Woodchuck hepatitis virus post-transcriptional regulatory element (WPRE)

β-D-galactose (β-D-Gal)

β-galactosidase (βgal)

β-glucuronidase (GUSB)

β-glucuronidase (βGlu)

LIST OF MULTIMEDIA FILES

Video 2.1 Male animals near humane endpoint of untreated βGal$^{-/-}$ mice. βGal$^{-/-}$ + 3e11 vg at 258 days, βGal$^{+/+}$ untreated at 258 days and βGal$^{-/-}$ + PBS at 221 days.

Video 2.2 Female animals near humane endpoint of untreated βGal$^{-/-}$ mice. βGal$^{-/-}$ + 3e11 vg at 260 days, βGal$^{+/+}$ untreated at 260 days and βGal$^{-/-}$ + PBS at 236 days.

Video 2.3 Male animals near humane endpoint of untreated βGal$^{-/-}$ mice βGal$^{-/-}$ + 1e11 vg at 249 days, βGal$^{+/-}$ untreated at 264 days and βGal$^{-/-}$ + PBS at 263 days.

Video 2.4 Female animals near humane endpoint of untreated βGal$^{-/-}$ mice. βGal$^{-/-}$ + 3e11 vg at 258 days, βGal$^{+/+}$ untreated at 278 days and βGal$^{-/-}$ + PBS at 264 days.

Video 2.5 Treated female βGal$^{-/-}$ + 3e11 vg at 590 days.

Video 2.6 Treated female βGal$^{-/-}$ + 3e11 vg at 563 days.

PREFACE

All chapters are original, unpublished works

All experiments were performed and data collected and analyzed by Weismann, C. unless otherwise noted

Figure 1.1: Structure was assembled by Schaffer, S. and modified by Weismann, C.

Figure 1.3: Was created by Sena-Esteves, M. and modified by Weismann, C.

Chapter II: AAV vector backbone was provided by Flotte, T.

Chapter II: AAV9-mβgal was cloned by Ferreira, J. and packaged by Su, Q. Animals were intravenously injected by Sena-Esteves, M.

Chapter II: Figure 3.2, 3.15 a & b, table 3.1, were performed and analyzed by Ferreira, J. and modified by Weismann, C. Figure 3.6 was assisted by Ferreira, J. with Weismann, C.

Chapter II: Figure 3.3 samples were collected by Keeler-Klunk, A. and analyzed by Weismann, C.

Chapter II: Figure 3.13 & 3.14 testing was set up by Qui, L. and collected and analyzed by Weismann, C.

Chapter III: Table 3.1 cloning of the viral vector CBA- transgene empty-WPRE by Golebiowski, D. Cloning of vector CB6-mβgal by Ferraira, J. All vectors packaged by Maitland, S. except original CBA-WPRE in Figures 4.1-4.9 packaged by Weismann, C.

Chapter III: Ferraira, J performed the following assays and animal support: Figures 4.10-4.18 maintenance of animal colony. Figures 4.10, 4.14 performed 4-Mu βgal assays and corresponding Bradford assays in 4.10, 4.14 and 4.18. Figure 4.10 performed Western Blot. Figure 4.13 performed RNA extraction and assisted in sample collection for microarray. Figure 4.18 assisted in sample collection and preparation for LC-MS/MS with Weismann, C.

Chapter III: Figure 4.11 genome copy analysis performed and analyzed by Sena-Esteves, M.

Chapter III: Figure 4.13 all micro array experiments performed by Genomics Core, Spatrick, P. and analyzed by Straubhaar, J.

CHAPTER I: Introduction

GM1-Gangliosidosis

Clinical Description

Lysosomal storage disorders (LSD) are a class of recessive diseases that are caused primarily by the reduction of a catabolizing lysosomal resident enzyme and subsequent storage of the substrate in the lysosome. These disorders result in lysosomal dysfunction, alterations in cell homeostasis, and cell death (1). There are more than 50 known LSD's, and ~70% of them have a central nervous system involvement. One well known LSD is GM1-gangliosidosis which was first identified in 1959 (2). GM1-gangliosidosis results from the lack of the enzyme β-galactosidase (βgal, encoded by the *GLB1* gene) and subsequent storage of GM1-ganglioside (GM1) and the asialo derivative GA1 (GM1 lacking sialic acid group), in the lysosomes in cells of the central and peripheral nervous system (CNS and PNS, respectively) (3). Also associated with this disease is the storage of other glycoconjugates with terminal β-galactose residues, along with oligosaccharides and keratan sulfate, in the lysosomes of cells of the visceral organs. Cells burdened with GM1 storage activate the unfolded protein response (UPR) and undergo endoplasmic reticulum (ER) stress which leads to Ca^{2+}-mediated mitochondrial apoptosis (4,

5) and inflammation (6), resulting in progressive neurological decline that leads to generalized paralysis and death (7).

There are three forms of GM1-gangliosidosis: infantile, juvenile and adult; in which severity, disease onset and progression are correlated with the amount of βgal activity which ranges from >1–9% of normal activity. Onset of infantile and juvenile GM1-gangliosidosis occurs between birth and 3 years. This form of the disease primarily affects the CNS, however, hepatosplenomegaly, and macular cherry red spots have also been documented (7). Two distinguishing features of the infantile form include the occurrence of facial dysmorphism, and skeletal abnormalities, which are not present in the juvenile form of this disease. In contrast to infantile and juvenile forms, onset of adult GM1-gangliosidosis occurs between 3 and 30 years of age. This disease manifests as primarily non-neurological, however, symptoms of dystonia with minimal skeletal abnormalities can also be present (7).

GM1-gangliosidosis occurs in 1:100,000-200,000 births with no known ethnic dominance, although some mutations in the *GLB1* gene have common lineages such as Italian, American, Brazilian and Japanese (7, 8). Diagnosis of this disease typically results from the presentation of abnormal neurological findings such as developmental regression or failure to meet milestones, which then trigger further investigation. The methods of diagnosis include the following: (1) retrospective analysis on dried blood spots from newborn screening panels (9), or on blood spots from high risk patients with suspected heredity inclinations

(10), (2) pre-natal diagnosis from amniotic fluid (11), and (3) molecular analysis of the *GLB1* gene (12). Known disease-carrying mutations in *GLB1* include gene duplication, insertions (which result in splicing defects), missense mutations, and nonsense mutations (7, 8). Currently, there is no cure for this disease.

GLB1 Gene

The human gene *GLB1* is located on chromosome 3p21.33. The gene is 62.5kb, contains 16 exons and encodes two, alternately spliced transcripts: a 2.4kb mRNA, 677 amino acid (aa) lysosomal acid β-galactosidase (βgal) and a 2.0kb variant mRNA, 546aa elastin binding protein (EBP) (7, 8, 13). EBP is a 67kDa protein that together with the elastin receptor and protective protein (carboxypeptidase A or cathepsin A), form an elastin complex on the cell surface to bind elastin peptides (8, 13). The functions of this complex include: the assembly of elastic fibers, cytoskeleton reorganization and cell proliferation through an increase of intracellular Ca^{2+} (8, 13, 14). Defects in EBP result in impaired elastogenesis (generation of elastic fibers) and results in a connective tissue disease (15). Interestingly, defects in elastogenesis that were believed to result from accumulation of keratan sulfate have also been implicated in patients with GM1-gangliosidosis with and without mutations in EBP (15).

The 677aa protein is the βgal prepropolypeptide which is processed in the ER to yield a 654aa product that is then glycosylated and phosphorylated to an 88kDa precursor. Final processing of the C-terminal end of βgal to a 67 then a

64kDa functional enzyme occurs in the lysosome (8). A multi-enzyme complex consisting of protective protein/cathepsin A, neuraminidase, and the 20kDa fragment from the C-terminal end of βgal are necessary for the correct processing and activity of the βgal enzyme (16). The catalytic nucleophile of βgal was identified by mass spectrometry (17) and mutation analysis confirmed the conserved residue Glu268 as an active site for βgal enzymatic activity (8). Recently, a crystal structure of βgal has been constructed which demonstrated mutations affecting ligand recognition, within the enzyme core or on the enzyme surface that indicates how these mutations may lead to disease (18).

GM1 Ganglioside Biosynthesis and Catabolism

Biosynthesis of gangliosides occurs through the stepwise addition of sugar moieties and sialic acid residues. This process is regulated both transcriptionally and post transcriptionally by enzymes expressed temporally in a cell-specific manner (19). GM1 synthesis (Fig. 1.1) begins with the lipid ceramide (Cer) in the ER that is transported to the Golgi by the ceramide transport protein, CERT (20). Glucose is transferred from uridine diphosphate glucose (UDP-glucose) to Cer in the golgi by glucosylceramide transferase (GlcT) which then becomes glucosylceramide (GlcCer). The final step prior to ganglioside production is the glycosylation of GlcCer to lactosylceramide (LacCer) by galactosyltransferase I (GalT I) from uridine diphosphate galactose (UDP-galactose) (21).
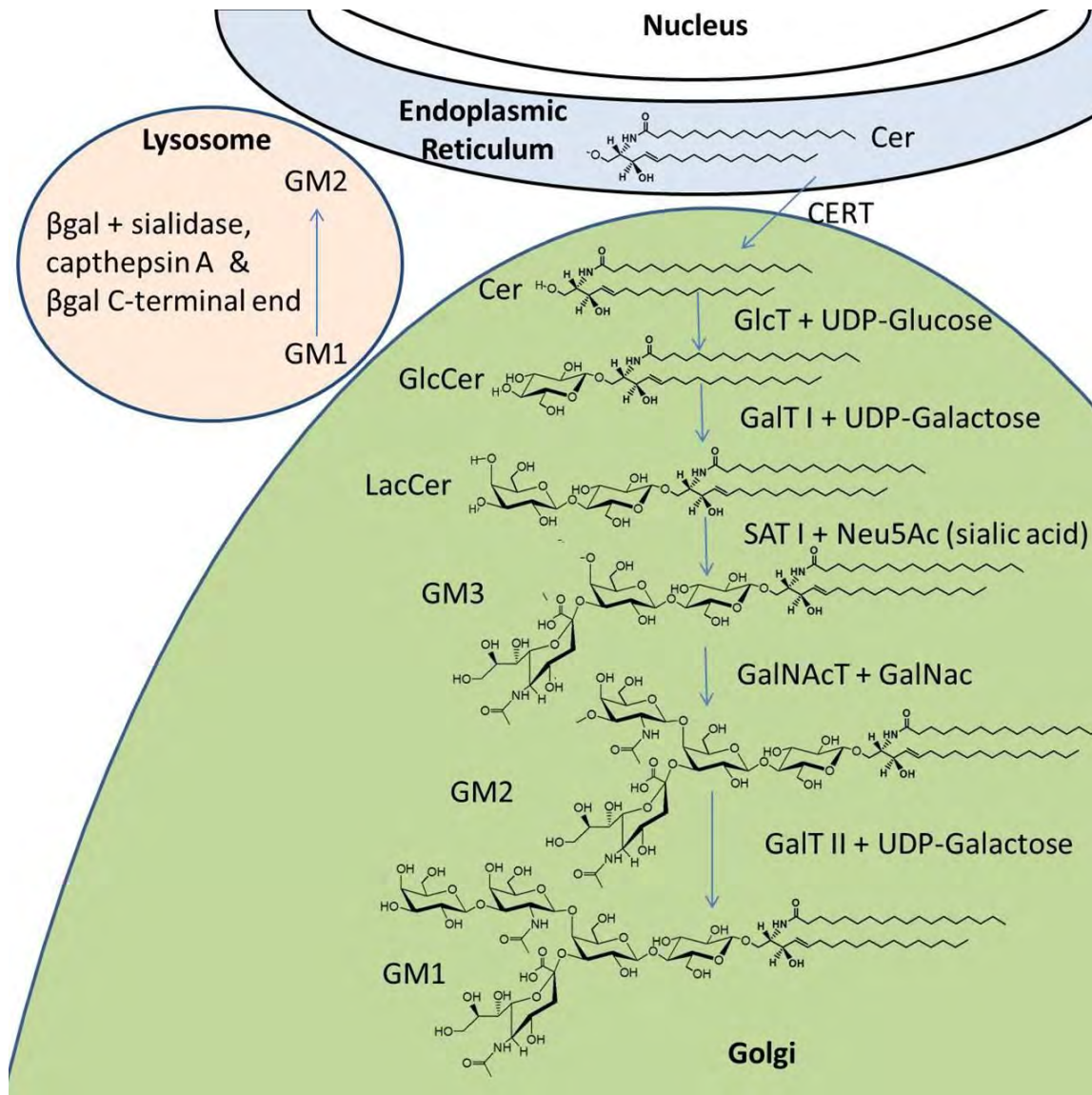
Figure 1.1 Ganglioside biosynthetic and catabolic pathway

Each ganglioside series is defined by the number of sialic acid groups: no sialic acid (0-series), 1 (A-series), 2 (B-series) and 3 (C-series) (19). Addition of one sialic group, N-acetylneuraminic acid (Neu5Ac, sialic acid) to LacCer occurs by sialictransferase I (SATI), which produces the GM3-ganglioside (GM3) and leads to the A series of gangliosides: GM3-GM2-GM1 (Fig. 1.1 and 1.2) (19). Sugar moieties N-acetylgalactosamine (GalNAc) and UDP-galactose are transferred by sequential addition by their respective, specific glycosyltransferases: N-acetylgalactosaminyltransferase (GalNAcT) (22) to obtain GM2-ganglioside (GM2) from GM3, then GM2-GM1 by galactosyltransferase II (GalT II) (19). Kotler and colleagues provide a comprehensive review of this process (19).

The mature gangliosides are transported to the cell surface by vesicular transport and become part of the cell membrane. Eventually, gangliosides are endocytosed from the plasma membrane and catabolizing enzymes then degrade the mature gangliosides back to their initial components within the lysosomes. The degradation of membrane bound GM1 is processed to GM2 by lysosomal acid β-galactosidase, which removes the terminal β-galactose residue. This process occurs in the presence of GM2 activator protein and saposin B (23). As discussed above, mature βgal activity requires a multienzyme complex of sialidase and capthepsin A and the presence of the proteolyzed C-terminal end of βgal (16). The process of ganglioside degradation has been recently reviewed (24).
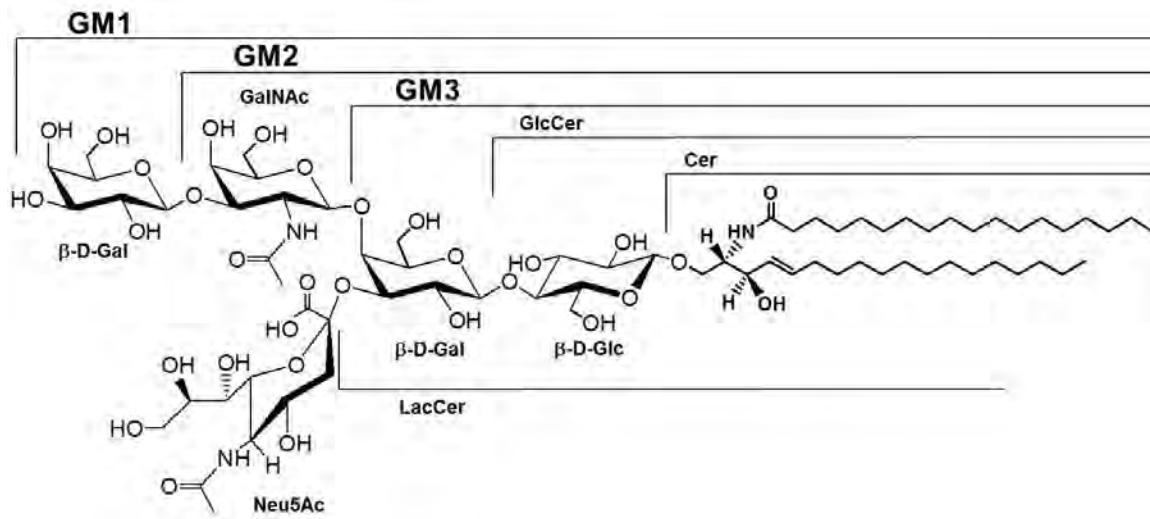
Figure 1.2 A Series Gangliosides

GM1-Ganglioside Function

Gangliosides are important components of cell membranes and have specific functions in the CNS. The concentration and complexity of gangliosides in the developing brain increase over time and have been studied in both mice and humans. Normal mice have an ~8-fold increase in ganglioside concentration from embryonic day E12 to adult (25). During this time, the composition of gangliosides shifts from simple GM3 ganglioside (GM3) (less sugar moieties) to complex GM1 and GD1a due to the differential expression of glycosyltransferases in neural precursor cells (25). This process is concomitant with neurogenesis and astrocytogenesis. In the human brain, it has been shown that total ganglioside concentrations increase 3-fold from fetal week 10-to-5 years of age, and during this time GM1 and GD1a increased 12-to-15-fold (26). Notably, the GM1 precursors GalCer and sulfatide also increase during development, specifically when myelin is forming and oligodendrocytes are differentiating (25). Importantly, mice deficient in glycosyltransferases and therefore lacking complex gangliosides, show axonal loss and decreased myelination within the nervous system (27). These findings further support the role of complex gangliosides in myelination and neuronal growth in the developing brain. In the adult brain, GM1 is located on the cell surface as a component of the membrane, specifically in lipid rafts, and has been shown to play a part in cell signaling (28-30). In these roles, GM1 has been demonstrated to have neuroprotective effects. One example is from an increase in nuclear

Ca^{2+} that can lead to apoptotic cell death, where a complex of GM1 with sodium/calcium exchanger NCX facilitates transport of nuclear Ca^{2+} to the ER (31, 32).

GM1 has been investigated as a therapeutic agent for aging and neurodegeneration due to identification of the ganglioside in several diseases. In Huntingtin's disease multiple groups had discovered a decrease in the amount of GM1 ganglioside in animal models of this disease (33, 34) as well as postmortem human brain samples (33, 34) and cultured fibroblasts from those patients (34). Therapeutic intervention for huntingtin was attempted to increase the amount of GM1 by an intraventricular infusion of the ganglioside in a mutant-huntingtin expressing mouse. Excitingly, this infusion led to phosphorylation of the mutant huntingtin which rendered the mutant less-toxic, and corrected motor behavior (35). In Parkinson's disease there has been no association with the disease state and the alternation of endogenous levels of GM1, however GM1 has been shown to inhibit the aggregation of α-synuclein (36) which is a major component of Lewy bodies present in this disease. In Parkinson's pre-clinical studies GM1 was demonstrated to partially restore dopamine levels within the mouse striatum after insult (37) and in parkinsonian monkeys (38), and in clinical trial subcutaneous administration of purified GM1 has shown great promise in improving motor function (39). In contrast, GM1 presence in Alzheimer's disease has been implicated in the formation of toxic Aβ fibrils by the recruitment of soluble Aβ to GM1 on lipid rafts specifically when GM1 is in a β-sheet

confirmation (40). GM1 concentration in the brains of Alzheimer's disease patients is significantly increased (41), however various mouse models of this disease show either no change or a decrease in GM1 (42). Interestingly, due to its neuroprotective roles GM1 has also been suggested to have therapeutic benefits in this disease. In one study, the pre-treatment of GM1 on rat hippocampal slices inhibited Aβ formation as well as the downstream activation of apoptosis pathways (43). Follow up work from this group treated rats with GM1 then challenged Aβ fibrils showing that GM1 played a role in preventing cognitive decline (44)

GM1-Gangliosidosis

Disease mechanisms of GM1-gangliosidosis have been examined in several studies using GM1-gangliosidosis mice ($\beta Gal^{-/-}$) (4, 6, 45, 46). (i) Autophagy is a major mechanism driving disease progression in this disease. Enhanced autophagy was observed in the brains of end-stage $\beta Gal^{-/-}$ mice, where GM1 was highly accumulated, but not in 10-day old mice (45). (ii) Inflammation and associated downstream effects were also identified. Jeyakumar *et al* demonstrated that GM1 accumulation over time resulted in inflammation in deep brain structures of the thalamus and brainstem (6). This inflammation leads to expression of activated macrophage or microglial cells, major histocompatibility complex class II (MHC class II) positive cells and nitric

oxide (NO) formation (6). NO accumulation leads to oxidative damage and can result in neurotoxicity (47). Inflammatory cytokines tumor necrosis factor alpha (TNF-α) and interleukin 1 beta (IL-1β) were also seen at the site of GM1 storage, however transforming growth factor beta (TGFβ1) was only in end stage βGal$^{-/-}$ mice providing a time course response to accumulation (6). (iii) ER stress was also shown to be factor leading to neurodegeneration. Tessitore *et al* investigated the excessive accumulation of GM1 in neurons, stress on the ER, and initiation of the unfolded protein response (UPR). They show that these actions lead to apoptosis, but that those effects were not seen in a double knockout mouse that did not produce GM1 (4). Further work from this lab demonstrated that the apoptotic effect was due to Ca^{2+} flux caused by GM1 presence from ER to the mitochondria, creating membrane permeabilization on the mitochondria leading to mitochondrial-mediated apoptosis (5).

Taken together, these studies demonstrate that a cascade of events beginning with accumulation of GM1 within the lysosome and initiation of compensatory mechanisms results in upregulation of autophagy. Continued accrual of GM1 storage recruits inflammatory cytokines and accumulation of neurotoxic NO species. Concomitantly, GM1 accumulation activates the UPR, causes Ca^{2+} flux through the ER membrane and results in apoptosis from the mitochondria.

Animal Models of GM1-Gangliosidosis

Murine Models

Two models of GM1-gangliosidosis currently exist for mice. (i) Matsuda *et al* produced a mouse through insertion of a neomycin and herpes simplex virus thymidine kinase (*tk*) gene into exon 15 of the *GLB1* gene in murine ES cells (48-50). (ii) Hahn *et al* created a mouse also through an insertion of the neomycin cassette with a downstream *tk* gene into ES cells, however this insertion was into the middle of exon 6 of the *GLB1* gene (51). Both of these models result phenotypically in the same βGal$^{-/-}$ mouse. They are both authentic representations of GM1-gangliosidosis with minimal exceptions. Each model resulted in disruption of the *GLB1* gene, loss of the βgal enzyme (50, 51) and subsequent storage of GM1 ganglioside within the CNS from birth (50, 51) with corresponding histological and neurological phenotypes (48, 49, 51). Interestingly, two β-galactosidases, lysosomal acid β-galactosidase and galactocerebrosidase, previously identified in human brains, were found to be capable of degrading GM1, GA1 and the experimental substrate 4-methylumbelliferyl β-galactoside *in vitro*, albeit with different efficiencies (52). Evidence that these two β-galactosidases can act on GM1 and corresponding substrates could lead to the low level of βgal activity found in the CNS (1-4%) as well as visceral tissues (1-8%) in both mouse models (50, 51).

Notably, GM1 content (µmol/g) in a the CNS of a 2.75 month old βGal$^{-/-}$ mouse was shown to be equivalent in concentration to an 8 month old infantile GM1 gangliosidosis patient (51). Despite the early accumulation of GM1 outward phenotypes do not present until ~4 months of age (48, 51). Both mouse models also demonstrated a higher total percentage accumulation of the GM1 asialo derivative GA1 (GM1 lacking the sialic acid group) present in the CNS compared to humans (49, 51, 53-55). This finding suggests that an alternate catabolic pathway utilizing sialidase is more active in the mouse than in humans. Interestingly, GM1 synthase activity was not found to be altered in a βGal$^{-/-}$ mouse in response to storage of the ganglioside, however patient fibroblasts from early infantile GM1 patients showed a compensatory down-regulation of the synthase that was correlated with decreased active βgal enzyme (56). This indicates that there is a feedback mechanism for regulation of GM1 content by GM1 synthase, however in these mouse models with alternate catabolic pathways, this feedback is somehow disrupted and may be one factor for the late onset of disease phenotypes.

Vacuolated neurons (50) and then severe gliosis were identified throughout the CNS and also increased with time (49, 51). In the mouse, CNS phenotypes of tremor, ataxia, huddled posture when held by tail and abnormal gait begin at ~4 months of age and progress until death by emaciation at ~10 months old (48, 51).

In contrast to humans, mice do not have keratan sulfate and therefore the bone abnormalities are not present in these animals (49, 51). Neither hepatosplenomegaly, nor correspondingly abnormal urinary oligosaccharides are present in the mouse models (50, 51), however thymus, liver, spleen and kidney show some pathology of foamy, ballooning or vacuolation phenotypes within the lysosome of these organs (49).

Feline Models

Feline models of GM1-gangliosidosis are naturally occurring and have been identified in Siamese (57, 58) and short-hair domestic cats (57) with slight variations between these animals studied. These models are representative of the juvenile form of the disease where CNS and visceral organ involvement are present, however with <10% (57), or 15-20% (58) of normal βgal activity in brain, kidney, skin and cultured fibroblasts . In this model, the primary storage material is GM1 which accumulates to levels 8-fold higher than normal animals (57, 58). These animals have appear normal until 2-3 months (57), or up to 4 months (58) of age, however tremors in the extremities are mildly evident . After the initial onset, the disease progresses rapidly with development of ataxia and subsequent quadriplegia by 6 months (58) or 7-8 months of age (57). These animals experience corneal clouding, vision loss, an extreme startle response, and grand mal seizures by 1 year (57). Hepatosplenomegaly or cherry red spot

in the retina are not present, but vacuolated macrophages and neuronal lipodosis results in neuronal degeneration, paralysis and death (57-59).

Canine Models

The first dog identified with GM1-ganglisidosis was a mixed breed beagle that presented with tremors, ataxia, hyperactivity and visual impairment that progressed over a 4 month period. The animal eventually developed paralysis and was euthanized at 9 months of age (60). Neuronal vacuolation with distended cytoplasm and membranous cytoplasmic bodies were found in the CNS. Elevations in GM1 and GA1 were noted in the liver, spleen and grey matter of the brain, which corresponded to a large decrease in βgal activity in these regions (60).

Since this time multiple naturally occurring canine models with GM1-gangliosidosis have been studied including, in English Springer Spaniels (ESS) (61), and a Portuguese Water Dogs (PWD) (61, 62), among others. Both ESS and PWD animals are different from the murine and feline models as skeletal dysplasia is evident at 2 months of age, and by 4.5 months neurologic manifestations of tremor, ataxia, and deteriorating responses from cranial nerves are present (61). ESS puppies with GM1-gangliosidosis are born dwarfed (61). These animals progressively decline until requiring euthanasia at 9 months of age where grey matter was increased in volume while white matter decreased

(61). Both dogs have <10% βgal activity of wild type (61, 62) and store GM1 in the CNS as well as visceral organs which results in enlarged, vacuolated cells (61). Non-lipid oligosaccharides have also been shown to be stored in the lysosome (61). In addition, these dogs showed decreased myelination accompanying the presentation of astrocytosis, microgliosis and minimal macrophages in the CNS (61). However, due to the heterogeneity of phenotypes in these animals, classification as to disease form in relation to human manifestation was not made.

In Shiba Inu dogs extensive study has occurred which advances the therapeutic investigation into GM1-gangliosidosis in humans. These dogs differ from the ESS and PWD model as no skeletal abnormalities, dwarfism, seizures (63, 64) or hepatosplenomegaly (63) were present in these animals. In addition, the course of the disease is slightly delayed with progressive neurological decline beginning at 5-6 months of age including tremors, ataxia, intermittent lameness and loss of balance resulting in an inability to stand by 8-10 months of age (63, 64). Visual impairments with corneal clouding, muscle rigor and lethargy (63, 64) lead to the animals being sacrificed at 14-15 months old (63). Vacuolated lymphocytes (63, 64) and distended neurons with membranous cytoplasmic bodies were present in the CNS (64). Severe reduction in βgal corresponded with increases in GM1-ganglioside 10-20 fold normal in the brain (64). Serial magnetic resonance imaging (MRI) had also been performed on these animals

showing progressive hyperintensity in white matter of the cerebrum beginning at 2 months of age and progressing through the course of the disease (65).

Studies in Shiba Inus have provided new tools for the diagnosis and monitoring of GM1-gangliosidosis (65-67). Satoh *et al* profiled the cerebral spinal fluid (CSF) of affected GM1-gangliosidosis canines and determined molecular signatures which indicate increases ganglioside concentrations and corresponding downstream effects until the humane endpoint (67) . Changes in aspartate aminotransferase (AST) and lactate dehydrogenase (LDH) increased until 7 months (67) of age which was hypothesized to represent leakage from the neurons as noted in other brain disrupting disorders. LDH has been indicated as a biochemical measure of cytotoxicity (68). In addition, more classical markers of degeneration or neuronal injury, neuron specific enolase (NSE) in the CSF (69, 70) was correlated with disease progression in these animals (67). Myelin basic protein (MBP) rose in CSF, but only after 9 months of age when it is suspected that myelin degeneration occurs in these animals (67). More recently, a matrix-assisted laser desorption ionization time-of-flight mass spectrometry (MALDI TOF) method was developed for GM1 ganglioside in the CSF of these animals (66).

Additional models

Other species with naturally occurring GM1-gangliosidosis include bovine (59, 71), sheep (72, 73) and black bears (74). Practical considerations of housing and studying such large animals do not lend these models easily to preclinical therapeutic investigation.

Current Therapeutic and Non-Viral

Approaches for GM1-Gangliosidosis

Clinical Approach

Despite significant research efforts, there is currently no cure for GM1-gangliosidosis. In the clinic the only treatment options are palliative. One therapy employed is substrate reduction therapy (SRT), with a drug named Miglustat (75-77). This orally administered therapy aims to reduce GM1-ganglioside accumulation by the inhibition of glycosylceramide synthase which in turn depletes GM1 precursor glycoslceramide (78). This regimen provides temporary modulation of symptoms in some patients although the disease still eventually progresses. Known side effects of Miglustat include chronic diarrhea and weight loss which makes it intolerable for certain patients (75-77).

Molecular Chaperone and Substrate Reduction Therapy

Currently, all other therapeutic approaches for GM1-gangliosidosis are in preclinical studies. Matsuda *et al* are utilizing molecular chaperone therapy which targets a specific mutation in the β-galactosidase enzyme (79). The objective of this therapy is to stabilize unstable and/or misfolded enzymes by the chaperone so it can be properly transported to the lysosome. In mice, chaperone N-octyl-4-epi-β-valienamine (NOEV) (79) lead to increased amounts of active βgal and reduced the storage of GM1 with minimal to no adverse responses. The limitation of chaperone therapy, however is that they are mutation specific and therefore lack application in the remaining *GLB1* resulting diseases. To increase the utility of chaperones, a combined treatment with SRT has also been attempted. Glycosphingolipid biosynthesis was targeted by competitive inhibition with imino-sugar N-butyldeoxygalactonojirimycin in mice (80) which successfully reduced total brain ganglioside as well as GM1-ganglioside content. In addition, an sp^2-immunosugar analogue SRT-chaperone combination *in vitro* (81) was able to increase βgal activity at levels similar to NOEV.

Bone Marrow or Cell Transplantation

The transplantation of bone marrow or intracerebral cell transplantation has been investigated for GM1-gangliosidosis in GM1 dogs (82), a human patient (83) and in mice with a mixture of cell types (84). In these studies,

successful donor cell engraftment was achieved, but therapeutic levels of βgal were not detected in the CNS and therefore disease progression and neurodegeneration occurred (82-84). Possible causes for the lack of therapeutic efficacy include the low level of endogenous enzyme from donor-derived migrating microglia (82, 83) and/or eventual rejection of newly resident cells (84).

Enzyme Replacement Therapy

Enzyme replacement therapy (ERT) is the practice of introducing recombinant enzymes into the organism by direct injection into the parachyma or vascular system. These enzymes are taken up via endosomes which contain a mannose-6-phosphate receptor (M6PR) on the surface that targets the payload to lysosomal compartments. Utilizing the property of cross correction (Fig. 1.3), those cells that receive the metabolically active enzyme are also able to excrete the from the loaded endosomes into the intracellular space to be taken up by neighboring cells (85-88). ERT has been investigated in GM1-gangliosidosis feline models, but no preclinical study has been published (89, 90) and this work has not advanced to human trials.

Disorders of the CNS are a challenge for intravenous ERT because the blood brain barrier restricts the entry of large, charged molecules into the parenchyma (91). Furthermore, the differential expression of M6PR such as in the skeletal
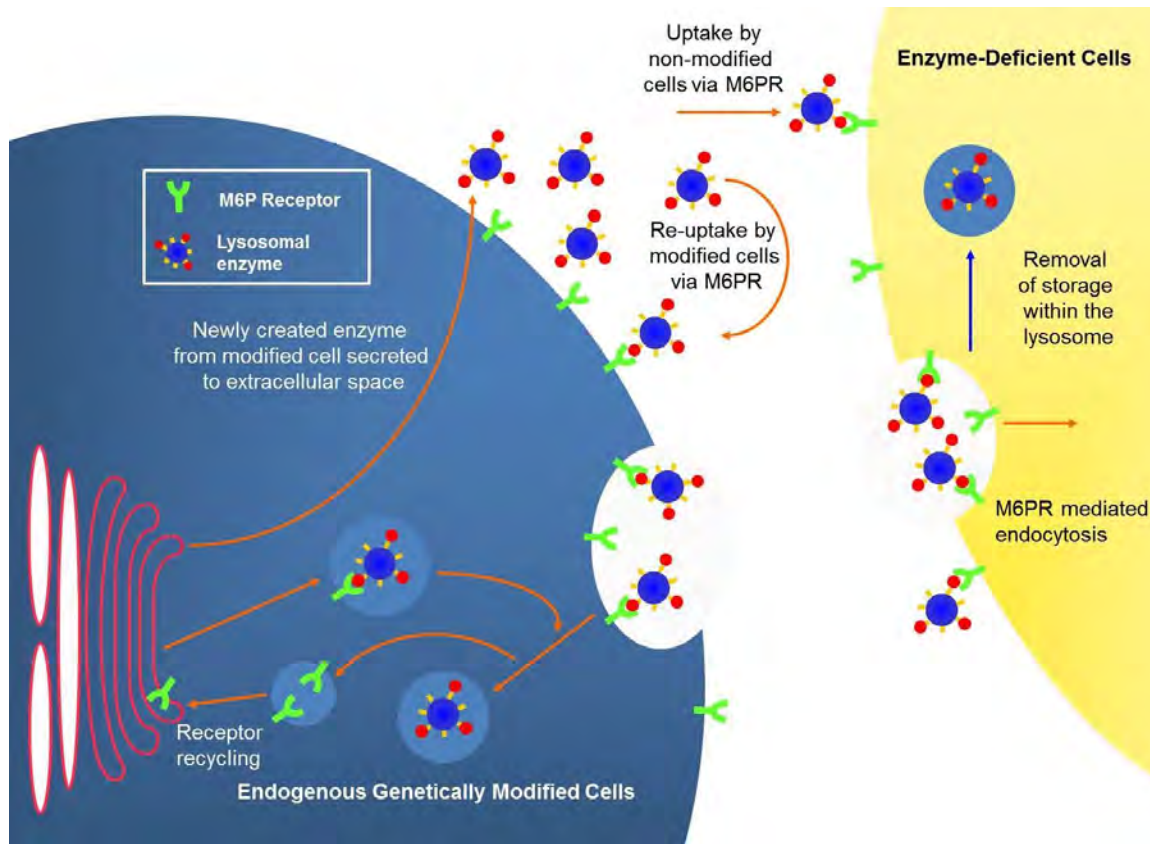
Figure 1.3 Cross correction mechanism

muscle of patients with the LSD Pompe disease can hinder therapeutic success. In Pompe disease, ERT presents a challenge as not only the uptake of the extracellular enzyme is restricted (92), but mouse studies suggest a decline in intracellular trafficking to the lysosome as indicated by reduction in storage clearance (93). One strategy to circumvent this obstacle utilized β_2 agonist Clenbuterol as an adjunct therapy to enhance M6PR expression in skeletal muscle and lead to increased enzymatic efficacy with ERT (94).

New approaches to deliver recombinant enzyme to the cerebral spinal fluid (CSF) either by intrathecal (IT) injection alone or in combination with intravenous (IV) administration indicates positive advancements in ERT in several models. An IT and/or IV approach in the LSD mucopolysaccharidosis I (MPS1) dogs (95-98) or cats (99) have shown great promise in increasing enzyme activity in the CNS. In addition, intracranial infusion in the lateral ventricles in the LSD late infantile neuronal ceroid lipofuscinosis (LINCL) mouse (100), wild type rat and non-human primates (NHP) (101) have shown moderate to extreme effectiveness in targeting the CNS. In larger models of dogs and NHP's, a gradient of enzyme concentration were demonstrated where areas of the brain closest to CSF at high levels and distal parenchyma considerably lower, however still above therapeutic range (95-97, 101). Sly *et al* indicate that the mannose receptors present on macrophages and Kupffer cells are responsible for the initial clearance of available enzyme from plasma shortly after administration of ERT (102). They suggest that previous approaches to ERT

using high doses saturated these receptors and allowed for uptake by M6PR and subsequent entry into the CNS. A final approach for the delivery of recombinant enzyme aims to capitalize on maternal transmission of IgG for therapeutic intervention *in utero.* This study in the LSD mucopolysaccharidosis VII (MPS VII) mice used β-glucuronidase tagged with an Fc receptor (103). Despite low amounts of enzyme transferred to the fetus, this route has the potential to combat prenatal disease phenotypes and provide tolerance to the absent enzyme.

Limitations to ERT include the need for expensive, frequent injections, or lack of endogenous protein in the host leading to the production of neutralizing antibodies. In addition, the absence of M6PR in certain diseases or cell types can result in less uptake of enzyme, the culmination of which is reduced efficacy in this therapy.

Gene Therapy for Lysosomal Storage Disorders

Gene Therapy Overview

The use of gene therapy for lysosomal storage disorders is quite promising. Gene therapy works on a simple premise – the addition or depletion of a gene into the system to achieve a therapeutic impact. As recessive diseases, LSD's are well suited for this therapeutic modality. In addition, the

majority of these diseases involve secreted enzymes that can also benefit from cross correction, where a transduced cell can essentially become an enzyme producing factory for neighboring cells (Fig. 1.3) (85-88).

Gene therapy can be employed as a modified viral vector, or utilizing non-viral approaches such as liposomes, polymers and modified peptides. For a comprehensive review on non-viral gene therapy, refer to O'Mahony *et al* (104). In viral gene therapy, the choice of which vector is appropriate is dependent on factors such as transgene size, cell type transduction, route of administration, integration capabilities and potential immune responses (105, 106). Lentiviral (LV) based vectors have a capacity up to 8kb in a single stranded (ss) RNA genome, transduce dividing and non-dividing cells, can randomly insert into the genome and have the risk of immune responses. Adenoviral (Ad) vectors have a transgene capacity of 36kb in a double stranded (ds) DNA genome, transduce dividing and non-dividing cells, show no integration into the host genome are highly immunogenic and can lead to toxicity in the CNS. Herpesviral (herpes simplex virus-1, HSV-1) vectors have an extra large capacity of 150kb in a dsDNA genome, transduce only dividing cells, do not integrate into the host genome, and have a high risk of immune reactions. Recombinant adeno-associated viral (AAV) vectors have a capacity of up to 4.7kb, in a ssDNA genome, transduce both dividing and non-dividing cells, are not known to integrate into the host genome (wild type AAV can integrate) and have little to no

immune concerns. For a review on viral gene therapy refer to Giacca and

Zacchigna (105) and Byrne *et al* (106).

For the work in this thesis, AAV has been chosen as the therapeutic

vector due to the transduction capability in non-dividing cells and safety aspects

of this virus. A detailed overview of AAV is provided below.

AAV Virology

AAV was originally identified as a contaminant of an adeno-viral

preparation and was hence named adeno-associated virus (107). AAV is a

linear, single stranded, non-enveloped virus, with a molecular weight of $1.4\text{x}10^6$

Da (108). It is a DNA parvovirus of the dependovirus group which is replication

deficient, and as the name implies, depends on another virus for replication

(107). The wild type virus consists of two 145bp inverted terminal repeats (ITR)

which contain elements that allow packaging of the viral DNA into the capsid

(108, 109). Two open reading frames encode the *Rep* and *Cap* genes which

function in the replication and capsid formation of the virus (110). Three

structural *Cap* proteins VP1, VP2, and VP3 exist at a ratio of 1:1:18, where VP1

expresses from the translation initiation codon, VP2 and VP3 results from

alternate splice sites expressed from two possible initiation sites either ACG or

AUG (111). More recently, a 23kDa protein has been identified from an alternate

open reading frame (ORF) within the *Cap* gene (112). This assembly-activating

protein (AAP) assists in the targeting of capsid proteins to the nucleous for

capsid formation (112, 113) by interaction with the C-terminus of the VP proteins (114). In general, capsid proteins function in cell recognition, entry, trafficking, uncoating, assembly and export. The structure of the capsid is a T=1 icosahedral, created from 60 total monomers of VP1, VP2, and VP3 proteins. The capsid is ~25nM in diameter (107). The *Rep* gene functions in DNA replication as well as expression of the AAV and encodes for 4 proteins. Transcription of Rep78 and Rep68 come from p5 promoter and are controllers of the AAV lifecycle, where Rep52 and Rep40 initiate from a downstream p19 promoter. AAV DNA is packaged as equal amount of either plus or minus ss genomes, and in the nucleus exists as a linear monomer, linear oligomers or duplex circles (108) or after transduction they exist as concatemers which are multi head to tail linear or circular dsDNA (115).

AAV enters the cell by interactions on the AAV capsid to receptors on the cell surface and into clathrin-coated vesicles via receptor-mediated endocytosis (116-118). Each capsid has a different composition and therefore a variety of receptors play a role in cell entry. More than 100 different versions or 'serotypes' of AAV have been identified which have been isolated from various species (119-121). However, serotypes of AAV capsids are not the classical definition as these capsids are not immunologically distinguished. The natural variations of these capsids lead to the ability to target a variety of cell populations. For example, AAV1 and AAV6 bind α2,3 and α2,6, N-linked sialic acid (122, 123) with a coreceptor for AAV6 of epidermal growth factor receptor (124). AAV2 and

AAV3 have a primary receptor of heparin sulfate proteoglycan (HSPG) binding domain (125) both with coreceptors of 37/67 kDa laminin receptor where this receptor also binds AAV8 and AAV9 (126). AAV2 has additional co-receptors of the fibroblast growth factor receptor (FGFR) (127), hepatocyte growth factor receptor (HGFR) (128) and integrin α5β1 (129). AAV4 and AAV5 both use α2.3 O-linked sialic acid (130, 131) with a co-receptor for AAV5 of platelet-derived growth factor receptor (132). Finally, AAV9 primarily binds galactose (133). Zinn and Vandenberghe provide a review of capsid evolution and tropism (134). Taken together, these studies allow for the intentional selection of capsids and in turn, specific cell populations and tissue targets according to experimental needs.

After cell entry, endosomes bearing AAV's are then trafficked to the golgi (118, 135), and interact with microtubules associated proteins (136, 137). Endosomal escape occurs as a change in conformation from the VP1 and VP2 proteins leads to exposure of the N-terminus (138-140) with phospholipase A2 domains (141) and nuclear localization signals (142, 143). Recent reports indicate that nuclear entry occurs through the native nuclear import pathway, using the host cell's machinery to enter the nuclear pore complex (144). Uncoating of the virus occurs in the nucleus (145-147). Two theories then exist for transgene expression i) second strand synthesis (148, 149) and ii) recruitment of plus and minus ssAAV genomes (150). i) Second strand synthesis is where the ssDNA then converts into dsDNA which is believed to be the rate limiting step to gene expression (148, 149). The generation of the second strand occurs as

the ITR's fold upon each other to form a hairpin (151). Only 125 nucleotides of the 145bp in the ITR are complementary, where unpaired bases are named the D sequence. DNA polymerase then synthesizes the second strand using the ITR as the origin of replication. ii) Recruitment of plus and minus strands occurs by first an accumulation of linear ssAAV genomes in the nucleus from AAV viral particles that contain either a plus or minus ss genome. The plus and minus strands then self-anneal and form a double stranded (ds) linear genomes which are then converted to ds circular monomers (150). Combination of the monomers to concatemers occurs through the intermolecular recombination of the ITRs (152). All ds forms are thought to be able to produce transgene expression (152, 153). AAV can persist within the nucleus of a non-dividing cell and produce transgene product for extended, unknown periods (>10 years) if not subject to an immune response elicited by the transgene (154) or capsid (155, 156).

When not replicating, wild type virus can use the ITR's and the Rep protein to integrate into the genome in a site specific manner into human chromosome 19q (AAVS1) locus which contains a Rep binding element (157, 158), and occurs in 0.1% of wild type infecting genomes. In contrast, recombinant AAV (rAAV) is not thought to integrate as long as no Rep gene is present in the rAAV transgene (159). The non-replicative nature of rAAV's lends to safety of the vector in therapeutic application. In addition, no known disease

has been caused by a wild type virus despite >90% of humans being seropositive (160).

AAV as a Gene Therapy Vector

In the creation of viral vectors for therapeutic intervention a dual vector approach was developed which removes all replicative and structural proteins, only retaining the ITR's for packaging (161). In this system, the *Rep* and *Cap* genes are provided in trans by an adenoviral helper plasmid while the AAV DNA of those genes are replaced with the transgene of interest (162). AAV2 wild type ITR's are retained for packaging with the AAV2 specific *Rep* gene, however the supplied *Cap* genes determine the resulting capsid which then provide user specificity and determine cell or tissue tropism as detailed above. AAV's have a packaging capacity of 4.7kb which can be limiting if employing a large cDNA or promoter. However, if the gene of interest is small, a self complementary (sc) AAV is also an option, which has a packaging capacity of 2.2kb. scAAV's have the added benefit of fast transcription as it bypasses the need for second strand synthesis by packing inverted terminal repeat DNA (163, 164).

Distribution of Lysosomal Enzymes in the Brain

Lysosomal enzymes distribute through the CNS in multiple ways including diffusion (165-167), axonal transport (167), and CSF (167). Formative work in this area was performed using AAV2-human β-glucuronidase (GUSB), and

corresponding adult mucopolysaccharidosis MPS VII mice (165). Diffusion is described as a sphere of enzyme in cells surrounding the injection site. Therefore, enzymes found in distal sites but lacking mRNA presence are investigated for axonal transport. Injections into brain regions with known axonal connections were performed into the hippocampus or dentate gryus. This resulted in enzyme expression which lacked mRNA presence in those predicted axonal connections in the contralateral hemisphere as early as 1 month and up to 18 months post-injection (165). Hippocampal injections demonstrated enzyme activity related to the clearance of storage product from axonal connections, but not in structures close to the injection site which do not have direct connections. This result indicated axonal transport and not diffusion lead to the clearance. Finally, injection into the subventricular zone (SVZ) resulted in enzyme expression, but not mRNA, in cells in the olfactory bulb demonstrating cross correction by secretion of GUSB from the SVZ and uptake by cells of the rostral migratory stream (RMS) (165). Davidson and colleagues further investigated the MPS VII mouse model utilizing AAV4-RSV-human β-glucuronidase unilaterally into the lateral ventricle of adult mice (166). Diffusion into the extracellular space from ventricular spaces, transduced ependymal cells, in conjunction with endocytosis and cross-correction in both the RMS and the SVZ lead to enzyme expression in the olfactory bulb. In addition, movement of enzyme through the CSF led to enzyme positive cells which were found near microvasculature throughout the cerebrum, cerebellum and brain stem, and resulted in large

reduction of storage materials and pathology as well as improvement in behavioral deficits (166). Work investigating GM1-gangliosidosis in adult mice with AAV1-mouse-βgal injected into the hippocampus showed presence of the enzyme βgal in projections consistent with anterograde transport, evidence of diffusion as indicated by enzyme activity in the surrounding cortex without mRNA presence, as well as enzyme activity in the leptomeninges and perivascular space indicative of CSF flow dissemination. A resulting correction of storage material was associated with all regions positive for enzyme. This study also exhibited anterograde and retrograde transport of mRNA as determined by *in situ* hybridization in the contralateral hippocampus and along the perforant pathway, respectively (167).

Targeting of the Central Nervous System in LSDs

Advances in targeting the CNS for treatment in LSDs have occurred through the injection of highly connected structures in the brain and development of new AAV capsids. A variety of novel AAV serotypes have been discovered whose tropisms provide gene therapy with many options for brain targeting (168-171). In a study utilizing MPS VII mice, AAV9-hGUSB injected into the striatum, hippocampus and ventral tegmental area (VTA) resulted in widespread distribution of vector mRNA and enzyme distal to the injection site which followed known projection sites specific to those targets. This work also presented

variable distribution patterns from AAV1, 9 and rh10 injected into the VTA. In

addition, AAV9-CY3 vector provided evidence of viral presence in neurons at 1

and 24 hrs post injection indicating distribution by fast axonal transport (170).

Further work by this group evaluated 17 additional serotypes in neonatal brains,

and further studied 6 of these in adult mice based on ability to transduce brain

tissues after lateral ventricular injection (169). In this study, AAV-GFP injections

into adult mouse cortex, striatum, hippocampus and thalamus indicated that rh8,

hu48R3, hu11, pi2, hu37, and hu32 all transduced more brain volume and cells

than AAV9. However, all but hu37 and hu48R3 were in distal sites with known

projections indicating axonal transport. Overall, AAVs appear to trend toward

neuronal transduction, and all but hu37 also transduced astrocytes and

oligodendrocytes which can be important in additional CNS diseases specifically

those involving demyelination (169). The Bankiewicz group continued to

investigate axonal transport in the primate brain with AAV2-glial-derived

neurotrophic factor (GDNF) and also with non-secreted AAV2-GFP injected into

the thalamus, where both provided delivery to the neurons of the cerebral cortex,

a known destination for efferent projections and indicative of anterograde

transport (172). In further studies, this group also examined AAV2 or AAV6-GFP

in the thalamus or striatum of rat brain, where thalamic injection resulted in GFP

positive cells in the striatum with AAV2, but not AAV6, indicating a lack of

anterograde transport with this capsid (171). Conversely, striatal injection of

AAV6 provided GFP expression in the cortex, thalamus and substantia nigra pars

compacta, but not substantia nigra pars reticulata which receives projections from the striatum. However, GFP positive fibers were found within the substantia nigra pars reticulata indicating the transduction of GABAergic neurons. This work implies a bias of AAV6 towards retrograde transport in the areas examined and demonstrates that the direction of axonal transport is serotype dependent (171). Recently, a study comparing the transport of AAV1, 8 and 9 in rat cultured cortical neurons and *in vivo* showed that conserved anterograde and retrograde axonal transport mechanisms existed in all three serotypes, and that increasing vector uptake by an increase in receptor availability lead to greater axonal transport (173). Additional studies focused on targeting the cerebellum were performed in mouse model of the LSD Niemann-Pick type A where the loss of Purkinje cells is a major phenotype (174). This work investigated AAV's 1, 2, 5, 7, and 8 encoding human acid sphingomyelinase (ASM) with bilateral injections into the deep cerebellar nuclei (DCN), a known projection site for Purkinje cells and highly connected to the brain stem and spinal cord. Results suggest AAV1 and 8 to be most widespread in the transduced area, where amount of enzyme expression and clearance of storage material appeared throughout cerebellum and surprisingly provided a reduction in storage in the cerebrum however without overt enzyme presence. Cell type transduction also varied, with AAV1 and 5 mainly transducing Purkinje cells, AAV2 in granular neurons, and AAV7 and 8 mostly in the molecular layer (174).

Potential Limitations to CNS Centric Approaches for LSD's

Considerable progress has been made in treatment of lysosomal storage diseases with central nervous system involvement. However, while CNS directed therapy mitigates the primary cause of mortality, additional phenotypes from peripheral involvement become more prominent. Successful treatment of the CNS was achieved in a mouse model of the LDS GM2 gangliosidosis, also known as Sandhoff disease (175). This study utilized AAV1-hexα and AAV1-hexβ plus 20% wt/vol mannitol with bilateral injections into striatum and DCN which resulted in unprecedented survival. Interestingly, despite successful correction of storage material throughout most of the CNS, many of these animals eventually succumbed to unanticipated peripheral organs disease, such as the urinary bladder and/or colon which was attributed to autonomic neuropathy (175).

Ex-vivo Lentiviral Modification Approaches for LSD's

Ex-vivo lentiviral (LV) mediated genetic modification of autologous hematopoietic stem and progenitor cells (HSC/HSPC) can be a useful technique to treat lysosomal storage disorders; however this method also faces some challenges. The treatment of LSD in the CNS has been shown to be extremely effective as it was revealed that donor HSPC's will enter the CNS, differentiate into microglia and engraft into the brain; a process that is enhanced by exploiting

intrinsic properties of these cells to migrate to the site of neuronal damage (176).

A study investigating the LSD metachromatic leukodystrophy (MLD) utilized

either modified purified donor HSPC's from mutated arylsulfatase A mice (As2$^{-/-}$

MLD) transduced with a lentiviral vector (LV) encoding the missing arylsulfatase

A (ARSA) enzyme, or non-modified HSPC's from wild type (WT) mice.

Transplanting mice with LV modified HSPC's, but not WT HSC's, resulted in

repopulation of CNS and PNS microglia and macrophages respectively, as well

as restored enzyme activity leading to resolution of storage material, and

provided almost total protection from demyelination where motor, learning and

coordination functions were retained. These results indicate cross correction

resulting from higher levels of enzyme from LV donor cells is necessary to

achieve therapeutic benefit in this model. Trepidation regarding this therapy is

from the possibility of insertional mutagenesis (177). Visigalli *et al* used LV

HSPC transplantation in the adult LSD MPS I mouse (178). This study

demonstrated a dose dependent correlation to therapeutic outcome, with ~100

fold > WT expression of enzyme activity from circulating hematopoietic cells

necessary to attain absolute resolution of disease. Most notably, this was the

first report showing correction of neurological and skeletal abnormalities in this

model. They also revealed that this supranormal level of expression had no

negative impact on the functionality of HSPC's *in vivo*, and that considerably

lower LV copy number (1 vs 5 on average) may be required for similar

expression in human HSPC's where the phosphoglycerate kinase promoter in

the transgene is more effective (178).   In some systems however, overexpression of an enzyme can have toxic implications as identified in the mouse model for the LSD Globoid cell leukodystrophy (GLD or Krabbe disease) where cultured GALC $^{-/-}$ mouse cells transfected with LV galactocerebrosidase (GALC), but not with LV GFP resulted in apoptosis, and LV GALC HSPC transplanted GALC $^{-/-}$ mice failed to engraft and had a severely reduced life span (179). An elegant solution to this issue was provided by the discovery that microRNA-126 (miR-126) was enriched in HSPC's, but severely decreased in differentiated hematopoietic cells. To this end, a microRNA de-targeting sequence (miRT) was added into the transgene and effectively regulated expression only to differentiated cells. Indeed, when applied to newborn GALC$^{-/-}$ mouse, the LV GALC-miRT-126 transplanted HSPC's led to increased enzyme activity in brain and liver, diminished storage and neuroinflammation, protection from peripheral demyelination and overall phenotypic improvement and survival (179). Another potential limitation in the treatment of some LSD's is the rapid progression of symptoms that may exceed the ability for efficient transgene expression through HSC therapy. For effective enzyme expression utilizing HSC's, enzyme deficient brain microglia must be replaced by LV modified HSC progeny, which can be a lengthy process. However, utilizing direct AAV brain parenchymal injections can reduce the time for therapeutic onset with expression ensuing in 3 weeks or less (180).

Systemic Administration of AAV Vectors for the CNS

Advent of new AAV vectors capable of targeting the brain after systemic delivery provides a therapeutic approach that may bridge the gap between direct CNS and peripheral treatment modalities. Successful demonstration of an IV approach resulting in AAV delivered transgene expression in the brain was shown with scAAV9-GFP injection into the facial vein of day 1 C57BL/6 mice or the tail vein of adult mice (181). This study established a tropism for transgene expression in the lower motor neurons (LMN) of the spinal cord, and pyramidal and Purkinje neurons in the brain from neonatal injections. However, a considerable reduction of LMN targeting from adult injections indicating restricted access to these cells in the post-developmental period. In contrast, adult injections led to mainly astrocyte transduction which were previously inaccessible utilizing parenchymal administration (181). Additional systemically delivered AAV serotypes were identified by injection into P1 neonates with scAAV-GFP into the superficial temporal vein (182). This study characterized AAVrh.10 > rh.39 > rh.43 as serotypes with similar or enhanced AAV transduction as compared to AAV9 in the brain, and AAVrh.43 > rh.39 > rh.10 in the spinal cord with gray and white matter GFP expression. Transduction of lateral, 3rd, and 4th ventricles, specifically in choroid plexus cells, were greatest in AAVrh.39 > rh.10 > rh.43 > 7 and followed by 9, where a descending gradation of expression was evident as distance from the ventricles increased. Finally, it was determined that this intravascular delivery did not activate microglial cells at the 3 week post injection

time point as compared to PBS or non-injected controls indicating a lack of immune response to this approach (182). Another direct comparison of vectors was performed in adult C57BL/6 mice which gave a profile of vectors in descending order of transduction capacity using GFP in the brain and spinal cord: AAVrh8 = rh10 = 9 > 8 = 7 = hr.43 = rh.39 > 6.2 > 6 > 1 > 2 (183). Further providing a transition into human studies, NHP were injected with scAAV9-GFP into the saphenous vein at P1, 30, or 90, or into the thoracic cord at 3 years of age (184), and recently with scAAVrh.10-GFP into the saphenous vein in adult marmosets with or without detargeting sequences miR1 and miR122 3x for heart and muscle or liver detargeting, respectively (183). The AAV9 animals all resulted in GFP expression throughout the brain in a pattern similar to the mouse study, however with minimal neuronal cells and a predominance of microglia and astrocytes targeted at all ages of NHP's tested (184). Spinal cord analysis revealed efficient motor neuron transduction through the entire length of the tissue in P1-P90 animals, and in the 3 year old NHP a similar pattern of transduction, but also with a slight reduction (184). Peripheral organs affirmed previous work with expression evident in all skeletal muscles taken in P1-P90 samples, with a slight decrease, but discernible in the aged animal; liver, heart, adrenal medulla from P1 intestines and testis were also positive in P1-P90 to varying degrees and with lung, kidney and spleen showing few positive cells (184). AAVrh10-GFP led to GFP expression throughout the motor neurons in the entire spinal cord (183). The brain expression was more restricted to particular

nuclei such as ventral midbrain, substantial nigra, inferior olivary nucleus, lateral reticular nucleus and red nucleus (183). Excitingly, these results demonstrate that motor neurons in the spinal cord (174, 184), and glia in brain of NHP's (184) are accessible to transduction at all ages studied indicating a larger therapeutic window for IV treatment of disorders involving these cell types then previously believed (184).

The ability to deliver a therapeutically relevant gene was demonstrated in several studies. Vascular endothelial growth factor (VEGF) in a scAAV9 vector was delivered into neonatal and adult mice, produced expression in the brain, spinal cord and peripheral organs (liver and heart) and sustained expression through the end of the study, up to 5 months post injection (185). In the lower motor neuron disease Spinal Muscular Atrophy (SMA), mice receiving treatment at P1-P5 showed therapeutic benefit in lifespan, weight gain and correction of synaptic current from an injection of a the missing gene scAAV9-survival motor neuron 1 (SMN1) (186). In the LSD MPS IIIB adult mouse IV injection into the tail vein successfully extended survival from 8-12M to >22M (187). This approach normalized rotarod performance, prevented astrocytosis and neurodegeneration, transduced neurons, glia and endothelia expressing enzyme throughout the brain, heart and muscle at supranormal levels, while normalizing enzyme in liver, lung, and intestine, and in turn providing correction of lysosomal storage (187). Ruzo *et al* investigated the IV treatment of the LSD MPS IIIA with AAV9-sulfamidase (Sgsh) in adult mice (188). In this work enzyme was effective

at targeting the CNS, clearing storage and significantly extending lifespan. Once

again, high liver expression was seen, but was restricted to levels of 5-fold in

males and wild type levels in females (188). Together, these unprecedented

results hold much promise for diseases involving CNS, PNS and peripheral

organ pathology; however extremely high expression in certain tissues could

indicate a "sink" for which the enzyme accumulates. If the transgene product is

expressing at high levels in particular tissues and leads to decreased availability

to the target organs, a high total vector dosing may be required in order to obtain

therapeutic impact and could possibly lead to long term toxic effects. As

mentioned earlier, microRNA's are a promising tool to repress expression in non-

desired cell or organ groups. This idea was exploited by engineering miRNA sites

with perfect complementary to liver miRNA, miR-122 and/or heart and muscle

miR-1 into the 3' untranslated region of a nLacZ or GFP transgene packaged into

AAV9 (189). This study elegantly revealed that expression of a transgene can be

modulated with addition of 1 or 3x the miRNA sites corresponding to non-target

organs. Target transgene mRNA's were cleaved at expected sites when bound to

Argonaute proteins, and that this addition does not affect the endogenous

function of miRNA's or their target proteins within those tissues (189).

Additional Approaches and Considerations for CNS Gene Therapy

Targeting to a specific organ or cell type as a source of enzyme

production is another approach for CNS gene therapy. One method employed in

an MPS III model was to utilize a liver directed promoter within an AAV8 capsid using systemic delivery (190). In this work, IV injection of AAV8 containing a liver directed promoter produced wild type or greater levels of circulating enzyme in the serum, led to an uptake of enzyme through M6PR on the cell surface and resulted in 10% wild type levels in the brain and a significant extension of lifespan. However, this effect was male specific due to the phenomenon identified by Davidoff *et al* where testosterone in the male animals enhanced transduction of liver cells (191). This interesting gender dependent finding was also identified within CNS where athymic NU/NU nude and C57BL/6N mice were injected with AAV9 expressing firefly luciferase (Fluc) (192). In this study, Fluc expression as well as vector genomes were found to be present in greater amounts in female versus male mice. Taken together, these studies indicate that in the IV administration of AAV one must consider a possible liver 'sink' for vector in male mice that could increase the availability of vector in the other organs of female mice and result in differing transduction amounts between the sexes.

Genetic targeting of disease specific brain endothelium can create a localized hub to deliver therapeutic proteins to the brain. This approach was investigated by modification of AAV2 capsid at site 587 (a known receptor binding location) after independent 5x phage panning in both WT and two LSD mouse models MPS VII or LINCL (193). Epitopes identified by this screening were unique to each mouse model signifying distinctive coinciding alternations in the vasculature, and upon tail vein injection of modified capsids only those

specific peptides provided novel tropism to the corresponding model's brain microvascular. CNS therapeutic outcomes included pathological correction, enzyme expression, and storage resolution in multiple cell types. Prevention of a tremor phenotype was also noted, indicating cross correction from the transduced endothelia, and providing a viable alternative to intracranial injections for CNS affecting diseases in which the therapeutic gene involves secreted proteins (193). In a subsequent study, the modified AAV2- brain targeting peptides (AAV2-PFG) and AAV9 were compared by injections into the tail vein of adult MPS VII mice (194). Surprisingly, the AAV-PFG-β-glucuronidase (βGlu) vector, but not AAV9-βGlu provided enzyme to the brain, reversed storage in the CNS, corrected learning phenotypes, and extended survival. Upon further investigation, a novel accumulation of sialic acid in the brain vasculature was revealed in the MPS VII mice, which lead to decreased transduction by AAV9 (194). This finding is extremely noteworthy, as it is further demonstration that despite common traits, researchers must consider biochemical features unique to each disease that can affect therapeutic outcomes.

Gene therapy for GM1-gangliosidosis

Previous attempts at gene therapy based approaches for GM1-gangliosidosis utilized RV (46), HSV-AAV hybrid (195), adenoviral (AD) (196), and adeno-associated viral (AAV) (197-199) vectors.

Sano *et a*l used the RV murine stem cell virus to transduce donor derived bone marrow cells (BMC) with human-β-galactosidase-(βgal)-GFP and introduced by tail vein into lethally irritated, 3-4 week old βGal$^{-/-}$ acceptor mice (46). These modified BMCs were successfully engrafted and expressed enzyme in both the CNS and peripheral organs. Reduction in GM1 storage, cytokines, inflammatory markers, unfold protein response hallmarks, as well as a reduction in histological pathology was noted from 3-6 months post transplant. Correction from bone marrow transplant (BMT) cells were mostly focused on areas which typically undergo inflammatory response in this disease (and thus recruit microglia derived BMC's) such as the thalamus, brain stem, cerebellum and spinal cord (6, 46). Behavior was also significantly improved, but not normalized in rotarod and open field testing (46). Notably, not all mice responded similarly which may reflect the success of the integration of the provirus in BMC in favorable regions for transcriptional activity, or those BMC that had higher transduction efficiencies prior to transplantation (46).

Oehmig *et al* employed a hybrid HSV/AAV vector for the integration of human βgal gene, *GLB1 in vivo* in cells of either a GM1-ganglioside patient or glioblastoma cell line (195). Expression of βgal enzyme was successful in 80% of clones tested, and provided 2 fold upregulation of activity for up to 4 months. Integration of the gene into the AAVS1 site was achieved in 33% of clones (195).

Takaura *et al* applied an AD vector encoding mouse-βgal in neonatal mice 24-48 hrs after birth into the superficial temporal vein (196). Animals were

evaluated at 30 and 60 days post infection. Both the CNS and periphery

demonstrated varying enzyme expression and reduction in GM1-ganglioside

storage in half the animals tested. Enzyme expression was increased in most

tissues at 10-20% of wild type levels, but ranged from normalized to

supraphysiological in the liver, lung and heart. The authors attribute the

variability in storage reduction in the CNS to age of injection and the permeability

of the blood brain barrier (196).

AAV therapy has been applied in both neonatal (197) and adult mice (198)

as well as adult cats (200). Neonatal animals were treated with AAV1-mouse-β-

galactosidase by intracerebroventricular (ICV) injection in P0 mice (197). At 3

months post injection, enzymatic activity was significantly increased in all brain

regions at levels 7-65 fold over wild type controls, but had no effect on the liver.

Storage of GM1-ganglioside in treated animals was significantly decreased

versus untreated βgal$^{-/-}$ controls and was similar to wild type levels. Interestingly,

analysis of neutral and acidic lipid species revealed a reduction in cerebrosides

and sulfatides (implicated as myelin-enriched lipids) in untreated βgal$^{-/-}$ controls,

but these lipids were normalized in treated animals (197). In adult mice at 6-8

weeks of age, AAV1 was injected bilaterally into the thalamus or the thalamus

and DCN (198). In addition, in another set of animals AAV with a liver-specific

promoter was infused intravenously prior to intracranial injections in order to

prevent immune responses; however, no immune responses were observed in

any cohort. *In situ* hybridization on sections from thalamic alone injections

reveled AAV-transduced cells only in the dorsal and lateral thalamic nuclei and slightly in the ipsilateral cortex. Enzyme expression and ganglioside content were analyzed at 1 and 4 months as well as at the humane point (~9 months for untreated βgal$^{-/-}$ compared to 12 months in treated mice). All treatment groups resulted in a 10 fold increase in enzyme expression over βgal$^{+/-}$ mice in the cerebrum, brainstem and subcortical regions, however only the thalamic + DCN group was > 10 fold higher than βgal$^{+/-}$ in the cerebellum. In contrast, the spinal cord was up to ~80% of βgal$^{+/-}$ levels at 4 months and to ~35% at endpoint in thalamic alone, versus a consistent ~50% of βgal$^{+/-}$ levels in the thalamic + DCN grouping. Notably, GM1-ganglioside content was similar in reduction for all regions in all groups (30-90% of untreated βgal$^{-/-}$ levels) except cerebellum where thalamic + DCN provided additional reduction of ~90% versus thalamic alone of ~25%. Markers of inflammation were also investigated and were found in the same CNS areas that had persisting storage after treatment in βgal$^{-/-}$ mice. Survival for both groups were significantly increased to 45 weeks for thalamic only and > 52 weeks for thalamic + DCN. Behavioral tests of rotarod for balance and coordination and open field testing did not provide any improvement over untreated βgal$^{-/-}$ mice with the exception of the thalamic + DCN group improved in distance traveled at and rearing at 2.5 months.

McCurdy *et al* presented a study in a feline juvenile GM1-gangliosidosis model with AAV1 or AAVrh8 encoding feline β-galactosidase (fβgal) injected intracranially into both the thalamus and DCN (200). This work resulted in

enzyme expression from 1.1-4.1 fold normal levels throughout the brain, and 0.9-4.2 fold normal levels in the spinal cord with both capsids. GM1 content was significantly reduced throughout the brain, but remained above normal in 4/15 sections of the CNS analyzed including the cervical spinal cord. The development of seizures occurred in 50% of the animals studied long term, but was well controlled by medication. Most importantly, these animals had significant extension of life span and obtained re-establishment of breeding function which was unprecedented in this model (200).

Taken together, studies in this disease either suffered from lack of enzyme expression in the intended regions, or a non-significant reduction of storage. Often, the lack of therapeutic efficacy resulted in secondary pathology and/or eventual disease progression.

The following chapters will discuss the investigation of a gene therapy based treatment for GM1-gangliosdiosis in a βgal mouse model. In Chapter II, an intravenous approach using a rAAV9-mβgal vector led to enzyme activity in the CNS, unprecedented motor retention and survival of these animals. In Chapter III, an intracranial technique using rAAVrh8-mβgal vector provided significant extension of lifespan and motor function, but also resulted in abnormal findings. These unusual results were then investigated in both normal and diseased animals leading to a re-engineered vector which provided a therapeutic benefit while minimizing negative impact. Taken together, these studies are an important step in the development of a safe and effective gene therapy treatment

for GM1-gangliosidosis and, in turn, other lysosomal storage disorders affecting

the central nervous system.

CHAPTER II: Systemic AAV9 gene Transfer in Adult GM1-Gangliosidosis Mice Reduces Lysosomal Storage in CNS and Extends Lifespan

Introduction

GM1-gangliosidosis is an autosomal recessive disorder resulting from mutations in the *GLB1* gene encoding lysosomal acid β-galactosidase (βgal) (3). Mutations resulting in enzymatic deficiency lead to storage of a number of metabolites in the lysosomes. Namely, storage of GM1-ganglioside (GM1) and its asialo derivative GA1 occur primarily in the central nervous system (CNS) (201) while oligosaccharides and keratan sulfate accumulate in visceral organs (202). GM1-gangliosidosis occurs at a frequency of 1:100K-200K births and manifests at different ages: The infantile form is diagnosed in the first 6 months of life, the late-infantile/juvenile form manifests between 3 and 36 months of age, and the less common chronic/adult form has a wide range of onset from 3-30 years of age, and disease progression over 10-30 years (7). The age of onset is directly correlated with the residual activity of mutant enzymes nearly absent in infantile-associated mutations, and up to 9% of normal in the adult forms (7). In infantile patients the disease is characterized by rapid neurological decline, loss of voluntary motor control resulting in generalized paralysis, extreme emaciation, and death. Other organs and tissues are also affected as evidenced by the

characteristic hepatosplenomegaly and skeletal dysplasia. These clinical findings are either milder or absent in late-infantile and chronic forms of the disease where some residual enzyme activity is present. Currently there is no treatment for GM1-gangliosidosis.

A number of gene therapy approaches have been tested in animal models of GM1-gangliosidosis, including *in vivo* infusion of adenovirus (196), adeno-associated virus (AAV) vectors (197, 198, 200), and *ex vivo* modification of autologous bone marrow stem cells with retrovirus vectors (46). The feasibility of these strategies is based on the ability of genetically modified endogenous cells, *in vivo* or *ex vivo*, to overexpress and release large quantities of functional lysosomal enzymes into the extracellular milieu. This secretion of enzyme allows for its distribution throughout the body via the blood stream. In the CNS several mechanisms contribute to the distribution of lysosomal enzymes including the flow of cerebral spinal fluid and interstitial fluid, as well as axonal transport (165, 167, 196). Most cells in the body are capable of taking up functional lysosomal enzymes and target them correctly to lysosomes via mannose-6-phosphate receptors on the cell surface (85). This targeting mechanism is the basis for enzyme replacement therapies that are the current standard of care for a number of lysosomal storage diseases affecting visceral organs. This is accomplished by regular parenteral infusion of recombinant enzymes. CSF infusion of recombinant enzyme is in clinical development for LSDs with neurological features (ClinicalTrials.gov: NCT01510028; NCT02055118). Direct infusion of AAV

vectors into CSF or brain parenchyma has been the most effective *in vivo* gene delivery approach in animal models of GM1-gangliosidosis (197, 198, 200) and other lysosomal storage diseases with neurological features (97, 98, 100, 203, 204). The distribution of AAV vectors after intraparenchymal infusion is largely restricted to the injection site, although some AAV capsids also undergo axonal transport (168, 170, 171). One approach to achieve widespread distribution of enzymes throughout the CNS via axonal transport is to infuse AAV vectors into highly interconnected structures such as striatum (205, 206), deep cerebellar nuclei (174), ventral tegmental area (170) or thalamus (198). In mouse and cat models of GM1-gangliosidosis, the combination of bilateral thalamic and deep cerebellar injection of AAV vectors has proven exceptionally effective to correct lysosomal storage in the CNS (198, 200). The therapeutic effect of this gene therapy approach in GM1 cats is remarkable with nearly complete correction of neurological symptoms and dramatic extension in their lifespan with restored reproductive capacity (200). Despite several CNS gene therapy clinical trials showing that intraparenchymal infusion of AAV vectors is well tolerated, it is still an invasive delivery approach (207-209).

AAV9 vectors are capable of crossing the blood brain barrier (BBB) after intravascular delivery and achieve widespread transduction of neurons and glia in neonatal (181) and adult animals (181, 184). This property of CNS transduction after vascular delivery appears to be a property shared by other AAV capsids (182, 183). These new BBB-penetrating AAV vectors are attractive

platforms to address the multisystemic nature of most LSDs as they also transduce peripheral organs at high efficiency and thus have the potential to become whole body therapies with a single intravascular infusion. Systemic infusion of AAV9 vectors in adult mucopolysaccharidoses (MPS) IIIA (188) and IIIB (187) mice has proven highly effective in addressing lysosomal storage in the CNS and peripheral organs with resulting extension in lifespan. Interestingly in MPS VII mice it appears the biochemical alterations inherent to the disease compromise the therapeutic efficacy of AAV9 (194).

In the present study, we assessed the therapeutic efficacy of vascular administration of an AAV9 vector encoding mouse lysosomal beta-galactosidase in adult GM1-gangliosidosis mice. A single administration of this single stranded AAV vector was sufficient to achieve enzyme expression and reduction of GM1–ganglioside content throughout the CNS. Most notably behavioral function remained stable longer and the lifespan was significantly increased in all AAV-treated cohorts.

Materials & Methods

AAV vector design and production

The vector AAV-mβgal contains a two flanking AAV2 inverted terminal repeats, cytomegalovirus enhancer fused to a chicken beta-actin promoter/rabbit beta globin intron (210), cDNA of mouse lysosomal acid β-galactosidase, and an

SV40 poly A. Vector stock was produced by transient transfection of 293 cells and purified by CsCl gradient ultracentrifugation (UMass Medical School, Gene Therapy Center, Worcester, MA).

Animal procedures

GM1 gangliosidosis mice (51) were obtained from Dr. Kunihido Suzuki (Neuroscience Center, University of North Carolina, Chapel Hill, NC). In our studies, animals reach humane endpoint either when paralysis of any limb is present or if weight loss is >15% of highest weight achieved per animal. βGal$^{+/+}$, $^{+/-}$ and $^{-/-}$ mice were generated by breeding of male βGal$^{+/-}$ or $^{-/-}$ to female βGal$^{+/-}$. Six-week old mice were injected with 200 μl of AAV9-mβgal vector at 1x10^{11} or 3x10^{11} vg via the tail vein using a 27G insulin syringe (BD Biosciences, Franklin Lakes, NJ). At 3 months, 9 months, or human endpoint, animals were sacrificed by an overdose of ketamine/xylazine (Fort Dodge Animal Health, Fort Dodge, IA and Lloyd Laboratories, Inc, Shenandoah, IA), cleared by transcardiac perfusion with ice cold PBS, and harvested according to assay needs. One brain hemisphere and half a spinal cord was embedded in freezing medium, Neg 50 (Richard-Allan Scientific, Kalamazoo, MI) and quick frozen in a dry ice/2-methylbutane bath (ThermoFisher Scientific, Waltham, MA). The remaining brain hemisphere was separated into cerebrum, cerebellum, and brain stem, and, along with the second half of the spinal cord, frozen over dry ice and stored at -80°C. All other organs were frozen over dry ice or fixed in 4% paraformaldehyde

in PBS (Sigma-Aldrich, St. Louis, MO). All procedures were approved by the University of Massachusetts Medical School, Institutional Animal Care and Use Committee and performed in compliance with the NIH Guide for Care and Use of Laboratory Animals.

Histological analysis

Fresh frozen, sagittal oriented brains and spinal cords were cut in 20 µm sections on a cryostat (ThermoFisher Scientific, Waltham, MA) at -12/-13°C. βgal enzyme presence was determined by an Xgal assay as described previously(197). GM1 storage was detected by Filipin staining as described previously(197). All histological analysis was performed as non-blinded, qualitative analysis on an N ≥ 2-3 animals with representative pictures shown in figures.

βgal enzymatic assay

Tissues were homogenized and βgal activity (nmol/hr/mg protein) was determined by reaction 4-methylumbelliferyl (4-MU) assay with βgal substrate = 1mM 4-Methylumbelliferyl-β-D-galactoside (4-MUG) with 4-methylumberlliferyl-β-D-galactopyranoside in a 96-well plate format and normalized for protein content by Bradford assay (Bio-Rad, Waltham, MA) as described previously(197).

Genome copy number

Tissue sections were extracted in a DNA clean environment and rinsed in sterile PBS. DNA was isolated by Qiagan DNeasy Blood and Tissue Kit (Qiagen, Valencia, CA). QPCR was performed on 100-400 ng of genomic DNA using Taqman probes (Applied Biosystems, Foster City, CA), with standard curve containing a known quantity of reference DNA containing an SV40 poly A. Probe to SV40 (TaqMan Probe, 6FAM- AGC ATT TTT TTC ACT GCA TTC TAG TTG TGG TTT GTC -TAMRA). Samples with genome copies ≥ 100 vg/ µg of DNA were considered positive for vector genomes. Data was represented as vg/diploid genome considering that 100 ng of mouse genomic DNA corresponds to 36,263 diploid genomes.

GM1 ganglioside content

A liquid chromatography-tandem mass spectrometry (LC-MS/MS) assay (Weismann et al, in preparation) was used for quantification of GM1-ganglioside in CNS. Briefly, 0.01-0.04 mg/µL of tissue homogenate was diluted to 25 µL in buffer containing 0.2M sodium acetate and 0.1M NaCl (pH 4.3). To each sample 3 µg of d_3-labeled GM1 (Matreya, LLC, Pleasant Gap, PA) was added as an internal standard. Calibration curves were made neat with GM1 (Avanti Polar Lipids, Alabaster, AL) over the range of 200-3,000 ng and spiked with 3,000 ng of d_3-GM1. Total lipids were extracted by the Folch method[211] two successive times in chloroform/methanol (1:1), the supernatants combined, and the

glycolipids partitioned to aqueous phase by adjusting the composition to

chloroform/methanol/water (2:1:0.6). The upper aqueous phase was removed

and the lower phase was washed once with chloroform/methanol/water (3:48:47)

and the upper phases combined. Samples were dried, re-suspended in 0.2 mL

0.1M NaCl and applied to an equilibrated 1cc C18 reverse-phase Bond Elute

column (Agilent Technologies, Santa Clara, CA), washed with 5 mL water, eluted

with 0.6 mL CH_3OH followed by 1 mL $CHCl_3$:CH_3OH (1:1), dried, and re-

suspended in 100 µL solution of 1:4 (A:B) where A is 0.1% (v/v) formic acid and

B is methanol:2-propanol:0.1% formic acid (47.5:47.5:4.9). Gangliosides were

separated on a Phenomenex (Torrance, CA) 2.1 x 50mm Kinetex 1.7 µm (100Å)

C18 column using a Waters (Milford, MA) Acquity UPLC using a fast gradient

program (0-1 min, 80%B; 1-5 min, 80-100%B; 5-7 min 100%B; 7.1, 80%B) and

eluted to a Waters Quattro Premier XE triple quadrupole mass spectrometer

operating in the negative ion mode. Multiple reaction monitoring (MRM)

transitions for all GM1 and GM2 species were monitored using a cone voltage of

90V, a collision energy of 70V, and recorded the common sialic fragment anion

at m/z 290. The area of all the individual GM1 lipid species (16:0, 18:0, 18:1,

20:0, 20:1) were combined for each ganglioside and the ratios were calculated to

the corresponding d_3-18:0 GM1 internal standard. Calculated concentrations

were normalized to protein content by Bradford (Bio-Rad, Waltham, MA).

Behavioral assays

Rotarod testing was conducted on a Rotarod apparatus (Med Associates, St Albans, VT) accelerating from 4 to 40 rpm over 5 minutes and latency to falling recorded. Testing was conducted with one practice trial of 1 minute accelerating from 2 to 20 rpm at the beginning of the session followed by 3 trials with 15-20 minute resting in between. Latency to fall for each mouse in a testing session was recorded, and the longest time on the rotarod in any of the 3 trials was reported.

Inverted screen testing was performed on an apparatus created in conjunction with UMass Machine Shop (UMass Medical School, Shrewsbury, MA) and implemented as described previously (212). Briefly, animals were placed on a square wire mesh of $30cm^2$ with $25mm^2$ holes, over a cushioned surface. The screen was inverted slowly over a 2 second period, head over tail, until a 60° angle was reached and the screen then locked in place. Animals were assessed for latency to falling up to 2 minutes and number of hind leg movements occurring during this time. One practice trial and one testing run were administered to each mouse per time point with 15-20 minute resting periods between trials.

Home cage testing was performed in an isolation cubicle (Med-Associates, St Albans, VT), where mouse movement was tracked by video camera and processed by HomeCageScan software (CeleverSys, Reston, VA) as described previously (213). Briefly, one animal was placed into the isolation

cubicle in a clean cage identical to normal housing and containing food and water. The background area was subtracted in both light and dark conditions, and the animal's dimensions identified by the software. Data was taken regarding the animal's movement or inactivity and reported in seconds/behavior for a 26 hour time period then collated according to behaviors.

Results

The therapeutic efficacy of systemic AAV9-mβgal delivery was evaluated in βGal$^{-/-}$ mice infused with 1x10^{11} vector genomes (vg) (low dose cohort; N = 20), or 3x10^{11} vg (high dose cohort; N = 34) via the tail vein at 6 weeks of age (± 2 days). Controls included PBS-injected βGal$^{-/-}$ mice (N=19), and naïve age matched βGal$^{+/-}$ and βGal$^{+/+}$ mice (N=49) (Fig. 2.15c, d, Table 2.2). Untreated βGal$^{-/-}$ mice appear normal until approximately 20 weeks of age when gait abnormalities and tremors become apparent. Untreated βGal$^{-/-}$ mice reach the humane endpoint at approximately 37 weeks of age, defined by >15% loss from maximum body weight or paralysis of any limb. Animals were removed for histological and biochemical studies at 37 weeks of age to compare with untreated βGal$^{-/-}$ mice at the humane endpoint, and ultimately when AAV-treated mice reached the humane endpoint. Behavioral testing was performed at 10 and 30 weeks of age.

Partial restoration of βgal activity in CNS and overexpression in peripheral organs

Histochemical staining of brain sections revealed an increase in βgal activity throughout the brain of 37-week old βGal$^{-/-}$ males and females in the high-dose (HD) cohort (Fig. 2.1, first and second rows, respectively) compared to PBS-injected βGal$^{-/-}$ animals (Fig. 2.1, bottom row). Distribution of βgal activity appeared largely similar to that in control βGal$^{+/-}$ animals (Fig. 2.1, third row).

Biochemical quantification showed a significant increase in βgal activity throughout the central nervous system (CNS) of AAV-treated βGal$^{-/-}$ mice compared to age-matched PBS-injected βGal$^{-/-}$ mice (Fig. 2.2a, b). The relative βgal activity (% WT) in cerebrum, cerebellum, and brainstem of AAV-treated βGal$^{-/-}$ mice was dose dependent and ranged 6-25% in males and 7-90% in females (Table 2.1). The relative βgal activity in the spinal cord of AAV-treated βGal$^{-/-}$ males and females ranged between 29-135% and 30-516%, respectively (Table 2.1). As expected βgal activity was dramatically elevated in liver, heart, muscle, and serum of AAV treated βGal$^{-/-}$ male and female mice (Fig. 2.2a; Table 2.1). The relative βgal activity (% WT) in peripheral organs ranged between 140-11,841% in males, and 29-5,150% in females (Table 2.1).

The content of AAV vector genomes in CNS and peripheral organs was consistent with enzymatic findings, with the highest amount of vector genomes/diploid genome (vg/dg) found in liver (22-173 vg/dg) and the lowest in CNS (3.4-13.5x10^{-3} vg/dg) (Fig. 2.3).
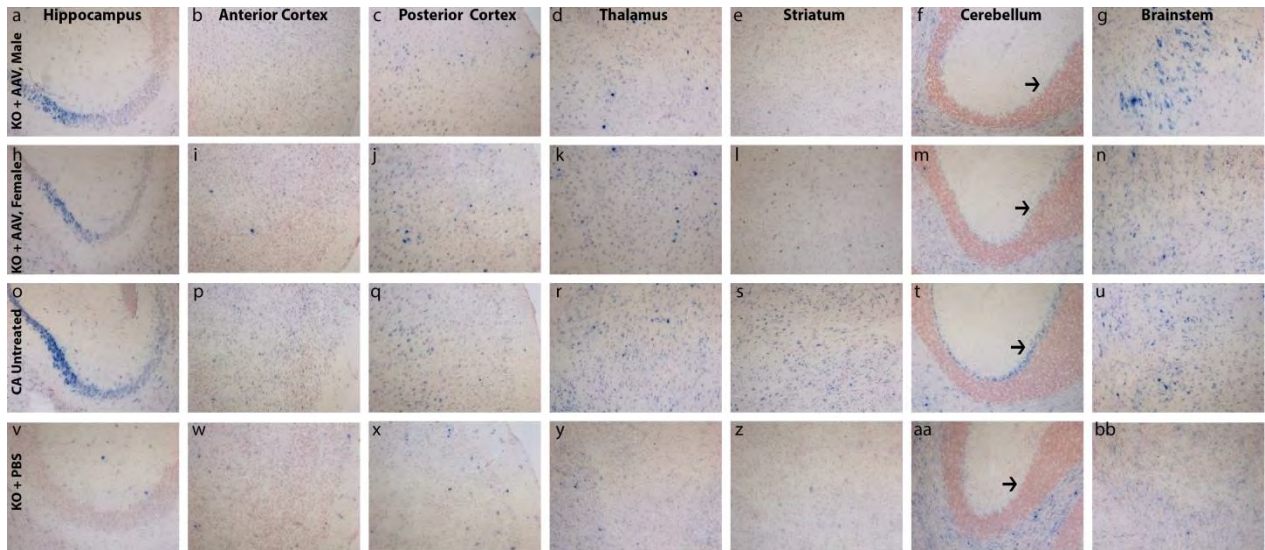
Figure 2.1 βgal enzyme expression and activity by Xgal in βGal$^{+/-}$, βGal$^{-/-}$ + PBS and βGal$^{-/-}$ + AAV 3e11vg treated mice

Xgal staining (blue) for βgal enzyme presence and counterstained with Nuclear Fast Red (red) at 37 weeks throughout the brain in a representative βGal$^{-/-}$ + AAV 3x10^{11} vg treated male (a-g) and female (h-n) (KO + AAV), untreated βGal$^{+/-}$ (CA Untreated, o-u), and βGal$^{-/-}$ mouse with mock treatment of phosphate buffered saline (PBS) (KO + PBS, v-bb). N = 3 per group.

β-galactosidase activity (range of %WT)				
	Male		**Female**	
Tissue	3e11vg	1e11vg	3e11vg	1e11vg
Cerebrum	7.9 - 23.6%	6.3 - 16.9%	14.4 - 37.3%	6.9 - 17.4%
Cerebellum	9.2 - 22.0%	9.1 - 11.0%	19.3 - 26.7%	11.2 - 13.2%
Brainstem	21.2 - 25.4%	9.2 - 10.4%	15.1 - 90.3%	7.4 - 26.7%
Spinal Cord	49.3 - 135%	29.1 - 41.9%	98.4 - 516%	30.2 - 131%
Serum	140 - 2,811%	1,529 - 2,399%	28.9 - 54.5%	43.1 - 121%
Liver	868 - 6,015%	4,501 - 11,841%	228 - 542%	128 - 1052%
Heart	2,397 - 6,486%	560 - 828%	1,434 - 3,583%	350 - 5,130%
Muscle	498 - 5,296%	226 - 358%	1,002 - 1,192%	129 - 1,347%

Table 2.1 β-galactosidase activity in CNS and peripheral tissues
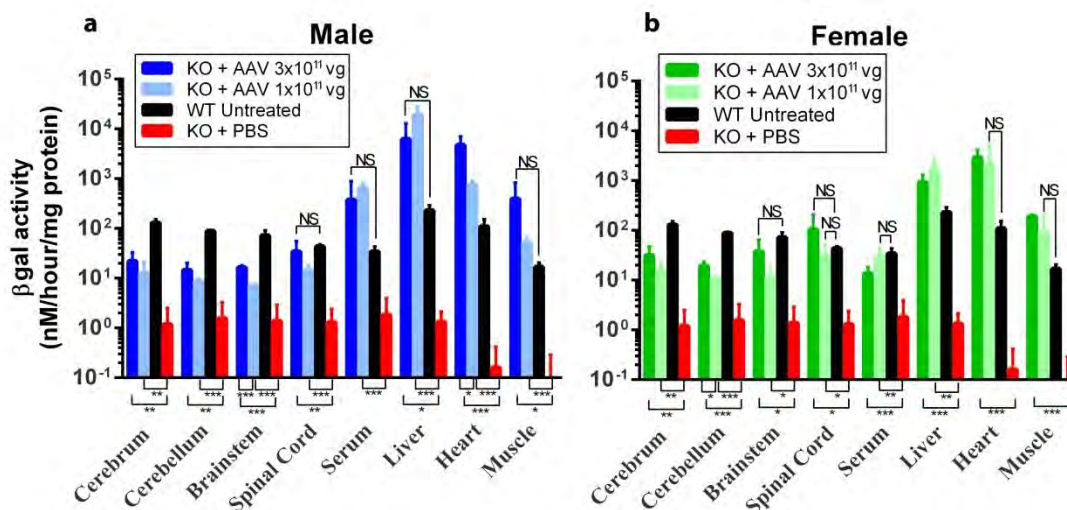
Figure 2.2 βgal enzyme activity in WT, βGal$^{-/-}$ + PBS and βGal$^{-/-}$ + AAV treated mice

(**a & b**) Enzyme activity in selected tissues determined by 4-MU assay at 37 weeks of age in (**a**) male or (**b**) female mice. Enzyme activity is normalized to protein concentration by Bradford, and is reported as nmol/hour/mg protein. Error bars represent mean + SD, N ≥ 3/group, and significance was determined by unpaired multiple T tests where * = $p < 0.05$, ** = $p < 0.01$, and *** = $p < 0.001$. In βGal$^{+/+}$ (WT) untreated or βGal$^{-/-}$ + PBS mice, both males & females are represented as no difference in enzyme activity between the sexes was observed in the untreated or mock-treated animals. NS = no significant difference.
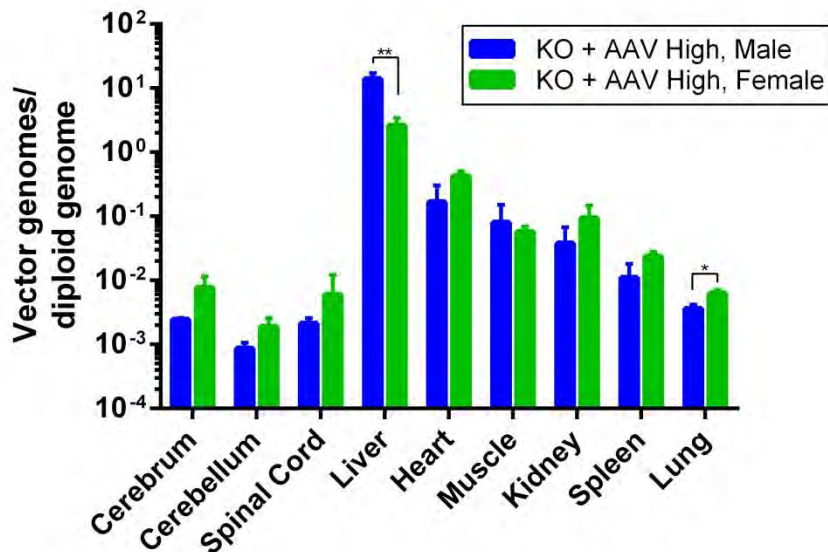
Figure 2.3 Viral induced transgene presence in tissues of βGal$^{-/-}$ + AAV 3e11vg treated mice

Vector amount was quantified per diploid genome in selected tissues for βGal$^{-/-}$ + AAV 3×10^{11} vg male and female mice as determined by qPCR to the SV40 poly A on the transgene. Samples were taken at 20 weeks of age. Error bars represent mean + SD, N ≥ 3/group, and significant difference of βGal$^{-/-}$ + AAV male vs. female was determined using unpaired multiple T tests where * = p < 0.05, ** = p < 0.01.

Reduction of GM1 ganglioside content and reduction in astrogliosis throughout CNS

In βGal$^{-/-}$ mice and humans with GM1 gangliosidosis, reduced βgal activity results in accumulation of GM1 ganglioside (GM1) in the CNS. Previously we have shown that filipin can be used to detect lysosomal storage in the brain of βGal$^{-/-}$ mice where it appears as bright perinuclear puncta (197). This histological marker correlates with GM1 ganglioside storage as AAV-mediated βgal delivery to the βGal$^{-/-}$ mouse brain corrects the neurochemistry and eliminates filipin staining (197). Recent work has shown that filipin binds cholesterol and GM1 (214). Filipin staining of βGal $^{+/-}$/βGal $^{+/+}$ brains does not reveal any defined cellular structures most likely due to the normal membrane localization of GM1 (197) (data not shown). Filipin staining of brain sections from males and female in the HD cohort at 37 weeks (Fig. 2.4 top and middle rows) revealed partial correction of lysosomal storage in most brain regions (Fig. 2.4, bottom row). The impact on lysosomal storage appeared to be modest in thalamus, striatum, and granule/Purkinje cell layers in the cerebellum. Interestingly we observed complete clearance of storage in deep cerebellar nuclei (DCN) (Fig. 2.4, top row and middle row thin and thick arrows respectively). The reduction in lysosomal storage material in the brain appeared to be more pronounced in female than in male mice (Fig. 2.4, top and middle row). Similarly, in spinal cord, there was a dramatic reduction in storage in HD cohort females (Fig. 2.5, third row), but variable response in males (Fig. 2.5, top two rows). The impact on lysosomal
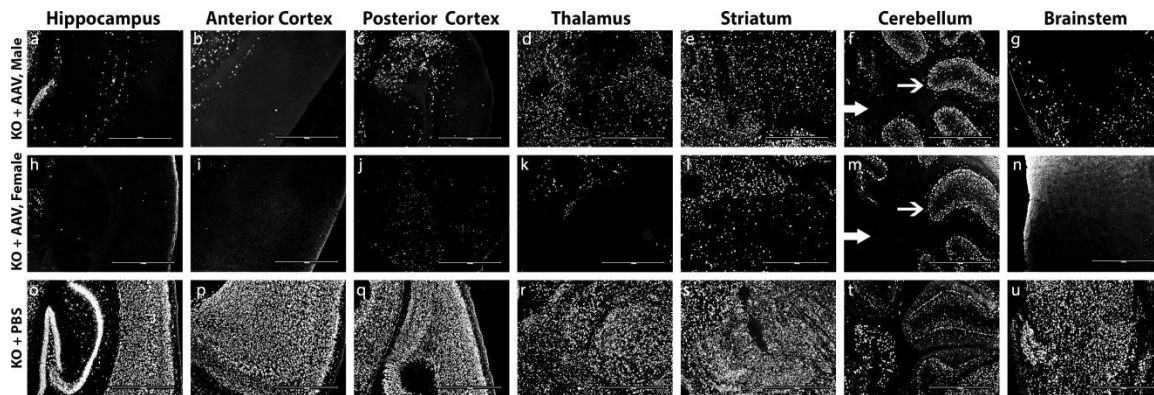
Figure 2.4 GM1 presence in the brain of βGal$^{-/-}$ + PBS and βGal$^{-/-}$ + AAV 3e11vg treated mice.

Filipin staining of selected brain regions in a representative βGal$^{-/-}$ + AAV 3×10^{11} vg treated male (a-g), female (h-n) (KO + AAV), and a βGal$^{-/-}$ + PBS (o-u, KO + PBS) mouse at 37 weeks of age. N = 3 per group. Scale bar =100 mm. Thick arrows indicate the DCN, thin arrows indicate the molecular and purkinje layers.
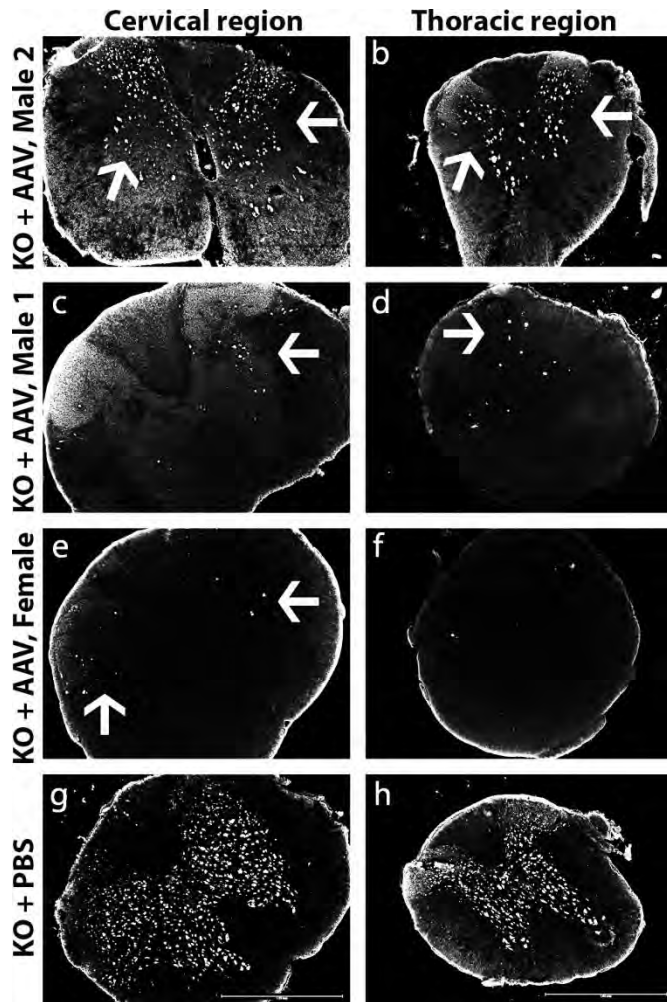
Figure 2.5 GM1 presence in the spinal cord of βGal$^{-/-}$ + PBS and βGal$^{-/-}$ + AAV 3e11vg treated mice

Filipin staining of cervical and thoracic region of spinal cord in 37 weeks old mice. Representative βGal$^{-/-}$ + AAV 3x10^{11} vg treated male (a-d), female (d-f) (KO + AAV), and a βGal$^{-/-}$ + PBS (g-h, KO + PBS) mouse. Arrows indicate areas of remaining storage. N = 3 per group. Scale bar =100 mm.
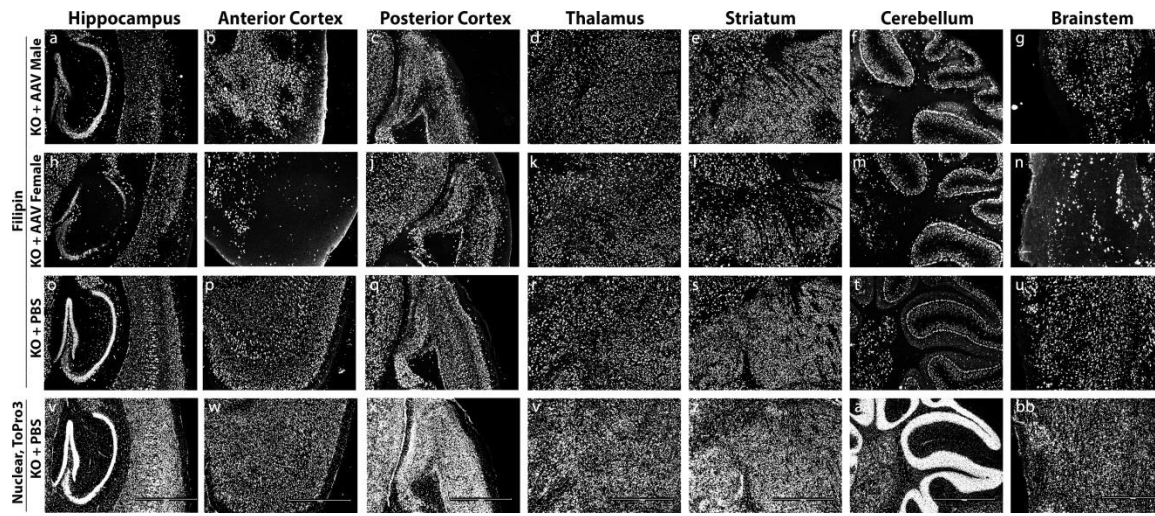
Figure 2.6 GM1 presence in the brain of βGal$^{-/-}$ + PBS and βGal$^{-/-}$ + AAV 1e11vg treated mice

Filipin staining of selected brain regions in a representative βGal$^{-/-}$ + AAV 1x10^{11} vg treated male (a-g), female (h-n) (KO + AAV), and a βGal$^{-/-}$ + PBS (o-u, KO + PBS) mouse at 37 weeks of age. ToPro3 staining for nuclear presence in βGal$^{-/-}$ + PBS (v-bb, KO + PBS) mouse. N = 3 per group. Scale bar =100 mm
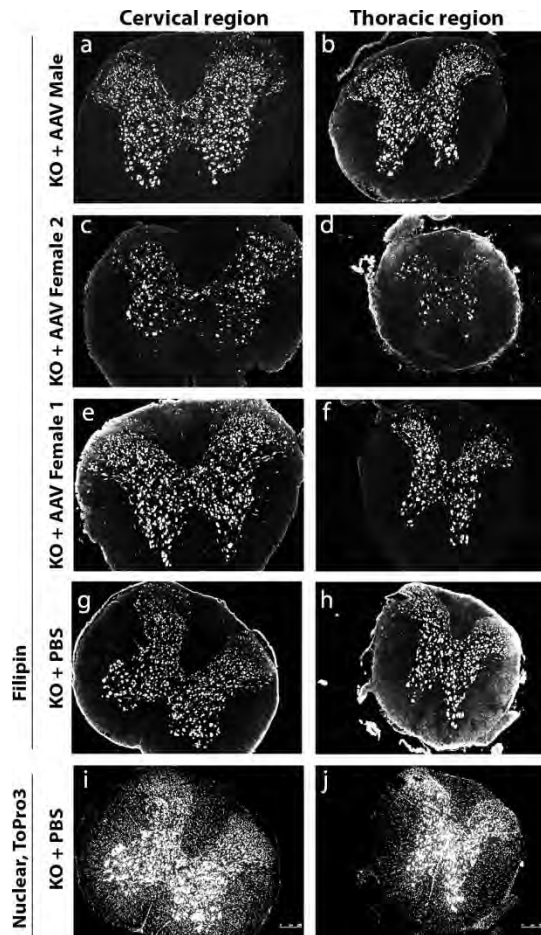
Figure 2.7 GM1 presence in the spinal cord of βGal$^{-/-}$ + PBS and βGal$^{-/-}$ + 1e11vg AAV treated mice

Filipin staining of cervical and thoracic region of spinal cord in 37 weeks old mice. Representative βGal$^{-/-}$ + AAV 1x10^{11} vg treated male (a-b), female (c-f) (KO + AAV), and a βGal$^{-/-}$ + PBS (g-h, KO + PBS) mouse. ToPro3 staining for nuclear presence in βGal$^{-/-}$ + PBS (i-j, KO + PBS) mouse. N = 3/group. Scale bar = 100 mm.
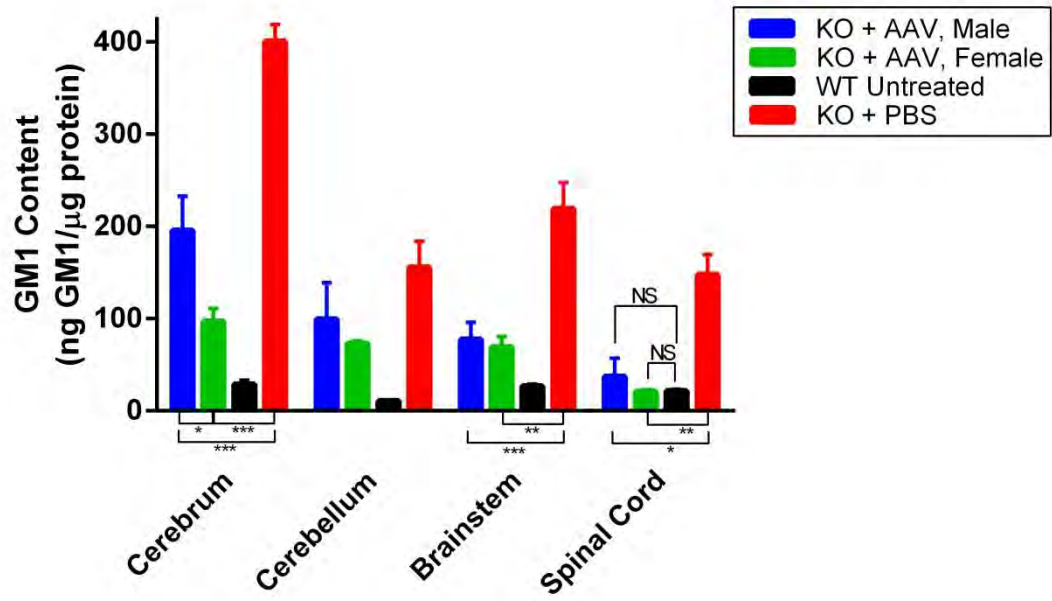
Figure 2.8 GM1 content in the CNS of WT, βGal$^{-/-}$ +PBS and βGal$^{-/-}$ + 3e11vg AAV treated mice

Figure 2.8 GM1 content in the CNS of WT, βGal$^{-/-}$ +PBS and βGal$^{-/-}$ + 3e11vg AAV mice

GM1 content quantitated by liquid chromatography tandem mass spectrometry in CNS tissues. βGal$^{-/-}$ + AAV from $3x10^{11}$ vg treated males and females (KO + AAV) at 37 weeks. βGal$^{+/+}$ (WT Untreated) or βGal$^{-/-}$ + PBS (KO + PBS) mice include both males and females as no sex difference in GM1 content was observed in the untreated or mock-treated animals. GM1 content was determined by ratio of d$_3$-GM1 internal standard to total GM1 content, normalized to protein concentration by Bradford, and represented as ng GM1/μg protein. Error bars represent mean + SD, N ≥ 3/group (except βGal$^{-/-}$ + AAV, female, N = 2). Significant difference of βGal$^{-/-}$ + AAV vs. KO + PBS, or βGal$^{-/-}$ + AAV males vs. females was determined using unpaired T tests where * = $p < 0.05$, ** = $p < 0.01$, and *** = $p < 0.001$. NS indicates no significant difference between βGal$^{-/-}$ + AAV vs. βGal$^{+/+}$ untreated.

storage in CNS was considerably smaller in the low dose (LD) cohort (1×10^{11} vg) (Figs. 2.6 & 2.7). Measurement of GM1 content in different CNS regions of male and female mice in the HD cohort by liquid chromatography-tandem mass spectrometry (LC MS/MS) (Fig. 2.8) showed significant reductions in the cerebrum (51 and 76%, respectively), brainstem (64 and 68%, respectively), and spinal cord (75 and 86%, respectively) compared to PBS-injected controls at 37 weeks of age. Interestingly, the impact of AAV9 treatment on GM1 content in cerebrum is significantly different between male and females ($p = 0.04$, Fig. 2.8). The GM1 content in cerebellum was not significantly changed by AAV9 treatment.

Astrogliosis was apparent throughout the CNS of PBS-treated βGal^{-/-} controls (Figs. 2.9 & 2.10, bottom rows), as described previously in these GM1 gangliosidosis mice (6). High dose AAV treatment resulted in marked reduction across the cerebrum (Fig. 2.9, first and second rows), but reactive astrocytes remained in some brain structures such as striatum, especially in males (Fig. 2.9, top row). In contrast, the spinal cords of AAV-treated animals of both genders were comparable to that of normal controls (Fig. 2.10).

Dose and gender dependent behavioral performance

A number of tests were carried out at 10 and 30 weeks of age to assess motor performance and behavior over time. In the rotarod test, 30 week-old AAV9-treated mice performed significantly better than age-matched PBS-treated
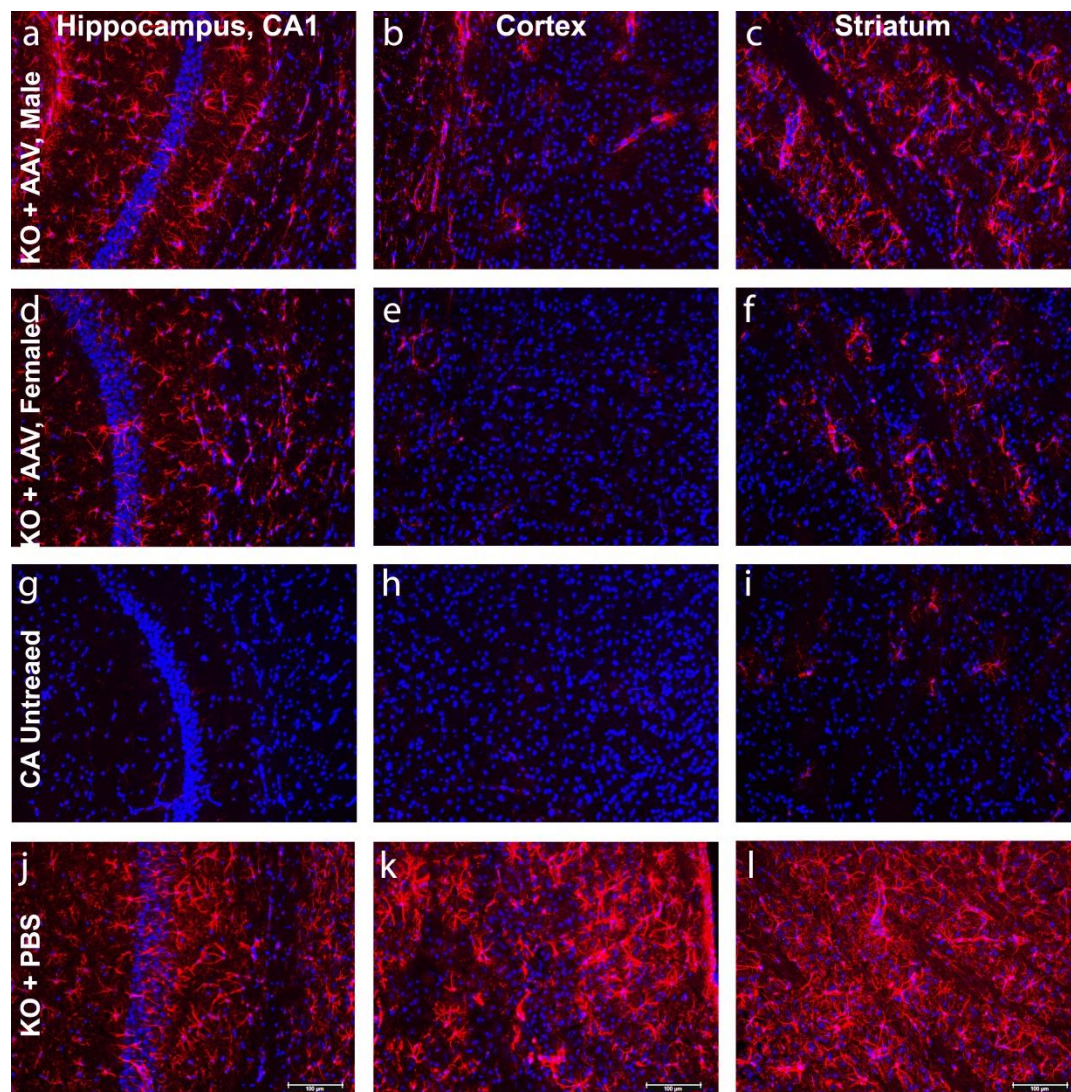
Figure 2.9 Astrogliosis in the brain of βGal⁺/⁻, βGal⁻/⁻ + PBS and βGal⁻/⁻ + AAV 3e11vg treated mice

GFAP staining in the hippocampal, CA1 region, cortex and striatum in a representative $\beta Gal^{-/-}$ + AAV 3×10^{11} vg treated male (a-c), female (d-f) (KO + AAV), an untreated $\beta Gal^{+/-}$ (g-I, CA Untreated) and a $\beta Gal^{-/-}$ + PBS (j-l, KO + PBS) mice at 37 weeks of age. N = 3/group. Scale bar = 100μm.
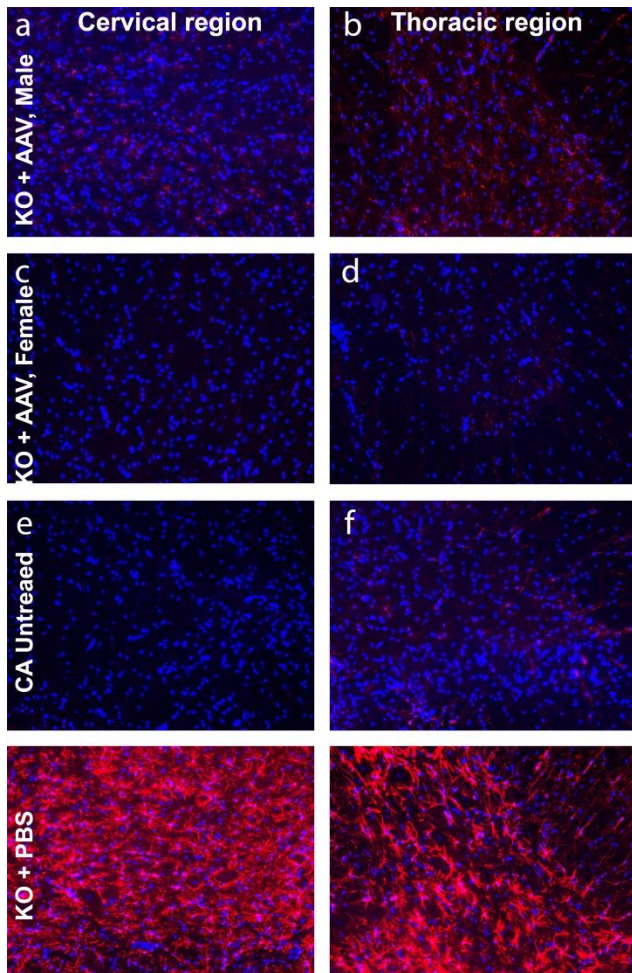
Figure 2.10 Astrogliosis in the spinal cord of βGal$^{+/-}$, βGal$^{-/-}$ + PBS and

βGal$^{-/-}$ + 3e11vg AAV treated mice

GFAP staining of cervical and thoracic region of spinal cord in 37 weeks old mice. Representative βGal$^{-/-}$ + AAV 3x10^{11} vg treated male (a-b), female (c-d) (KO + AAV), an untreated βGal$^{+/-}$ mouse (e-f, CA Untreated), and a βGal$^{-/-}$ + PBS (g-h, KO + PBS) mouse. N = 3/group.
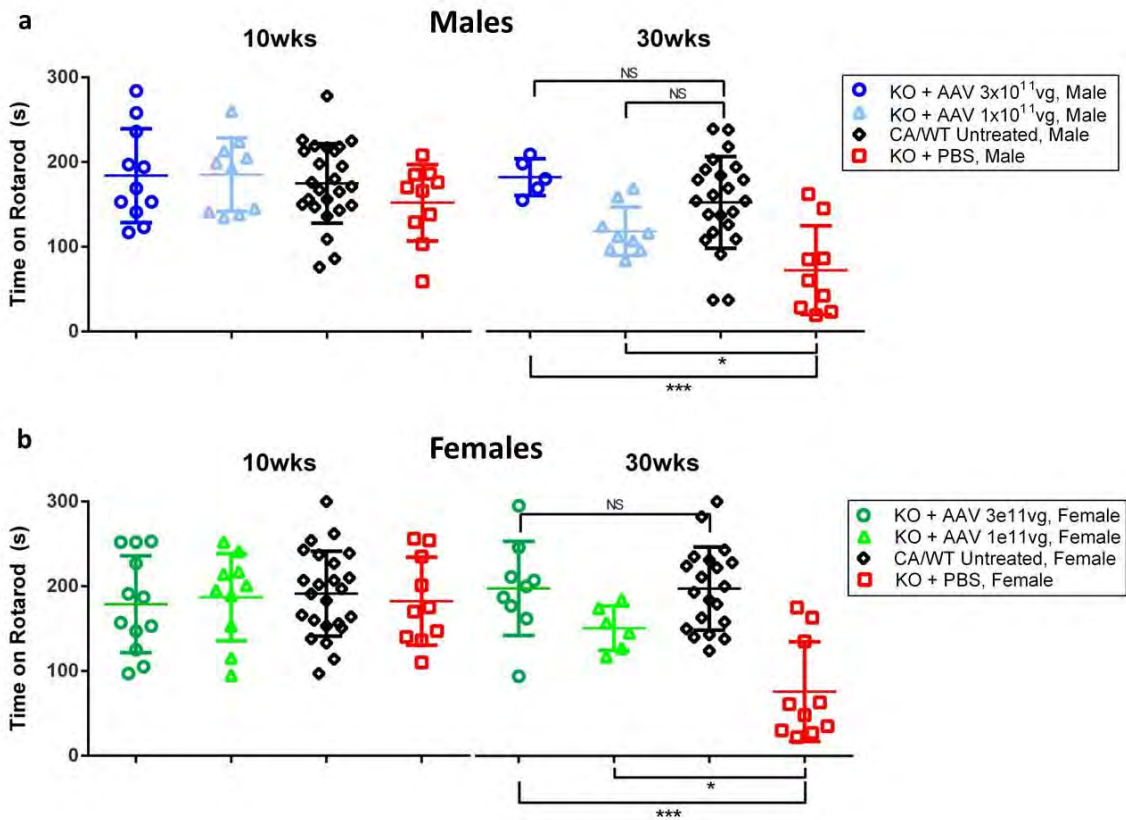
Figure 2.11 Rotoard performance of WT/βGal$^{+/-}$, βGal$^{-/-}$ + PBS and βGal$^{-/-}$ +

AAV treated mice

Figure 2.11 Rotoard performance of WT/βGal$^{+/-}$, βGal$^{-/-}$ + PBS and βGal$^{-/-}$ +

AAV treated mice

Rotarod testing of βGal$^{-/-}$ + AAV, 1x10^{11} and 3x10^{11} vg (KO + AAV) treated males

(a) or females (b). Untreated βGal$^{+/-}$, and βGal$^{-/-}$ (WT/CA Untreated), mock

treated βGal$^{-/-}$ + PBS (KO + PBS). Rotarod testing was performed on a 4-40 rpm

accelerating rotarod over 300 seconds at both 10 and 30 weeks of age. Highest

score of 3 trials reported. Symbols indicate performance of one animal, error

bars represent mean + SD, N=5-25 animals/group. * indicates significant

difference of βGal$^{-/-}$ + AAV vs. βGal$^{-/-}$ + PBS, or βGal$^{-/-}$ + AAV, 1x10^{11} vs.

3x10^{11}vg using unpaired T tests where * = p < 0.05, ** = p < 0.01, and *** = p <

0.001. NS indicates no significant difference between βGal$^{-/-}$ + AAV vs. βGal$^{+/+}$

untreated or 1x10^{11} vs. 3x10^{11}vg βGal$^{-/-}$ + AAV.

Figure 2.12 Inverted screen testing performance of WT/βGal$^{+/-}$, βGal$^{-/-}$ + PBS and βGal$^{-/-}$ + AAV treated mice

Figure 2.12 Inverted screen testing performance of WT/βGal$^{+/-}$, βGal$^{-/-}$ + PBS and βGal$^{-/-}$ + AAV treated mice

Inverted screen testing of βGal$^{-/-}$ + AAV, 1×10^{11} and 3×10^{11} vg (KO + AAV) treated males (a, c) or females (b, d). Untreated βGal$^{+/-}$, and βGal$^{-/-}$ (WT/CA Untreated), mock treated βGal$^{-/-}$ + PBS (KO + PBS). Inverted screen testing is shown as (a & b) percentage of time on screen up to 2 minutes and (c & d) number of hind leg movements during this time. The second score of two trials is reported. Symbols indicate performance of one animal, error bars represent mean + SD, N=5-25 animals/group. * indicates significant difference of βGal$^{-/-}$ + AAV vs. βGal$^{-/-}$ + PBS, or βGal$^{-/-}$ + AAV, 1×10^{11} vs. 3×10^{11}vg using unpaired T tests where * = $p < 0.05$, ** = $p < 0.01$, and *** = $p < 0.001$. NS indicates no significant difference between βGal$^{-/-}$ + AAV vs. βGal$^{+/+}$ untreated or 1×10^{11} vs. 3×10^{11}vg βGal$^{-/-}$ + AAV.

controls and were comparable to normal controls (βGal $^{+/-}$/βGal $^{+/+}$) except

females in the LD cohort (Fig. 2.11a, b). In the inverted screen test, AAV9-

treated females in the HD cohort, but not the LD cohort, scored significantly

better in both time on screen and number of hind limb movements than PBS-

treated females at 30 weeks of age (Fig. 2.12a, b). In contrast, only males in the

LD cohort performed better than PBS-treated males in percentage of time on

screen at 30 weeks of age (Fig. 2.12a).

Home cage testing captures a large number of behaviors of an animal in a

familiar environment and can identify phenotypic alterations not detectable by

traditional motor function testing (213). Animals were evaluated over a 24 hr

period that spans the 12 hr light cycle when animals are less active (Fig. 2.13a,

b, left graphs), and the 12 hr dark cycle when animals are most active (Fig.

2.13a, b right graphs). AAV-treated males in HD and LD cohorts performed

significantly better than PBS-treated males in vertical reaching in both periods

(Fig. 2.13a) and in exploratory behavior during the day (Fig. 2.13a, left side).

However, only the HD males performed significantly better than PBS controls in

exploratory behavior during the night (Fig. 2.13a, right side). Females in HD and

LD cohorts performed significantly better than PBS-treated females in daytime

vertical movements and exploratory behavior (Fig. 2.13b, left side), however only

females in the HD cohort retained significantly better performance than PBS-

treated controls in these measured behaviors during the nighttime (Fig. 2.13b,

right side). Females in the HD cohort were able to hang from the overhead wire

Figure 2.13 Home cage testing: verticals, hangs and exploratory analysis of WT/βGal$^{+/-}$, βGal$^{-/-}$ + PBS and βGal$^{-/-}$ + AAV treated mice

Figure 2.13 Home cage testing: verticals, hangs and exploratory analysis of WT/βGal$^{+/-}$, βGal$^{-/-}$ + PBS and βGal$^{-/-}$ + AAV treated mice

Home cage testing of βGal$^{-/-}$ + AAV, 1x10^{11} and 3x10^{11} vg (KO + AAV) treated males (a) or females (b). Untreated βGal$^{+/-}$, and βGal$^{+/+}$ /βGal$^{+/-}$ (WT/CA Untreated), mock treated βGal$^{-/-}$ + PBS (KO + PBS). Evaluation of daytime activity (left graphs) and nighttime activity (right graphs) of verticals, hangs and exploratory behaviors were assessed by time reaching, hanging and moving around the cage, respectively. Home cage testing behavioral data was collected per second, tabulated per hour, averaged per animal and consolidated to represent a 10 hour period of day or night. Error bars represent mean + SD, N=5-7 animals. Significant difference of βGal$^{-/-}$ + AAV vs. βGal$^{-/-}$ + PBS, or βGal$^{-/-}$ + AAV, 1x10^{11} vs. 3x10^{11} vg was calculated using non-paired T tests where * = $p < 0.05$, ** = $p < 0.01$, and *** = $p < 0.001$. NS indicates no significant difference between βGal$^{-/-}$ + AAV vs. βGal $^{+/+}$ /βGal$^{+/-}$ untreated.
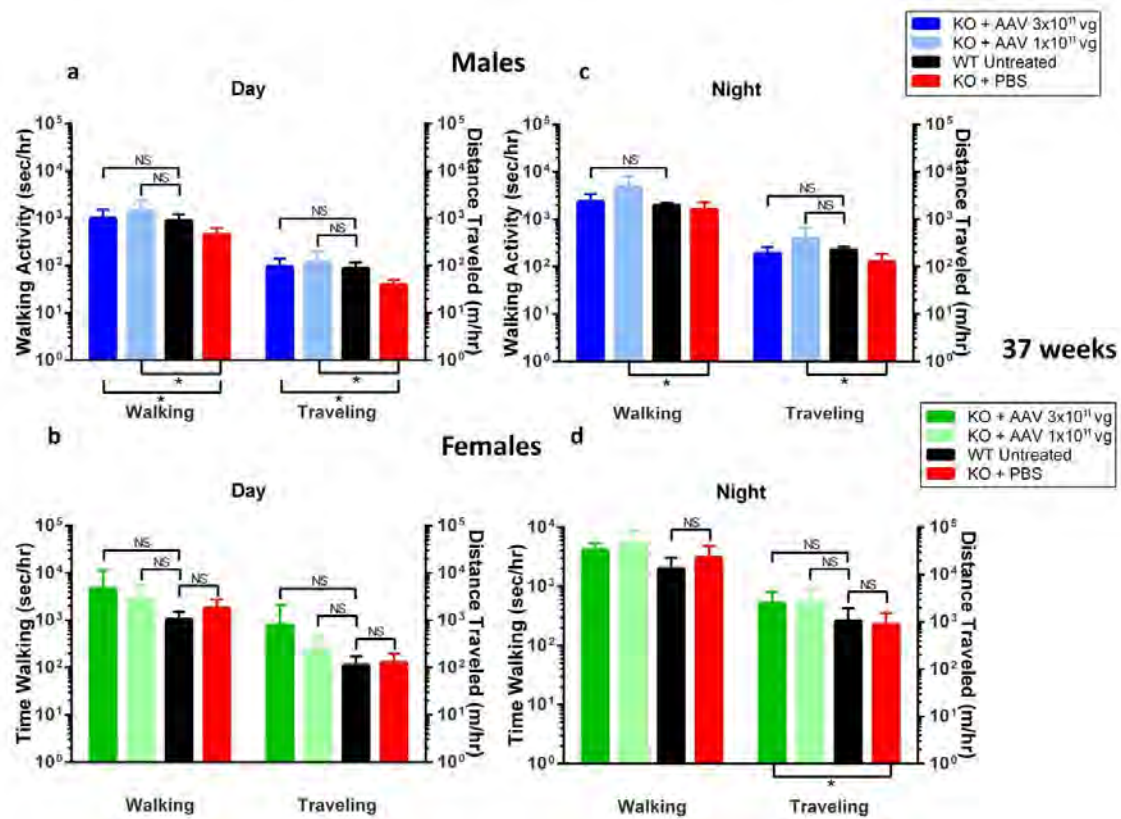
Figure 2.14 Home cage testing: walking and traveling analysis of WT/βGal$^{+/-}$, βGal$^{-/-}$ + PBS and βGal$^{-/-}$ + AAV treated mice

Figure 2.14 Home cage testing: walking and traveling analysis of WT/βGal$^{+/-}$, βGal$^{-/-}$ + PBS and βGal$^{-/-}$ + AAV treated mice

Home cage testing of βGal$^{-/-}$ + AAV, 1x10^{11} and 3x10^{11} vg (KO + AAV) treated males (a) or females (b). Untreated βGal$^{+/-}$, and βGal$^{+/+}$ βGal$^{+/-}$ (WT/CA Untreated), mock treated βGal$^{-/-}$ + PBS (KO + PBS). Evaluation daytime activity (a & c) and nighttime activity (b & d) of walking and traveling behaviors were assed by time moving around the cage and distance traveled, respectively. Home cage testing behavioral data was collected per second, tabulated per hour, averaged per animal and consolidated to represent a 10 hour period of day or night. Error bars represent mean + SD, N=5-7 animals. Significant difference of βGal$^{-/-}$ + AAV vs. βGal$^{-/-}$ + PBS, or βGal$^{-/-}$ + AAV, 1x10^{11} vs. 3x10^{11} vg was calculated using unpaired T tests where * = $p < 0.05$, ** = $p < 0.01$, and *** = $p < 0.001$. NS indicates no significant difference between βGal$^{-/-}$ + AAV vs. βGal$^{+/+}$ untreated.

feed tray significantly better than PBS-treated control females in both light cycles (Fig. 2.13).

Animals were video recorded at 220-260 days old to document phenotypes of treated and untreated animals close to the median humane endpoint of untreated βGal$^{-/-}$ mice. In all videos with PBS-treated control mice (Videos 2.1 - 2.4), hallmark phenotypes of GM1 gangliosidosis were noted as previously reported in this model (48, 51). Whole body tremors and gait abnormalities were evident in these mice. The front legs were tucked under the torso but remained functional and the body was consistently tilted forward suggesting weakness in forelimbs or shoulder muscles. The hind legs were splayed outward but remained capable of supporting body weight. Interestingly, hind leg movement appeared to be initiated by hip rotation suggestive of quadriceps weakness, which may also be the cause for reduced rearing or vertical movements. Tail stiffness and curling over the body was also a common phenotype in these control mice as described previously in the GM1 mouse model (48). Male mice in the HD cohort displayed some tail stiffness, but normal body position, mobility, and rearing activity at 258 days (Video 2.1). Male mice in the LD cohort at 263 days showed tail stiffness, unsteady gait, and slight tremors. Rearing was still apparent during grooming (Video 2.3). Female mice in the HD cohort at 260 days (Video 2.2) were largely indistinguishable from normal βGal$^{+/+}$ controls. Female mice in the LD cohort at 264 days (Video 2.4) displayed some tremors, but body position was close to normal albeit lower to the ground, and gait abnormalities such as occasional

hopping were milder than in PBS-treated controls at comparable age. Long lived

females in the HD cohort remained ambulatory but displayed clear signs of

decline with stiff tails, jerky movements, whole body tremors, and walking low to

the ground at 590 days old (Video 2.5) and 566 days old (Video 2.6).

AAV treatment extends lifespan of βGal$^{-/-}$ mice

PBS-treated control βGal$^{-/-}$ mice reached maximum weight at an average

of 175 $\pm$ 21 days of age, (>15% body weight loss from maximum) (Fig. 2.15a b;

Table 2.2). Maximum body weight was comparable across all groups. AAV9-

treated βGal$^{-/-}$ males reached maximum body weight at 245.7 $\pm$ 53.2 days (p =

0.007, LD cohort) and 278.6 $\pm$ 61.6 days (p = 0.001, HD cohort). AAV9-treated

βGal$^{-/-}$ females reached maximum body weight at 230.3 $\pm$ 38.5 days (p = 0.004,

LD cohort) and 458.8 $\pm$ 76.3 days (p = 0.0007, HD cohort) (Fig. 2.15a, b; Table

2.2). Survival analysis showed a significant increase in median survival for both

genders and doses (p < 0.0001) compared to PBS-treated βGal$^{-/-}$ mice (Fig.

2.15c, d; Table 2.2). In addition, there was a significant difference in survival

between doses for females (p = 0.0007), and between males and females in the

HD cohort (p = 0.01) (Fig. 2.15c, d; Table 2.2).
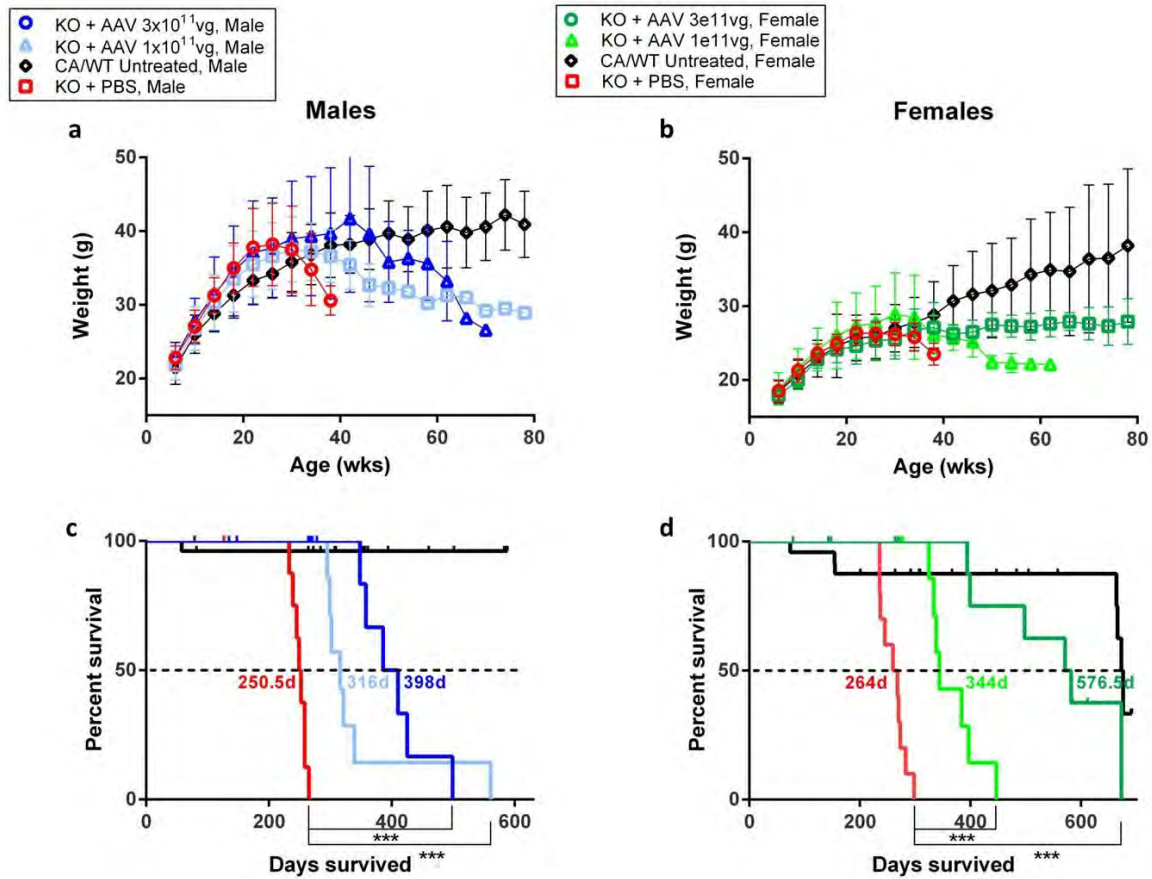
Figure 2.15 Weight and survival of WT/βGal$^{+/-}$, βGal$^{-/-}$ + PBS and βGal$^{-/-}$ +

AAV treated mice

Figure 2.15 Weight and survival of WT/βGal$^{+/-}$, βGal$^{-/-}$ + PBS and βGal$^{-/-}$ +

AAV treated mice

(**a & b**) Weights and (**c & d**) survival of βGal $^{-/-}$ + AAV, 1×10^{11} and 3×10^{11} vg

treated (KO + AAV), βGal$^{+/-}$ and βGal $^{+/+}$ untreated (WT/CA Untreated) and βGal$^{-/-}$

+ PBS mock treated (KO + PBS) male and female mice. Error bars represent

mean + SD, N=9-26 animals/group. (**a & b**) Weights are represented as an

average of 1 weighing during a 4 week period beginning at pre-injection (6

weeks) and continued until removal from the study up to 80 weeks of age. (**c &**

d) Survival analysis of all animals entered into the study. *** indicates significant

difference vs. KO + PBS using Log-rank (Mantel-Cox) test where p=0.0001.

				Weight and survival statistics of βGal and βGal^{-/-} + AAV treated mice			
Gender	Genotype	Treatment	Enrolled animals	Max weight (g ± std, N)	Age at max weight (days)	Median survival (days)	Max survival (days)
Male	CA/WT	Untreated	25	42.3 ± 4.7, 7	513.8 ± 10.5	N/A	N/A
Male	KO	PBS	9	38.8 ± 5.9, 8	178.5 ± 23.1	250.5	265
Male	KO	1×10^{11} vg	10	38.6 ± 4.6, 7	245.7 ± 53.2**	316.0***	339[†]
Male	KO	3×10^{11} vg	17	42.2 ± 9.1, 6	278.6 ± 61.6**	398.0***	499
Female	CA/WT	Untreated	24	38.9 ± 10.5, 7	510.3 ± 42.0	N/A	N/A
Female	KO	PBS	10	26.9 ± 1.8, 10	179.2 ± 24.5	264.0	298
Female	KO	1×10^{11} vg	10	27.2 ± 3.3, 7	230.3 ± 38.5**	344.0***	447
Female	KO	3×10^{11} vg	17	28.7 ± 2.2, 7	458.5 ± 76.3***	576.5***	673

[†] 1 animal survived until 561 days.

Table 2.2 Weight and survival statistics of WT/βGal^{+/-}, βGal^{-/-} + PBS and βGal^{-/-} + AAV treated mice

Significant difference for age at max weight for βGal^{-/-} + AAV vs. βGal^{-/-} + PBS was calculated using unpaired T tests where ** = p < 0.01, and *** = p < 0.001. Significant difference for median survival of βGal^{-/-} + AAV vs. βGal^{-/-} + PBS was calculated using Log-rank (Mantel-Cox) test where *** p = 0.0001.

Discussion

Previous studies from our lab have shown intracranial delivery of recombinant AAV vectors in neonatal (197) and adult GM1 mice (198) to be effective approaches to achieve widespread expression of functional βgal and reduce lysosomal storage of GM1-ganglioside in the CNS. The intracranial AAV delivery approach in adult GM1 mice delayed the onset of disease symptoms, but had little to no impact on the decline of motor function and only a modest improvement in survival (198).

In this study we show that vascular delivery of a single-stranded AAV9 vector in adult GM1 gangliosidosis mice (βGal$^{-/-}$) extended the survival of all AAV-treated animals (Fig. 2.15c, d; Table 2.2), but was not successful in arresting disease progression at the doses tested ($1x10^{11}$ and $3x10^{11}$ vg/mouse). The therapeutic impact was considerably better in females with a median survival in the high dose cohort of 576.5 days compared to 398.0 days for males (Fig. 2.15c, d; Table 2.2). The therapeutic outcomes correlate well with the findings from biochemical and histological studies of the CNS where we observed increased βgal activity (Figs. 2.1, 2.2a, b; Table 2.1) and partial correction of GM1 ganglioside content (Figs. 2.4, 2.5 & 2.8).

Histological analysis of lysosomal storage revealed dramatic reduction in HD cohort cerebral cortex, hippocampus, brainstem, and spinal cord, but lesser impact in deep brain structures such as thalamus, and striatum, and importantly in the cerebellum (Figs. 2.4 & 2.5). The reduction in lysosomal storage observed

in deep brain structures likely contributed to slower disease progression as the onset of symptoms in GM1 gangliosidosis mice coincides with the detection of inflammatory markers in different brain regions, especially in thalamus, brainstem, and spinal cord (6). Despite partial correction in several CNS regions, the impact of AAV treatment on disease physiology was nonetheless profound in the HD cohort as indicated by the dramatic reduction in reactive astrocytes throughout the brain (Fig.2.9) that correlated with reduction in GM1 storage (Figs. 2.4 & 2.8). The therapeutic impact in the spinal cord with normalization of GM1 ganglioside content (Figs. 2.5 & 2.8) and resolution of astrogliosis (Fig. 2.10) was likely a major factor in extending the lifespan and preserving ambulation of AAV9-treated animals (Videos 2.1, 2.2, 2.5 & 2.6). Nonetheless, AAV9-treated animals eventually developed whole body tremors and jerky movements, which may be related to the marginal therapeutic impact in the cerebellum (Videos 2.5 & 2.6). AAV9-HD cohort treated animals showed little or no change in lysosomal storage in granular, molecular, or Purkinje cell layers, but complete correction in deep cerebellar nuclei (Fig. 2.4f, m; thin and thick arrows, respectively). The failure to resolve storage in the Purkinje cell layer was also reported in another study using systemic delivery of an AAV9 vector to treat MPSIIB mice (187). As the output centers of the cerebellum, the deep cerebellar nuclei send projections to different levels of the spinal cord and other regions of the brain (215). Given the connectivity of those nuclei and that βgal can be distributed over long distances via axonal transport (167), storage correction in DCN is most likely the

result of enzyme uptake at axonal terminals in successfully treated structures, such as the spinal cord, and its retrograde transport to the cell body where most lysosomes reside. Disease progression in other cerebellar nuclei or cell populations may have led to the phenotypes that developed over time in AAV9-treated GM1 gangliosidosis mice.

The pattern of lysosomal storage correction in the CNS of GM1 gangliosidosis mice in this study matches closely with the transduction profile of other studies where AAV9 vectors were delivered systemically in adult mice. The most effectively transduced CNS regions are the cerebral cortex, hippocampus, and spinal cord (181, 216). Neuronal transduction in adult mice seems to be most pronounced in the spinal cord and hippocampus, but mostly glia and endothelial transduction throughout the rest of the brain (181, 216). Transduction of striatum and thalamus is relatively inefficient by comparison to other brain regions, and especially inefficient in cerebellum at comparable doses (216). Nonetheless previous studies have reported exceptional therapeutic effects using systemic delivery of single-stranded AAV9 vectors in mouse models of mucopolysaccharidosis type IIIA (188) and IIIB (187). The difference in therapeutic outcomes may be related to rates of disease progression specific to each lysosomal storage disease or mouse model. Also the minimum level of enzyme necessary to achieve complete correction of storage in cross-corrected cells may be considerably higher for βgal compared to other lysosomal enzymes. During synthesis βgal forms a megacomplex with neuraminidase-1 (NEU1) and

protective protein/cathepsin A (PPCA) important for transport of NEU1 to lysosomes, and processing/protection of βgal (reviewed in (217)). Since only βgal is overexpressed, secreted, and transported into enzyme-deficient cells, it is possible that its half-life may be lower in the lysosomes of cross-corrected cells because it may not interact with PPCA as the βgal-PPCA complex is normally formed before transport to lysosomes (217). This may render the recombinant βgal more susceptible to proteolytic degradation. In addition the enzymatic efficiency of βgal by itself may be lower than in its native multienzyme complex. Other aspects such as AAV vector design and dosing may also explain the difference in outcomes between our study and others. Finally, biochemical changes intrinsic to a particular lysosomal storage disease may affect the efficiency of AAV9 CNS gene transfer as shown in MPS VII mice due to sialic acid deposition in brain vasculature (194).

The impact of AAV9 treatment on lysosomal storage in CNS was better in females than males in the HD cohort (Figs. 2.4, 2.5 & 2.8), and this likely explains the difference in therapeutic outcome between genders. Survival was comparable between genders in the low dose cohort, but females survived 45% longer than males in the high dose cohort (Fig. 2.15c, d, Table 2.2). The difference in therapeutic impact between genders is likely the result of a difference in CNS gene transfer efficiency as suggested by the analysis of vector genome content (Fig. 2.3). Although the difference between genders did not reach statistical significance in most tissues, it is interesting that the average

value is 2-3-fold higher in females across all brain regions (p = 0.07 for cerebrum

and cerebellum) and in most other organs except liver and muscle (Fig. 2.3).

The higher efficiency of AAV liver gene transfer in male mice has been

documented in a multiple models (190, 191) and appears to be testosterone

dependent (191, 218). Our results show the same gender difference in AAV liver

gene transfer with a 5-fold higher vector genome content (Fig. 2.3) and 6-7-fold

higher enzyme activity in males than females in the high dose cohort (Fig. 2.2a,

b; Table 2.1). The notion that AAV9 CNS gene transfer after vascular delivery in

adult GM1 mice is more efficient in females is supported by a recent study

showing an identical gender difference in different mouse strains infused

systemically with an AAV9 vector encoding firefly luciferase (192). In our study

the higher efficiency of AAV9 CNS gene transfer in females after systemic

delivery may be partly due to lower affinity to liver as its vector genome content is

5-fold lower than in males (Fig 2.3). This suggests that liver tropism/affinity may

be a major factor in determining the bioavailability of AAV9 (and possibly other

AAV capsids) to transduce other organs after systemic delivery. The gender

effect on AAV liver transduction has not been documented in other mammalian

species such as cats (218). Nonetheless, liver tropism remains an important

issue in the development of systemic AAV9 gene delivery approaches for

neurological diseases. The liver tropism of AAV9 is a concern for vascular

delivery approaches to treat neurological diseases as the high doses required to

target CNS effectively could lead to collateral liver toxicity related to transgene

expression. Transient liver toxicity may explain the paradoxical finding that the range of βgal activities in liver and serum was lower in mice (both sexes) receiving higher vector dose (Table 2.1). Further studies will be necessary to assess this possibility and uncover the causes, which could be related to βgal overexpression. Whether this is a finding unique to this enzyme or also applies to other lysosomal enzymes remains to be determined. Different approaches have been employed to reduce or eliminate transgene expression in liver after vascular delivery of AAV9 vectors, namely using the CMV promoter that is down-regulated over time (187), or incorporation of perfect miR-122 (highly expressed in liver) target sequences in the expression cassette 3' untranslated region (189). These transcriptional de-targeting approaches are likely to increase safety of vascular delivery of AAV9 vectors, but have no impact on its liver tropism properties. Interestingly AAV9 mutants engineered to reduce liver tropism by more than 10-fold show only marginal increases in CNS gene transfer (219). Presently the molecular basis for decreased liver tropism is unknown, namely whether the introduced mutations change the affinity to the same cell surface receptor, or re-direct the capsid to another receptor entirely. Clearly, achieving higher CNS gene transfer with AAV9 vectors, or derivatives, is not as simple as reducing liver tropism. Other AAV capsids may display higher CNS gene transfer efficiency than AAV9 in adult mice, as recently shown for AAVrh8 (183).

The therapeutic outcome in this study is superior to that obtained by intracranial injection of an AAV1 vector into thalamus and deep cerebellar nuclei

of adult GM1 gangliosidosis mice (198). This finding is somewhat paradoxical as in the present study there was only partial correction of GM1 ganglioside content in the brain compared to complete normalization in the intracranial approach, while the findings are reversed in the spinal cord. This suggests that disease progression in the spinal cord may be an early driver of disease phenotypes in this mouse model, but ultimately partial treatment of other CNS regions will compromise survival. It is possible that treatment of adult GM1 gangliosidosis mice with higher doses of AAV9 vector may lead to complete correction of lysosomal storage in the CNS and arrest disease progression completely.

This is the first study reporting on the therapeutic efficacy of vascular delivery of an AAV9 vector encoding βgal in adult GM1 gangliosidosis mice. We showed successful widespread expression of functional enzyme throughout the CNS with resulting reduction in GM1 ganglioside storage and significant extension of lifespan with retention of motor function. To improve overall therapeutic outcomes, a focus on increasing enzyme delivered to the CNS is warranted as enzyme levels achieved in this study were insufficient to normalize GM1 ganglioside levels. This inability to normalize GM1 ganglioside content everywhere may have lead to an eventual inflammatory cascade resulting in loss of function in partially corrected regions. Intravascular infusion of AAV9 vector at higher doses, or using AAV capsids with higher CNS gene transfer efficiency (183), may result in complete biochemical correction of disease with normalization of phenotype and lifespan.

CHAPTER III: AAVrh8-Mediated Intracranial Gene Delivery of a Lysosomal Enzyme to the CNS: Therapeutic Benefits, Challenges and Considerations in a GM1 Mouse Model

Introduction

Lysosomal storage disorders (LSD) are a class of >50 disorders associated with malfunction of a resident enzyme which leads to accumulation of undegraded substrates in lysosomes (7). Over time, this accumulation can lead to lysosomal malfunction which results in a cascade of events (220-223) often resulting in cell death (4, 5, 7). LSDs with central nervous system (CNS) involvement require the intended therapy to cross or bypass the blood brain barrier in order to deliver functional enzyme to target cells to achieve disease resolution (91). However, obtaining enzyme levels at high enough concentrations or with sufficient distribution throughout the CNS to achieve a therapeutic impact has been challenging. Strategies employed to overcome these obstacles in the CNS focus on utilizing inherent properties of these enzymes such as cross correction (the release and uptake of enzymes from neighboring cells) (85-87), CSF-mediated distribution, and axonal transport (165, 167). A successful approach has been to target gene delivery to highly connected structures in the brain for maximum spread of enzymes (100, 165-167, 170-172, 174, 175, 198, 203, 204, 215, 224, 225).

Gene therapy by intracranial injection of adeno-associated virus (AAV) vectors has been the most effective approach to obtain high levels gene transfer to target structures (165, 166, 170-172, 174, 175, 198-200, 215). Typical approaches seek to express the highest amount of enzyme possible in order to obtain maximum therapeutic benefit and have been optimized by addition of enhancers, ubiquitous promoters (210, 226, 227), and post transcriptional regulatory elements (228, 229). However, accumulation of undegraded substrates or dysregulation of the lysosomal compartment can lead to responses to upregulate lysosomal biogenesis (220, 221), substrate reduction (222) or exocytosis (223). It is also possible that introduction of supraphysiological levels of a therapeutic protein can also trigger deleterious "protection" cascades which may be associated with unfolded protein response common in these disorders (4).

GM1-gangliosidosis is a LSD resulting from the deficiency in the catabolizing enzyme β-galactosidase (βgal) (3, 7). GM1-gangliosidosis is primarily a disease of the CNS where accumulation of GM1 ganglioside (GM1) results in lysosomal dysfunction, ER stress and calcium mediated apoptosis leading to neuronal loss, generalize paralysis and death (4, 5, 7). The amount of residual enzyme activity determines the severity and age of disease onset. Infantile and late infantile/juvenile patients usually have 1-4% of normal activity, while adult onset or chronic patients have 4-<10% βgal activity (7). As no cases of GM1-gangliosidosis have been reported with >10% βgal activity, it is thought

that 10-20% of normal activity should be sufficient to treat this disease.

Currently, there is no cure or effective treatment for GM1-gangliosidosis patients.

Attempts at therapies for GM1-gangliosidosis include enzyme replacement (89,

90), bone marrow (82, 83) or cell transplantation (84), molecular chaperones (79,

230), substrate reduction therapy (75, 78, 80, 81), and gene therapy (196-198).

Despite success in cell lines or animal models in delivering or regaining active

enzyme (79, 83, 84, 90, 197, 198), reducing substrates (75, 78, 80), and

resolution of GM1 storage (80, 84, 197, 198), no experimental approach has

been successful in treating all disease aspects and eventually animals succumb

to disease progression. Previous work in our lab focused on the delivery of

enzyme to the CNS through AAV vectors injected into the lateral ventricle of

neonatal mice (197), or intracranial bilateral injections into the thalamus and

deep cerebellar nuclei of adult mice (197). Both of these approaches achieved

high expression of active βgal in the brain with an AAV1 capsid, but found some

regions of the CNS lacking in enzyme expression and without resolution of GM1

storage.

In this current study, we first investigated possible reasons for the lack of

overall efficacy by employing i) an AAVrh8 vector (121) as it has been shown

very effective at expressing enzyme in the mouse CNS (169), and cat brain (199,

200), and ii) modification of target coordinates for the DCN. We were able to

achieve widespread distribution of βgal throughout the cerebrum and cerebellum,

significant retention of motor function and extension of lifespan. The resulting

expression of βgal was very high in the injection sites, and surprisingly was one of the remaining regions in brain with strong staining of our storage marker, Filipin. In addition, we found evidence of neuropathology at the injection sites suggestive of toxicity, which decreased with lower vector dose. We examined these unexpected results in both GM1-gangliosidosis βgal$^{-/-}$ mice and unaffected βgal$^{+/-}$ animals and found this abnormal Filipin staining to be consistent. To investigate the cause for this unusual result we constructed a variety of AAVrh8 vectors with decreasing enzyme expression levels. Microarray analysis of the thalamic target showed increased expression of a number of genes associated with microglia and astrocyte activation, which did not occur in a low expressing vector or in control animals. Finally, we tested these AAVrh8 vectors in βgal$^{-/-}$ mice for therapeutic efficacy and identified a vector that both minimized consequences of over expression and maximized therapeutic benefit.

Taken together, this work demonstrates that in treatment of a lysosomal storage disorder by intracranial injection one must consider impact of supraphysiological levels of enzyme as well as transgene delivery efficiency for a safe and effective therapeutic intervention.

Materials and Methods

Vector design, construction and viral creation.

Construction of the original AAV vector was previously described (197) and carries an expression cassette driven by a promoter composed of cytomegalovirus immediate early enhancer (CMV) fused to the chicken beta-actin promoter followed by a chimeric chicken beta-actin/rabbit beta globin intron (CBA), the mouse lysosomal acid β-galactosidase cDNA (mβgal), a woodchuck hepatitis virus post-transcriptional regulatory element (WPRE), and two polyA signals in tandem derived from the bovine growth hormone (BGH) and SV40. This vector is called AAV-CBA-mβgal-WPRE. AAV-CBA-mβgalE269Q-WPRE was generated by PCR mutagenesis with of the following primers: AAA CGT CTC ACT AGT CCG CGG AAT TC , Rev1: AAA CGT CTC ACT GAG AAT TGA TCA AA , For2: AAA GGT CTC CGG CCG CTA GCG TCA G, Rev2: AAA GGT CTC ATC AGT TCT ATA CTG GC. The resulting PCR product was digested with SpeI and Not I restriction enzymes and cloned in place of the wild type βgal cDNA. All other AAV vectors were generated by removal of different elements from AAV-CBA-mβgal-WPRE vector. All AAVrh8 vector stocks were produced as previously described (231).

Animal procedures.

GM1-gangliosidosis mice ($\beta gal^{-/-}$), a knock out version created by insertion of a neomycin cassette in exon 6 of the β-galactosidase gene, GLB1 (51), were obtained from Dr. Kunihido Suzuki (Neuroscience Center, University of North Carolina, Chapel Hill, NC). $\beta gal^{-/-}$, $\beta gal^{+/-}$, and $\beta gal^{+/+}$ mice weregenerated by mating of male $\beta gal^{-/-}$ and female $\beta gal^{+/-}$ mice or $\beta gal^{+/-}$ males and females.

Intracranial injections.

Six to eight week-old $\beta gal^{-/-}$ or $\beta gal^{+/-}$ mice were anesthetized by intraperitoneal injection of ketamine (125 mg/kg) and xylazine (12.5 mg/kg) in 0.9% saline and placed in a rodent stereotaxic frame (Stoelting, Wood Dale, IL). The fur around the incision site was clipped, and the was skin scrubbed with povidine-iodine pads and 70% EtOH. The skull was exposed by a small longitudinal incision (< 1 cm) along the midline. The periosteum was removed from the surgical area with sterile cotton tipped applicators. Small burr holes (< 1 mm) were made using a high-speed drill (Dremel, Robert Bosch LLC, Waltham, MA) at the appropriate stereotaxic coordinates. AAV vectors, or PBS, were infused in $\beta gal^{-/-}$ or $\beta gal^{+/-}$ mice with 1 µl bilaterally into the thalamus (stereotaxic coordinates: AP –2.0 mm, ML ±1.5 mm from bregma; DV -3.5 mm from brain surface) and in $\beta gal^{-/-}$ mice with 0.3 or 1 µl into the deep cerebellar nuclei (AP - 6.0 mm, ML ±1.5 mm from bregma; DV -3.5 mm from brain surface) at a rate of

0.2 µl/min using an Ultramicro Pump (World Precision Instruments, Sarasota, FL) to drive a 10 µl gastight glass syringe fitted with a 33G needle (Hamilton, Reno, NV). Infusions were started 1 min after placement of the needle in the target structures and slowly withdrawn 2.5 min after conclusion of the infusion. The scalp was closed with sterile wound clips (9 mm). All animal experiments were approved by the Institutional Animal Care and Use Committee at the University of Massachusetts Medical School, and complied with the National Institutes of Health Guide for the Care and Use of Laboratory Animals.

Behavioral assays.

Rotarod testing was conducted on a Rotarod apparatus (Med Associates, St. Albans, VT) accelerating from 4 to 40 rpm over 5 minutes, with latency to fall recorded. Testing was conducted with one practice trial of 1 minute accelerating from 2 to 20 rpm at the beginning of the session followed by 3 trials with 15-20 minute resting in between. Latency to fall for each mouse in a testing session was recorded, and the longest time on the rotarod among the 3 trials was reported.

Tissue processing.

For biochemical studies in βgal$^{+/-}$ mice, the brain was removed and sliced into 2 mm coronal blocks using a brain matrix (Stoelting, Co., Wood Dale, IL), and immediately frozen on dry ice. The block containing the thalamus was identified by morphology and the presence of needle entry points on the dorsal brain surface. A 2 mm diameter biopsy punch (Integra Miltex, York, PA) was used to sample the thalamus and the tissue plug placed in the appropriate buffer for analysis. For histological studies the brain and spinal cord were removed and placed in Neg 50 freezing medium (Richard-Allan Scientific, Kalamazoo, MI) and frozen in a dry ice/2-methylbutane bath (ThermoFisher Scientific, Waltham, MA). For biochemical studies in βgal$^{-/-}$ mice, cerebrum, cerebellum + brainstem, and spinal cord were removed and immediately frozen on dry ice.

Histological analysis.

20 µm brain (sagittal and coronal) and spinal cord (transverse) sections were cut in a cryostat (ThermoFisher Scientific, Waltham, MA) and stored at -80°C.

Brain sections were stained with X-gal to assess the distribution of βgal as described previously (197), with modifications. Briefly, slides were fixed in 0.5% glutaraldhyde in PBS, washed 3x in ice cold citrate phosphate buffer (CPB)

(50mM C_6H_8O, 50mM Na_2HPO_4, 10mM NaCl, pH=4.2) incubated overnight at 37°C in X-gal staining solution [20mM $K_4Fe(CN)_6$, 20mM $K_3Fe(CN)_6$, 2mM $MgCl_2$, 0.01% $C_{24}H_{39}NaO_4$, 0.02% $(C_2H_4O)nC_{14}H_{22}O$ (IGEPAL CA-630, SigmaAldrich),97% CPB @ pH=4.2, 2mg/ml 5-bromo-4-chloro-3-indolyl-β-D-galactosidase (X-gal) in $HCON(CH_3)_2$). The next day, slides were rinsed in CPB then water, counterstained with Vector Nuclear Fast Red (Vector Laboratories, Inc., Burlingame, CA), dehydrated through a series of ethanol 50%-100%, cleared with CitriSolv (ThermoFisher Scientific, Waltham, MA) and mounted with Permount (ThermoFisher Scientific, Waltham, MA).

Brain and spinal cord sections were stained with Filipin to assess lysosomal storage as described previously (197), with modifications. Briefly, slides were fixed in 4% paraformaldehyde in phosphate buffered saline (PBS), washed with PBS, incubated with 1.5% glycine in water, washed with PBS, incubated with 100 µg/ml of Filipin (Santa Cruz Biotechnology, Inc., Dallas, TX) and 1 µg/ml of ToPro3 Iodide (Life Technologies, Grand Island, NY) for 1-2 hours, washed with PBS and mounted with fluorescence mounting media, PermaFluor (ThermoScientific, Fremont, CA).

Brain sections were stained with Mayer's Hematoxylin and Eosin to assess morphological changes in the tissue. Briefly, slides were dried at room temperature, fixed in 4% paraformaldehyde in phosphate buffered saline (PBS), washed with water, incubated with Mayer's Hematoxylin (Sigma-Aldrich, St.

Louis, MO), washed in running tap water, counterstained with Eosin (Sigma-Aldrich, St. Louis, MO), rinsed with deionized water, dehydrated through a series of ethanol 50%-100%, cleared with CitriSolv (ThermoFisher Scientific, Waltham, MA) and mounted with Permount (ThermoFisher Scientific, Waltham, MA).

Whole brain slice images were captured using white light on a Nikon Super CoolScan 5000 ED with a medical slide holder (Nikon, Inc., Melville, NY). Microscope images were captured on a Leica DM550 B microscope, equipped with Leica DFC425 C and DFC365 FX digital cameras (Leica Microsystems, Buffalo Grove, IL). Filipin was imaged at 405nm and ToPro3 Iodide at 636nm. H&E was imaged using brightfield.

All histological analysis was performed as non-blinded, qualitative analysis on an N ≥ 2-3 animals with representative pictures shown in figures.

βgal enzymatic assays and Immunobloting.

Biopsy punches, one hemisphere of brain tissue or one half spinal cord were homogenized in lysis buffer (0.1% Triton X-100 in 0.2M CH_3COONa , 0.1M NaCl, pH 4.3) and assayed for βgal enzymatic activity as described previously (197, 199). Briefly, a reaction with βgal substrate = 1mM 4-Methylumbelliferyl-β-D-galactoside (4-MUG) was performed in a 96-well plate format and the amount of 4-methylumbelliferyl (4-MU) released was measured against a standard curve

with fluorescence detection by excitation at 360 nm and emission at 460nm using a BioTek Synergy HT plate reader (BioTek, Winooski, VT). Enzymatic activity was normalized to protein content as determined by Bradford assay (Bio-Rad, Waltham, MA) and reported as nmol (of substrate converted)/hour/mg protein. For immunobloting injection site biopsy punches were homogenized in T-PER buffer (ThermoFisher Scientific, Waltham, MA) supplemented with Complete Mini protease inhibitor cocktail (Roche Molecular Systems, Inc., Branchburg, NJ), incubated on ice for 10 min and then centrifuged at 10,000 x g for 5 min. The supernatant was collected and protein concentration determined using a Bradford assay (Bio-Rad, Waltham, MA). Total protein (20 µg) was separated by polyacrylamide gel electrophoresis using Mini-PROTEAN TGX precast gels (Bio-Rad, Waltham, MA), and protein transferred to NitroPure nitrocellulose membrane (Maine Manufacturing, LLC, Sanford, ME). Blots were blocked in Tris-buffered saline-Tween-20 (TBST) with 5% fat-free milk, and then incubated with primary antibodies to α-rabbit GLB1 (β-galactosidase antibody) (1:250; Proteintech, Chicago, IL) and α-mouse β-Actin (1:1000; GenScript, Piscataway, NJ). HRP-conjugated anti-rabbit and anti-mouse secondary antibodies were used (1:4000; GE Healthcare, Westborough, MA) and signal detection was done with Pierce ECL Western Blotting Substrate (ThermoFisher Scientific, Waltham, MA) and blots exposed to Amersham Hyperfilm ECL (GE Healthcare, Westborough, MA).

Genome copies

Genomic DNA from injection site biopsy punches was isolated using Qiagen DNeasy Blood and Tissue Kit (Qiagen, Valencia, CA), and concentration determined using a Nanodrop spectrophotometer (ThermoFisher Scientific, Waltham, MA) The number of AAV vector genome copies in 100 ng of genomic DNA were determined by qPCR using the following primers and Taqman probe specific for BGH polyA in the vector genome: (TaqMan Probe, 6FAM- AGC ATT TTT TTC ACT GCA TTC TAG TTG TGG TTT GTC -TAMRA) (Integrated DNA Technologies, Coralville, IA). Samples with ≥ 100 vg genome copies per µg of DNA were deemed positive for vector genomes. Data was represented as vg/diploid genome considering that 100 ng of mouse genomic DNA corresponds to 36,263 diploid genomes.

Microarray

Total RNA was isolated from biopsy punches using Trizol (Life Technologies, Woburn, MA) and further purified using RNeasy Plus Mini Kit (Qiagen, Valencia, CA), and its quality analyzed on an Agilent Bioanalyzer (Agilent Technologies, Santa Clara, CA). Bioanalyzer RNA integrity number (RINs) values were 8.7-9.5, which indicates high quality RNA (data not shown). Sample preparation and microarray hybridization was done at the UMass Medical School Genomics Core using Affymetrix Mouse Gene 2.0ST Arrays

(Affymetrix, Santa Clara, CA). Three independent samples were analyzed per group. Resulting data was processed and P values <0.05 and 1.5-fold change in relation to PBS controls were considered differentially expressed genes.

Quantification of GM1 ganglioside content

A liquid chromatography-tandem mass spectrometry (LC-MS/MS) assay (Weismann et al, in preparation) was used for quantification of GM1-ganglioside in CNS. Briefly, 0.01-0.04 mg/µL of tissue homogenate was diluted to 25 µL in buffer containing 0.2M sodium acetate and 0.1M NaCl (pH 4.3). To each sample 3 µg of d_3-labeled GM1 (Matreya, LLC, Pleasant Gap, PA) was added as an internal standard. Calibration curves were made neat with GM1 (Avanti Polar Lipids, Alabaster, AL) over the range of 200-3,000 ng and spiked with 3,000 ng of d_3-GM1. Total lipids were extracted by the Folch method(211) two successive times in chloroform/methanol (1:1), the supernatants combined, and the glycolipids partitioned to aqueous phase by adjusting the composition to chloroform/methanol/water (2:1:0.6). The upper aqueous phase was removed and the lower phase was washed once with chloroform/methanol/water (3:48:47) and the upper phases combined. Samples were dried, re-suspended in 0.2 mL 0.1M NaCl and applied to an equilibrated 1cc C18 reverse-phase Bond Elute column (Agilent Technologies, Santa Clara, CA), washed with 5 mL water, eluted with 0.6 mL CH_3OH followed by 1 mL $CHCl_3$:CH_3OH (1:1), dried, and re-

suspended in 100 µL solution of 1:4 (A:B) where A is 0.1% (v/v) formic acid and

B is methanol:2-propanol:0.1% formic acid (47.5:47.5:4.9). Gangliosides were

separated on a Phenomenex (Torrance, CA) 2.1 x 50mm Kinetex 1.7 µm (100Å)

C18 column using a Waters (Milford, MA) Acquity UPLC using a fast gradient

program (0-1 min, 80%B; 1-5 min, 80-100%B; 5-7 min 100%B; 7.1, 80%B) and

eluted to a Waters Quattro Premier XE triple quadrupole mass spectrometer

operating in the negative ion mode. Multiple reaction monitoring (MRM)

transitions for all GM1 and GM2 species were monitored using a cone voltage of

90V, a collision energy of 70V, and recorded the common sialic fragment anion

at m/z 290. The area of all the individual GM1 lipid species (16:0, 18:0, 18:1,

20:0, 20:1) were combined for each ganglioside and the ratios were calculated to

the corresponding d_3-18:0 GM1 internal standard. Calculated concentrations

were normalized to protein content by Bradford (Bio-Rad, Waltham, MA).

Results

AAV dose dependent distribution of βgal in brain

AAVrh8-CBA-mβgal-WPRE vector (Fig. 3.1) was infused into the brain of

6-8 week old GM1 gangliosidosis mice (βgal$^{-/-}$) by bilateral injections in the

thalamus and deep cerebellar nuclei at total doses of 4e10vg, 2.6e10vg and

2.6e9vg. Animals in the highest dose cohort received bilateral injections of 1 µl

in thalamus and DCN, while animals in the other two cohorts received 1 µl in

thalamus and 0.3 µl in DCN. The βgal distribution pattern in brain at 3 months

post-injection appeared to be dose dependent with the highest intensity of βgal

activity at the injection site (Fig. 3.2). The highest dose (4e10vg) provided

enzyme activity throughout much of the section in the cerebrum (Fig. 3.2a) and

cerebellum (Fig. 3.2b). Middle dose, 2.6e10vg had similar level of activity in the

cerebrum (Fig. 3.2e), and the cerebellum (Fig. 3.2f) appeared to provide slightly

less activity but still spread of enzyme throughout the structure. Low dose,

2.6e9vg had less spread in both the cerebrum and cerebellum (Fig. 3.2i & j,

respectively).

AAV treated animals retain motor function in a dose dependent manner.

The motor function of AAVrh8-treated mice was assessed over time using

the rotarod test (Fig. 3.3). All cohorts of AAVrh8-treated βgal$^{-/-}$ performed

significantly better than untreated βgal$^{-/-}$ controls at the 6 month post-treatment

time point (high dose 4e10vg p = 0.006, middle dose 2.6e10vg p = 0.0009, and

low dose 2.6e9vg p = 0.005). N = 6-10 animals/group at 6 months post-

treatment. Nonetheless, the rotarod performance of AAVrh8-treated animals

declined over time.
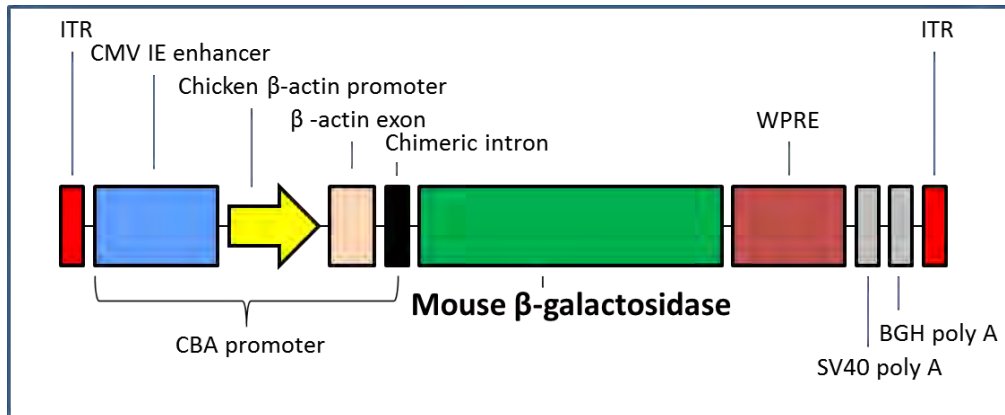
Figure 3.1 Vector design and components

Vector CBA-mβgal-WPRE. Two inverted terminal repeats (ITRs) from AAV2 flank the vector on each end. The CBA promoter is composed of a cytomegalovirus immediate early enhancer (CMV) fused to the chicken beta-actin promoter followed by a chimeric chicken beta-actin/rabbit beta globin intron (CBA), the mouse lysosomal acid β-galactosidase cDNA (mβgal), a woodchuck hepatitis virus post-transcriptional regulatory element (WPRE), and two polyA signals in tandem derived from the bovine growth hormone (BGH) and SV40. This vector was then packaged in an AAVrh8 capsid.
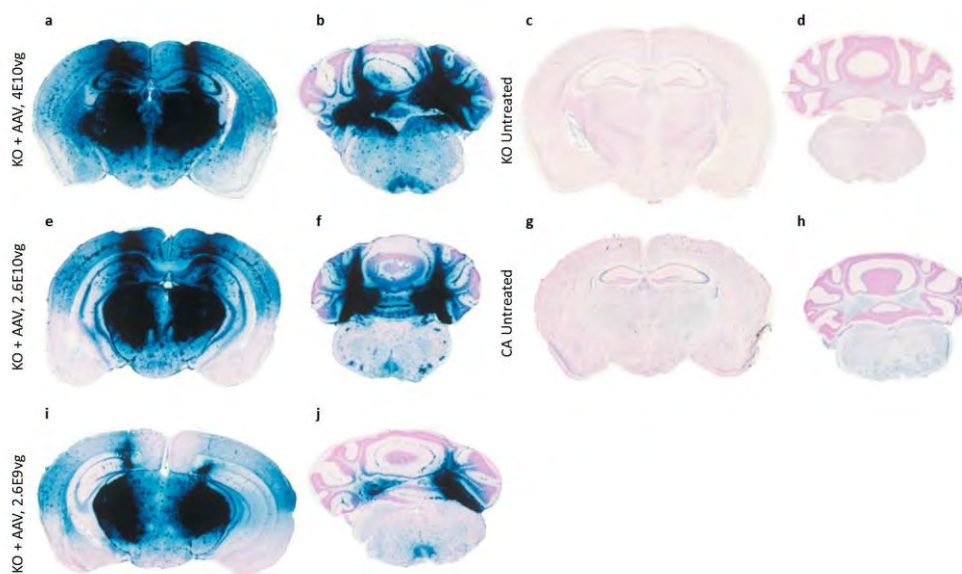
Figure 3.2. AAVrh8-mβgal intracranially injected in βgal$^{-/-}$ mice produces dose dependent enzyme distribution

βgal expression in the brain of representative AAVrh8-injected animals and age-matched controls was analyzed at 2 weeks (4e10vg) or 3 months (2.6e10vg and 2.6e9vg) post-injection by histochemical staining of 20 μm coronal brain sections with X-gal and counterstaining with Nuclear Fast Red. (a, b) 4e10vg (e, f) 2.6e10vg (i, j) 2.6e9vg (c, d) naïve βgal$^{-/-}$ and (g, h) naïve βgal$^{+/-}$ mice. Images are representative of N ≥ 3 mice/group.
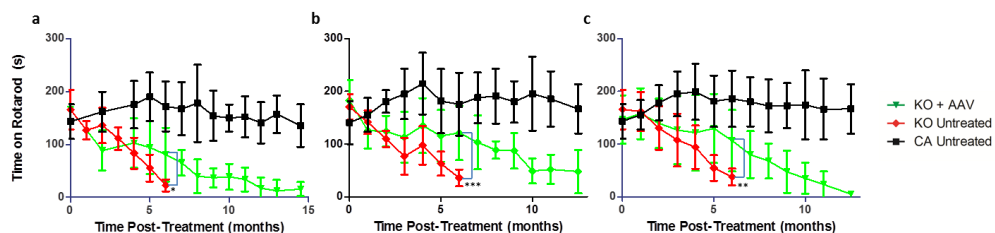
Figure 3.3. βgal$^{-/-}$ mice intracranially injected with AAV retain significant motor performance on the rotarod

Animals were assessed for motor function on an accelerating rotarod test (4-40 rpm over 5 minutes). Highest value from three trials was recorded. βgal$^{-/-}$ animals treated with a total dose of AAVrh8 vector of (a) 4e10vg (b) 2.6e10vg and (c) 2.6e9vg all retained motor performance significantly better than naïve βgal$^{-/-}$ controls at 6 months post injection using non-parametric, unpaired Student T Test and Welsh-correction (P = 0.006, 0.0009, 0.005 respectively). N = 3-15 animals/group at each time point, and N = 6-10 animals/group at 6 months post-treatment.

AAV treatment extends lifespan

The lifespan of AAVrh8-treated βgal$^{-/-}$ mice was significantly increased compared to naïve βgal$^{-/-}$ controls (Fig. 3.4). Median survival for naïve βgal$^{-/-}$ controls was 245.5 days (N = 18), 293.5 days for the 4e10vg cohort (N = 12, p = 0.0004), 349 days for the 2.6e10vg cohort (N = 13, p = 0.002) and 389 days for the 2.6e9vg cohort (N = 12, p < 0.0001). Of note, there were a subset of animals in the 4e10vg that developed tremor and circling behavior ~2weeks post injection. These animals were excluded from lifespan and behavioral testing. We retained these animals for analysis to understand this phenomenon.

GM1-ganglioside storage persists at the injection site and in the spinal cord of long-lived AAV treated animals

Histological analysis of lysosomal storage by Filipin staining in the CNS of animals at 3 months post injection (data not shown) revealed nearly complete correction in the brain and cerebellum that was corresponding to enzyme presence as seen in Xgal staining at the same time point (Fig. 3.2). Surprisingly Filipin-positive cells were only found at the injection sites, or along the injection track (Fig 4.5c, e). Filipin was originally identified as a potent anti-fungal with UV-VIS and IR properties (232), but was found to also bind directly to cholesterol and GM1 ganglioside (214).
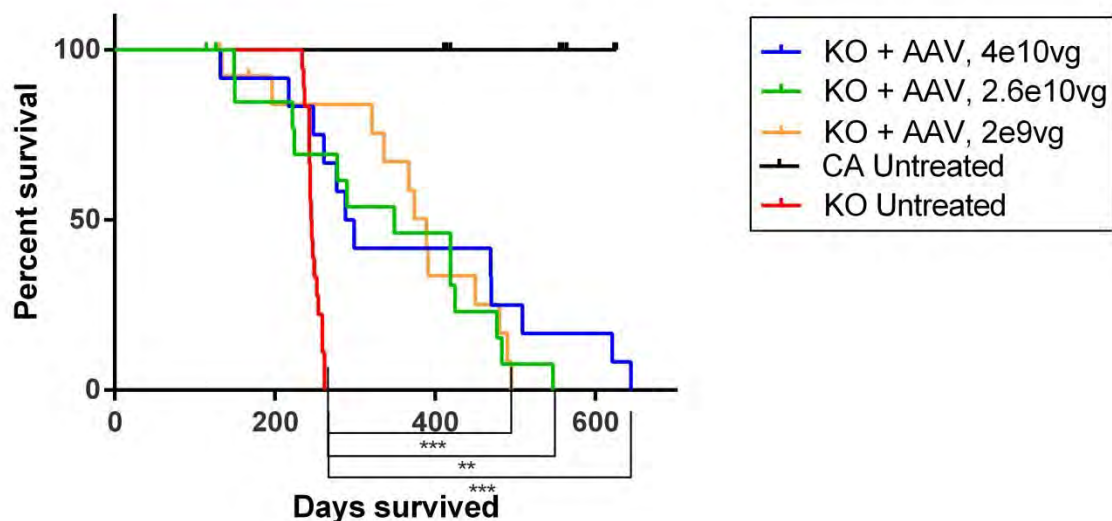
:Figure 3.4 AAVhr8 intracranially injected βgal$^{-/-}$ mice achieve significant extension in lifespan

Kaplan-Meier survival curves for intracranial AAVrh8 treated βgal$^{-/-}$ mice. Treated mice with a total dose of AAVrh8 vector of (blue) 4e10vg (green) 2.6e10vg and (orange) 2.6e9vg all had a significant extension of life span vs. naïve βgal$^{-/-}$ controls using Log-rank (Mantel-Cox) test (p = 0.0004, 0.002, < 0.0001 respectively). Median survival was increased from (red) naïve βgal$^{-/-}$ controls (245.5 days, N = 13) to 4e10vg cohort (293.5 days, N = 12), 2.6e10vg cohort (349.0 days, N = 13) and 2.6e9vg cohort (389.0 days, N = 13).
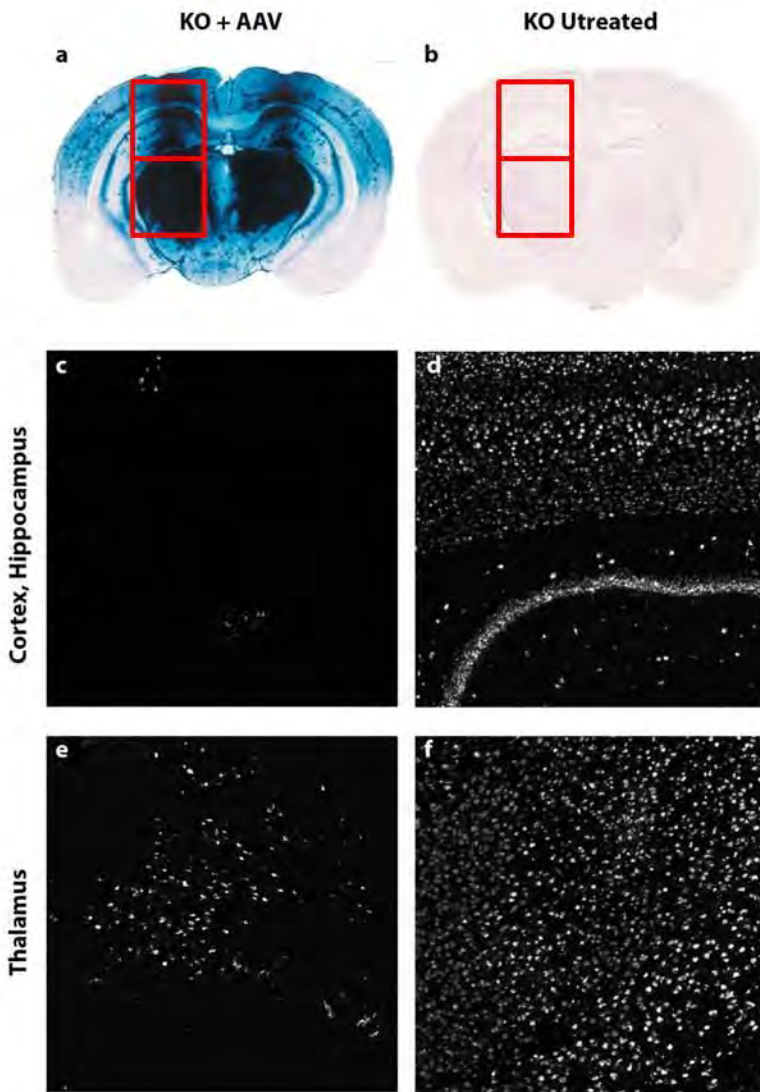
Figure 3.5 Intracranial injections of AAV in βgal$^{-/-}$ mice result in abnormal Filipin staining in areas of highest enzyme expression.

Figure 3.5 Intracranial injections of AAV in βgal$^{-/-}$ mice result in abnormal Filipin staining in areas of highest enzyme expression.

Coronal sections of mouse brain stained with Xgal (blue) for βgal enzyme presence and counterstained with Nuclear Fast Red (red) at 12 weeks post injection in (a) representative βgal$^{-/-}$ (KO + AAV) injected with 1μl of AAVrh8-CBA-mβgal-WPRE (2.6e10vg total dose) bilateral into the thalamus and (b) βgal$^{-/-}$ mouse untreated (KO Untreated). Red boxes represent location of pictures in (c)-(f), Filipin staining on adjacent brain sections in (c, e) βgal$^{-/-}$ animal treated with 2.6e10vg of AAVrh8-CBA-mβgal-WPRE or (d, f) a βgal$^{-/-}$ mouse untreated (KO Untreated). Filipin images taken at 10X magnification. . Images are representative of N ≥ 3 mice/group.

The presence of Filipin-positive cells in the thalamus of AAVrh8-injected $\beta gal^{-/-}$ mice was surprising as it is also the brain region that displays the most intense X-gal histochemical staining in the brain (Fig. 3.5a, red boxes), which we interpret as a semi-quantitative indicator of high βgal enzyme activity. In the spinal cord of long-lived AAV-treated mice (495-612 days) the impact on lysosomal storage was variable ranging from regions with very few remaining Filipin-positive cells to regions with no apparent change compared to untreated $\beta gal^{-/-}$ controls (Fig. 3.6a, d, f and b, c, e, respectively).

Neuropathology at the injection sites

Animals were histologically assessed with Hematoxylin & Eosin (H&E) after early loss or at 3 months post injection. These animals were found to have morphological changes at the injection site that correlated with dose. $\beta gal^{-/-} +$ AAV 4e10vg at 2 weeks post injection demonstrated large amounts of changes in the thalamus such as vascular cuffing (large amount of cells with small nuclei surrounding a blood vesicle) and the appearance of inflammation (concentration of cells with small nuclei) (Fig. 3.7a & b, thick and thin arrows, respectively), and in the DCN with vascular cuffing and apparent neuronal engulfment (Fig. 3.8a, thick arrow and b, arrow heads, respectively). In $\beta gal^{-/-} +$ AAV 2e10vg at 3 months post-treatment thalamic alterations were also seen with vascular cuffing and inflammation (Fig. 3.7e & f, thick and thin arrows, respectively). However,
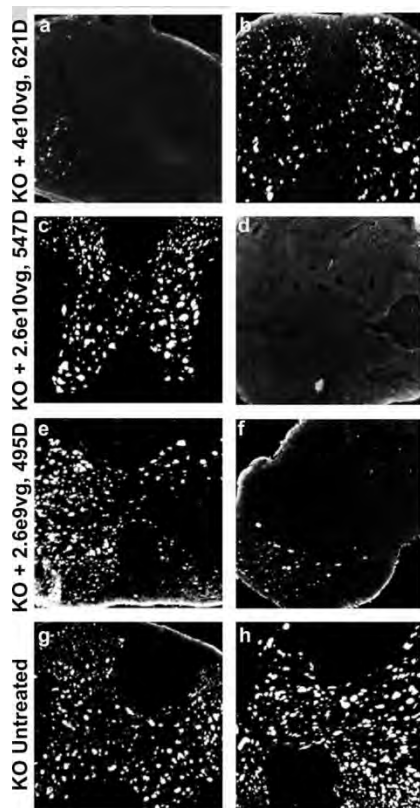
Figure 3.6 Lysosomal storage persists in the spinal cords of long-lived AAV intracranial injected βgal$^{-/-}$ mice

Spinal cord sections cut at 20μm were stained with Filipin for GM1-ganglioside storage. All long-lived animals showed some amount of clearance in the spinal cord, but also contained regions where clearance did not occur. (a, b) 4e10vg at 621 days (c, d) 2.6e10vg at 547 days, (e, f) 2.6e9vg at 495 days and (g, h) Naïve βgal$^{-/-}$ ~250 days with storage throughout. Images are representative of N ≥ 2 mice/group.
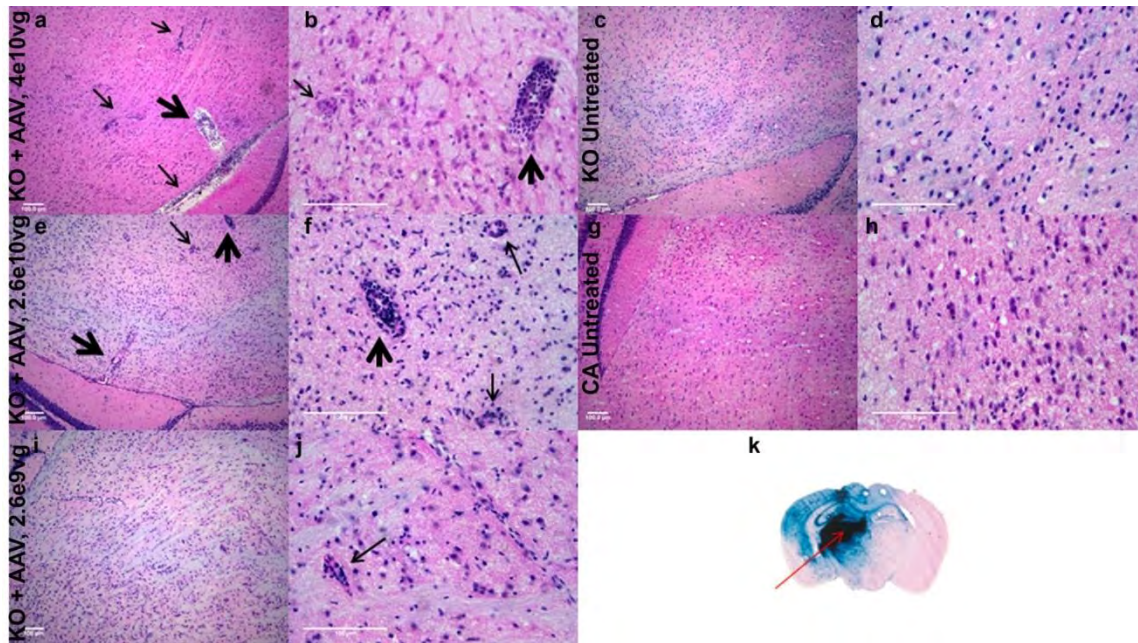
Figure 3.7 Intracranial injections of AAV in βgal$^{-/-}$ mice result in morphological changes at the site of injection in the thalamus

Figure 3.7 Intracranial injections of AAV in βgal$^{-/-}$ mice result in morphological changes at the site of injection in the thalamus

Intracranially injected βgal$^{-/-}$ mice were analyzed at 2 week (4e10vg) or 3 months (2.6e10vg and 2.6e9vg) post-injection by H&E staining of 20 μm coronal brain sections. Morphological changes in the injected region of the thalamus: thick arrow denotes vascular cuffing, thin arrow indicates inflammation. Left panel taken at 10x, right panel a 40x picture (from regions on the left panel). Morphological changes and neuronal loss appear to lessen at lowest inject dose. (a, b) 4e10vg at 2 weeks post-treatment (e, f) 2.6e10vg at 3 months post-treatment, (i, j) 2.6e9vg at 3 months post-treatment, (c, d) Naïve βgal$^{+/-}$ at age of treated animals, (e, f) Naïve βgal$^{-/-}$ at age of treated animals, (k) example cerebrum injected with AAVrh8-mβgal. Red arrow indicates injection site in βgal animals and location of pictures shown here. Scale bar represents 100um. Images are representative of N ≥ 3 mice/group.
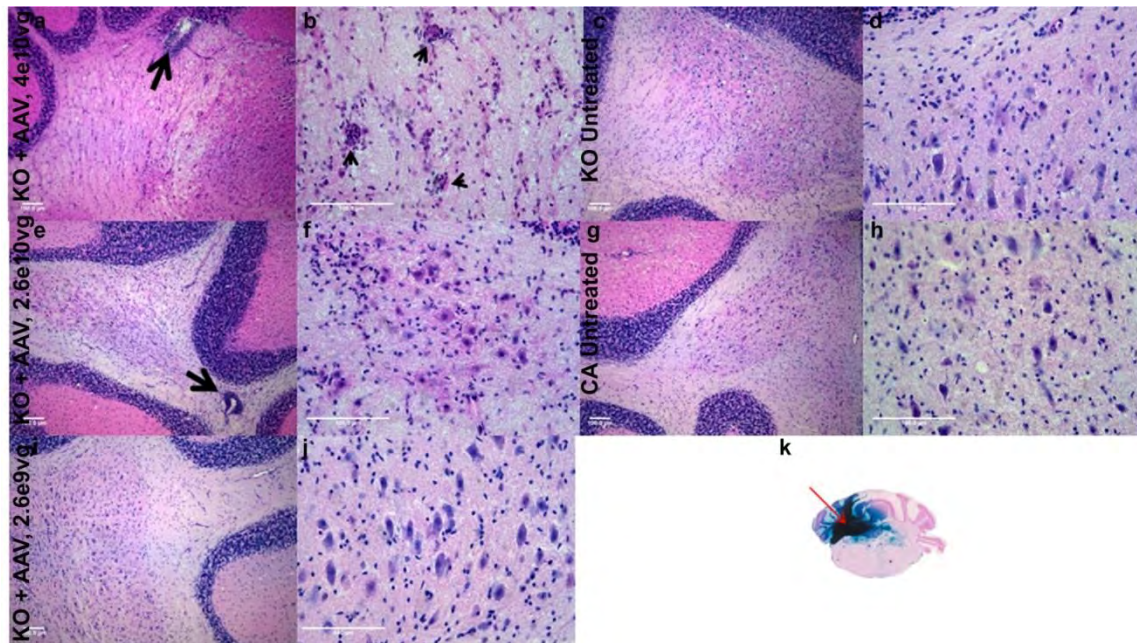
Figure 3.8 Intracranial injections of AAV in βgal$^{-/-}$ mice result in morphological changes at the site of injection in the deep cerebellar nuclei

Figure 3.8 Intracranial injections of AAV in βgal$^{-/-}$ mice result in morphological changes at the site of injection in the deep cerebellar nuclei

Intracranially injected βgal$^{-/-}$ mice were analyzed at 2 week (4e10vg) or 3 months (2.6e10vg and 2.6e9vg) post-injection by H&E staining of 20 μm coronal brain sections. Morphological changes noted in the injected region of the DCN. Thick arrow denotes vascular cuffing. Arrowhead indicates suspected neuronal engulfment. Left panel taken at 10x, right panel at 40x (from regions depicted on the left panel). Morphological changes and neuronal loss appear to lessen at lowest inject dose. (a, b) 4e10vg at 2 weeks post-treatment (e, f) 2.6e10vg at 3 months post-treatment, (i, j) 2.6e9vg at 3 months post-treatment, (c, d) Naïve βgal$^{+/-}$ at age of treated animals, (e, f) Naïve βgal$^{-/-}$ at age of treated animals, (k) example DCN injected with AAVrh8-mβgal. Red arrow indicates injection site in βgal animals and location of pictures shown here. Scale bar represents 100um. Images are representative of N ≥ 3 mice/group.

βgal$^{-/-}$ + AAV 2e10vg dose in the DCN had less vascular cuffing only (Fig. 3.8e,

thick arrow). In the lowest dose representative animal, βgal$^{-/-}$ + AAV 2e9vg at 3

months post injection only very minimal inflammation was seen in the thalamus

(Fig. 3.7j, thin arrow) and this effect was absent in the DCN (Fig. 3.8i & j).

Neither vascular cuffing nor inflammation was seen in untreated βgal$^{-/-}$ controls

(Fig. 3.7c, d and Fig. 3.8c, d) or in untreated βgal$^{+/-}$ controls (Fig. 3.7g, h and Fig.

3.8g, h).

High levels of βgal induce an unexpected response in injected brain structure.

The paradoxical presence of Filipin-positive cells at the injection sites (Fig.

3.5c, e) could be the result of treatment failure, or an unexpected response to

AAV gene transfer in βgal$^{-/-}$ mice. To understand this phenomenon, normal,

unaffected βgal$^{+/-}$ littermates were injected intracranially with AAVrh8 vector to

distinguish between those two possibilities. Similar to the results in βgal$^{-/-}$ mice

(Fig. 3.5c & e), large numbers of Filipin-positive cells were present in brain

regions with the highest βgal staining intensity (Fig. 3.9a, b) in AAVrh8-injected

βgal$^{+/-}$ mice (Fig. 3.9d, g, j). This result indicates that the presence of Filipin-

positive cells in the targeted brain structures is an unexpected adverse response

to an aspect of AAV gene transfer.
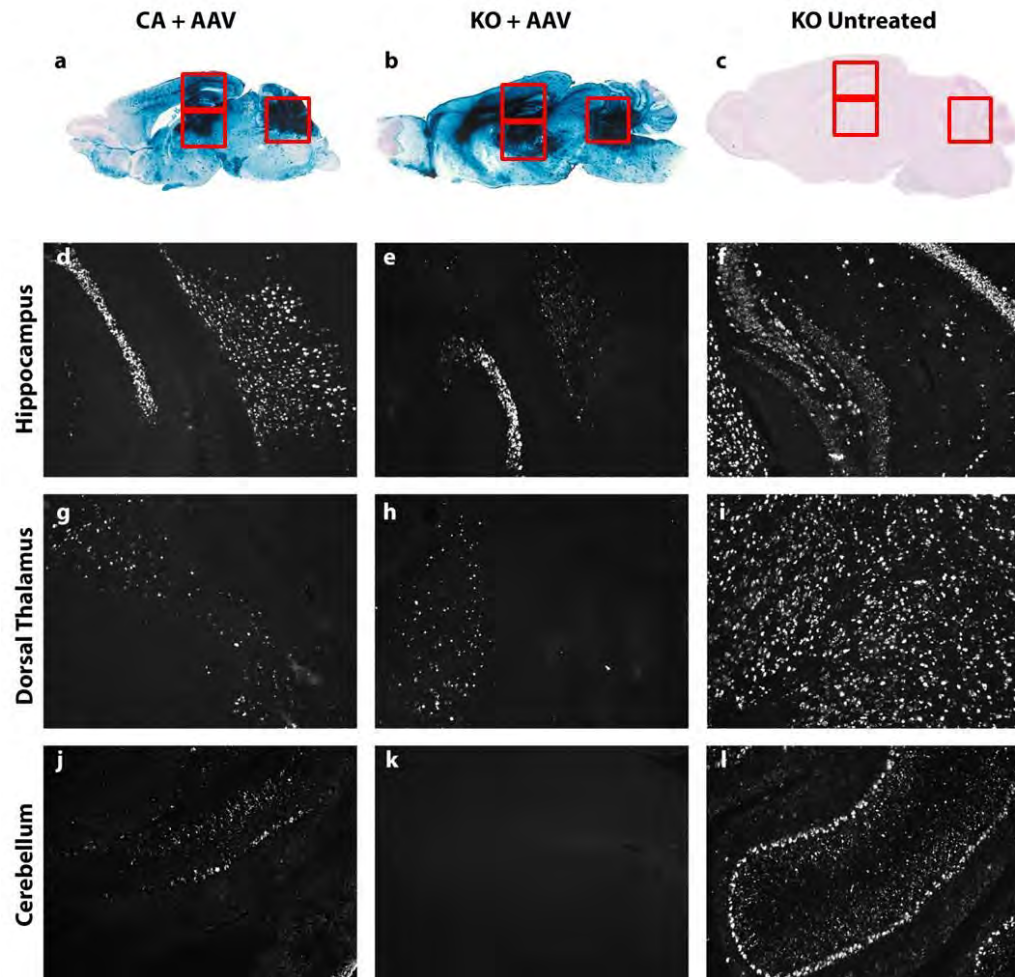
Figure 3.9 Intracranial injections of AAV in βgal$^{+/-}$ and βgal$^{-/-}$ mice result in abnormal Filipin staining in areas of most intense enzyme expression.

Figure 3.9 Intracranial injections of AAV in βgal$^{+/-}$ and βgal$^{-/-}$ mice result in abnormal Filipin staining in areas of most intense enzyme expression.

Sagittal sections of mouse brain stained with Xgal (blue) for βgal enzyme presence and counterstained with Nuclear Fast Red (red) at 10 weeks post injection in representative (a) βgal$^{+/-}$ (CA + AAV) (b) βgal$^{-/-}$ (KO + AAV) injected with 1μl of AAVrh8-CBA-mβgal-WPRE at 1.7x10^{12}vg/μl bilateral into the thalamus, 2ul into intracerebral ventricles and 0.3ul in the deep cerebellar nuclei, and (c) βgal$^{-/-}$ mouse untreated (KO Untreated). Red boxes represent location of pictures in (d)-(i). Filipin staining was positive in regions of most intense enzyme expression in both (d, g, j) βgal$^{+/-}$ (CA + AAV) (e, h, k) βgal$^{-/-}$ (KO + AAV) injected animals. (f, i, l) βgal$^{-/-}$ mouse untreated (KO Untreated) had no change in Filipin content. Filipin staining on brain sections taken at 10X magnification. Images are representative of N ≥ 3 mice/group.

Validation of AAVrh8 vector series to assess contribution of enzyme activity, protein levels, and AAVrh8 capsid to Filipin-detected response.

A series of AAVrh8 vectors were designed to understand the nature of this unexpected response at the injection sites (Table 3.1). This series of AAVrh8 consisted in sequential removal of elements that influence transgene expression levels in the original vector, AAVrh8-CBA-mβgal-WPRE, which will be referred to as 'CBA-WPRE' from here on. In vector 2 'CBA', the woodchuck hepatitis virus post-transcriptional regulatory element (WPRE) was removed. Vector 3 'CBA-EI-WPRE' has the exact same backbone as vector 1 but encodes a βgal protein carrying an E269Q mutation in the putative active site (8, 17). This vector was designed to assess whether the observed response was caused by enzymatic activity or protein production. Vector 4 'CB6' contained mβgal cDNA, but did not carry WPRE or the chimeric intron present in the other vectors. This vector was tested at two doses, 'CB6 Low' (same dose as all other vectors), and 'CB6 High' **(**2.0e10vg). Vector 5 'transgene empty' or 'T. Empty' contained all components of vector 1, but lacked the mβgal cDNA.

The newly constructed AAVrh8 vectors were injected bilaterally into the thalamus of normal βgal$^{+/-}$ mice (1 µl/site for total dose of 3.4e9vg), except the CB6 vector, which was also injected at a higher dose (1 µl/site for total dose of 2.0e10vg). Controls were βgal$^{+/-}$ mice injected with phosphate buffered saline (PBS), and naïve βgal$^{+/-}$ mice. Enzyme activity and protein production in the

1) CBA-mβgal-WPRE, **CBA-WPRE** – original vector
2) CBA-mβgal (no WPRE), **CBA** – decrease enzyme expression
3) CBA-enzyme inactive mβgal-WPRE, **CBA-EI-WPRE** – eliminate enzyme function
4) CB6-mβgal (no WPRE), **CB6** – further decrease enzyme expression
5) Transgene empty, **T. Empty** – eliminate protein expression
6) PBS injection, **PBS** – control for surgery
7) Untreated βGal$^{+/-}$, **CA Untreated**

Table 3.1 List of alterations in vectors designed to evaluate storage biomarker Filipin persistence
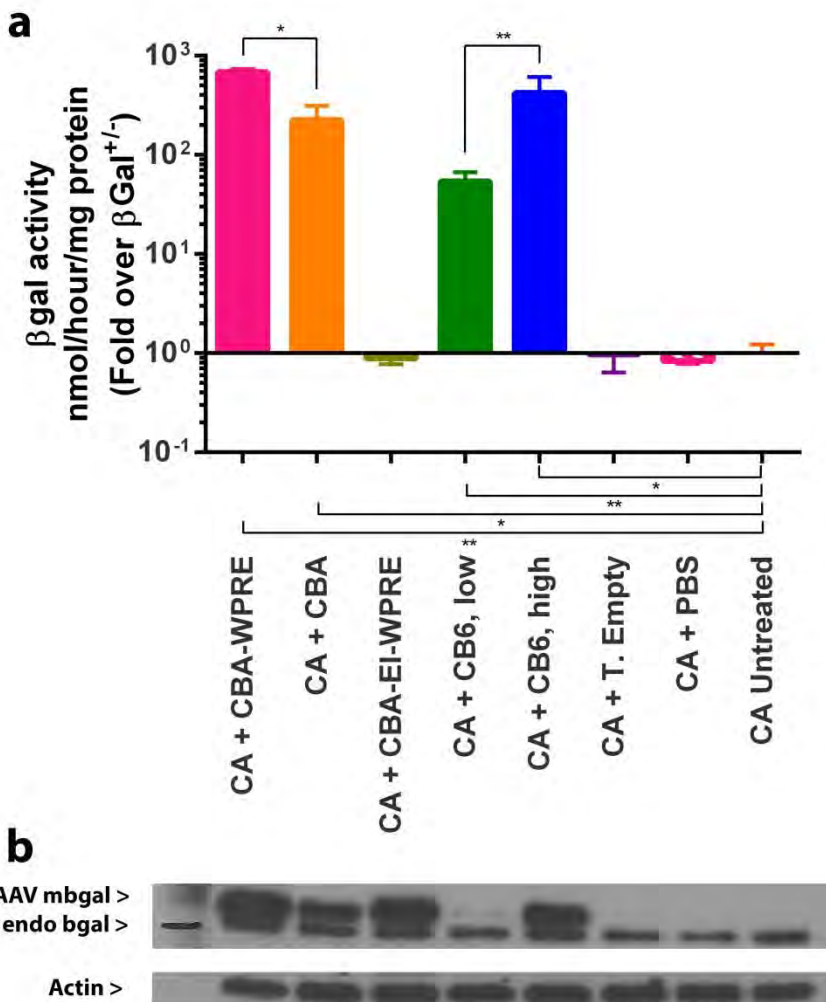
Figure 3.10 Alterations in vector design lead to a changes in βgal protein presence and/or enzyme activity in βgal$^{+/-}$ mice

Figure 3.10 Alterations in vector design lead to a decrease in βgal protein presence and/or enzyme activity in βgal$^{+/-}$ mice.

(a) βgal enzyme activity in 2mm x 2mm biopsy punches in injected structures. 1μl of AAVrh8-vector (total dose 3.4e9vg, or 2.0e10vg, CB6 High only) or mock treated PBS bilateral into the thalamus, as determined by 4-MU assay at ~6 weeks post injections. Enzyme activity is normalized to protein concentration by Bradford, and is reported as nmol/hour/mg protein. Error bars represent mean + SD, N = 3/group, and * indicates significant difference of βgal$^{+/-}$ + AAV (CA + *vector name*) vs. βgal$^{+/-}$ Untreated (CA Untreated) or as indicated by connecting line. P value calculated using unpaired multiple T tests (Holm-Sidak) where * = $p < 0.05$, ** = $p < 0.01$, and *** = $p < 0.001$. (b) Endogenous βgal protein presence as determined by Western blot which appears at 67kd, where transgene expression from the AAV vector appears as a higher weight band. Loading control is Actin appearing at 42kd. Western blot shown is representative of N = 3 blots ran. Samples analyzed for enzyme activity (a) are from either the contralateral side of animals in (b) or from injected animals in the same cohort .

thalamus were measured by 4-methylumbelliferyl (4-MU) biochemical assay and western blot 6 weeks after injection (Fig. 3.10).

The CBA-WPRE vector generated the highest enzyme activity at 686 fold above that in thalamus of naïve βgal$^{+/-}$ mice (Fig. 3.10a), and corresponding elevation in protein (Fig. 3.10b, lane 1). The CBA vector resulted in βgal activity 224 fold over βgal$^{+/-}$ level, which was significantly lower than that obtained with CBA-WPRE vector (Fig. 3.10a, orange bar, p = 0.001) and an apparent corresponding decrease in protein product (Fig. 3.10b, lane 2). In thalami of mice injected with CBA-EI-WPRE vector the βgal activity was comparable to that in naïve control mice (Fig. 3.10a), but the protein was expressed at comparable levels to those in CBA-WPRE injected thalami (Fig. 3.10b, lane 3 vs. lane 1). Therefore, the E269Q mutation abrogates enzyme activity but does not seem to affect protein expression levels. Injection of CB6 vector at the same dose as the other vectors (CB6-Low) resulted in βgal activity 54 fold above over βgal$^{+/-}$ level (Fig. 3.4a, green bar), and protein presence at a correspondingly lower amount that with the other vectors (Fig. 3.10b, lane 4). Injection of this vector at higher dose (CB6-High) resulted βgal activity 420 fold above over βgal$^{+/-}$ level, which is significantly higher than in the CB6-Low cohort (Fig. 3.10a-b, p = 0.03). The βgal activity level in the CB6-High cohort was comparable to that measured in the CBA-WPRE cohort, and appeared similar in protein levels (Fig. 3.10a-b, blue bar & lane 1 vs. pink bar & lane 5). The thalami of animals injected with transgene empty vector (T. Empty) or PBS showed no change in βgal activity or protein
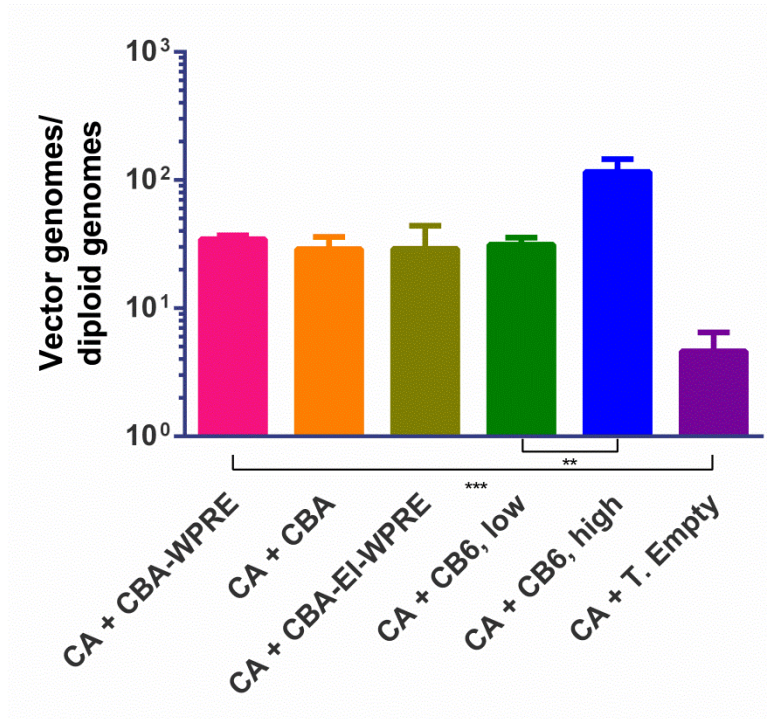
Figure 3.11 Vector genome presence in injected structure biopsy punches in βgal$^{+/-}$ mice

Vector genomes per diploid genome in a 2mm x 2mm biopsy punches in injected structure where 1µl of AAVrh8-vector (total dose 3.4e9vg, or 2.0e10vg, CBA High only) bilateral into the thalamus of βgal$^{+/-}$ mice (CA + *vector name*) as determined by qPCR to the SV40 poly A on the transgene. Samples were taken at 6 weeks post injection. Error bars represent mean + SD, N=3/group, and * indicates significant difference indicated by connecting line and using unpaired multiple T tests (Holm-Sidak) where * = $p < 0.05$, ** = $p < 0.01$ and *** = $p < 0.001$.

level compared to naïve βgal$^{+/-}$ levels (Fig. 3.10a-b). The number of vector

genome copies in AAV-injected thalami were shown to be comparable in most

cohorts injected with a total dose of 3.4e9 vg, except in the T.empty cohort (Fig.

3.11). As expected, the CB6-High cohort infused with 2.0e10 vg showed

significantly increased number of vector genome copies (Fig. 3.11, blue bar).

Filipin-detected response correlates with protein levels.

The brains of AAVrh8-injected and control βgal$^{+/-}$ mice were analyzed for

βgal enzymatic activity by Xgal staining (Fig. 3.12a, d, g, j, m, p, s) and for

presence or absence of Filipin-positive cells in the thalamus (Fig. 3.12b, e, h, k,

n, q, t).. The thalamic regions with the most intense βgal staining (Fig. 3.11a & d,

red boxes) also contained Filipin-positive cells in CBA-WPRE and CBA injected

animals, albeit at apparently lower numbers in the latter cohort (Fig. 3.11b, e).

The thalami in the CBA-EI-WPRE cohort had large numbers of Filipin-positive

cells, but no active βgal enzyme (Fig. 3.11k & j, respectively). Similar Filipin

staining was apparent in the thalami of T-empty and CB6-low cohorts (Fig. 3.11 k

&q), but it appeared as small puncta distinct from the pattern observed in the

CBA-WPRE and CBA-EI-WPRE cohorts. Filipin staining was also observed in

the thalami of CB6-High cohort and the pattern appeared a mix of that observed

in the CBA-WPRE and CB6-Low cohorts (Fig. 3.11h). These results suggest the
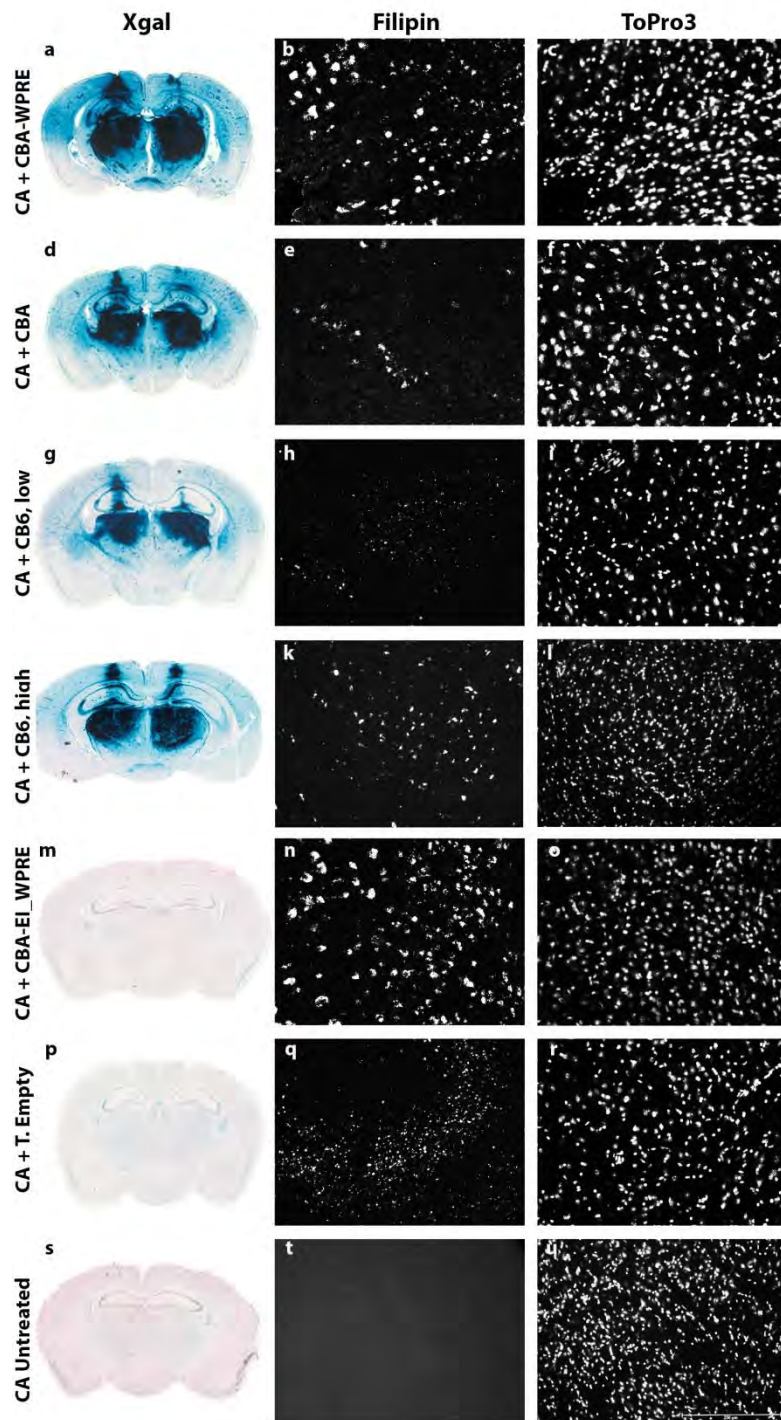
Figure 3.12 Vectors with decreasing protein presence lead to decrease in Filipin positive regions in βgal$^{+/-}$ mice

Figure 3.12 Vectors with decreasing protein presence lead to decrease in Filipin positive regions in βgal⁺/⁻ mice.

Coronal sections of mouse brain stained with Xgal (blue) for βgal enzyme presence and counterstained with Nuclear Fast Red (red) at 6 weeks post injection in (a, d, g, j, m, p) in representative βgal⁺/⁻ (CA + *vector name*) injected with 1µl of AAVrh8-vector (total dose 3.4e9vg, or 2.0e10vg in the CBA High only) bilaterally into the thalamus or βgal⁺/⁻ un-injected (CA Untreated). (b, e, h, k, n, q) Filipin staining and ToPro3 nuclear stain (c, f, i, l, o, r) in parallel sections of the same animals in (a, d, g, j, m, p). Red boxes represent approximate location of pictures in (b, c, e, f, h, i, k, l, n, o, q, r) Filipin and ToPro3 staining on brain sections taken at 20x magnification. Scale bar = 250 µm. Images are representative of N ≥ 2 mice/group.

abnormal Filipin accumulation at the injection site is related to protein expression levels and not enzyme activity.

Transcriptomic changes in injected thalami correlate with Filipin-detected abnormal response.

Microarray analysis was performed in the thalami to further characterize the tissue response to this apparent pathological change induced by gene transfer. Total thalamic RNA was isolated from CBA-mβgal-WPRE, CB6-Low, T.Empty and PBS-injected cohorts. Transcriptomic changes (fold change > 1.8-fold, $p<0.05$) for all samples analyzed are represented in a heat map (Fig. 3.13a). CB6-low and T.Empty samples cluster together with PBS, and are different from CBA-WPRE samples. The number of genes with >2-fold change in expression levels ($p<0.05$) is considerably larger in CBA-WPRE samples compared to CB6 and T.Empty with a few overlapping genes (Fig. 3.13b). A number of genes up-regulated in the CBA-WPRE samples are characteristic of activated microglia and reactive astrocytes (Table 3.2). None of these genes showed significant changes in CB6 or T.Empty samples.
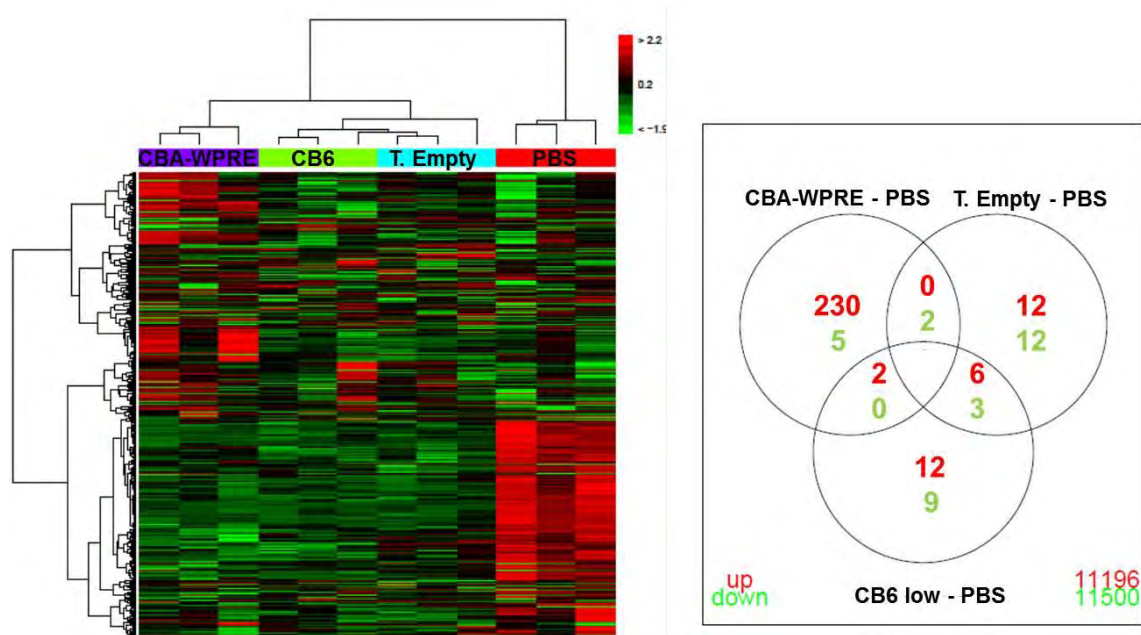
Figure 3.13 Clustering heatmap and Venn diagram of all differentially expressed genes in βGal$^{+/-}$ mice demonstrate transgene expression dependent variation.

(a) Heatmap and (b) Venn diagram of all differentially expressed genes from a 2mm x 2mm biopsy punch of thalamus injected with 1 µl of AAVrh8-vector (3.4e9vg total dose) or mock treated with PBS bilaterally, at ~6 weeks post injection in βgal$^{+/-}$ mice (CA + *vector name).* Microarray results determined by Affymetrix Mouse Gene 2.0ST, N = 3/group, P<0.05 and >1.8 fold change.

Genes upregulated in CBA-WPRE				
Gene	Gene name	Function	Fold change	Reference
Serpina3n	serine (or cysteine) peptidase inhibitor, clade A	Peptidase inhibitor, response to cytokine, marker of reactive gliosis	1.9	Winkler *et al*, 2005; Zamanian *et al*, 2012
Gbp3	guanylate binding protein 3	Response to interferon β, response to interferon γ, upregulated in LPS reactive astrocytes	3.2	Burckstummer *et al*, 2009; Degrandi *et al*, 2007; Zamanian *et al*, 2012
B2m	beta-2-microglobulin	Antigen processing and presentation, cellular defense response, upregulated in LPS reactive astrocytes	2.2	Uginovic *et al*, 2005; Zijilstra *et al*, 1989; Zamanian *et al*, 2012
Cd86	Cd86 antigen	Costimulatory ligand, upregulated in SOD1^{G93A} microglia	2.3	Chiu *et al*, 2013
Trem2	triggering receptor expressed on myeloid cells 2	Transmembrane protein - triggers myeloid cells, increase phagocytic activity, supress cytokine production, upreglated in SOD1^{G93A} microglia	3.0	Melchior *et al,* 2010; Trash *et al,* 2009; Chiu et al, 2013
C1qa	complement component 1, subcomponent, alpha polypeptide	Complement activiation, upregulated in SOD1^{G93A} microglia	3.0	Azeredo da Silveira *et al*, 2002; Chiu *et al*, 2013
Gfap	glia fibrillary acidic protein	Marker of reactive gliosis, upregulated in SOD1^{G93A} microglia	3.6	Jessen & Mirsky, 1980; Chiu et al, 2013
Cybb	cytochrome b-245, beta polypeptide	Proinflammatory oxidase, upregulated in SOD1^{G93A} microglia	4.8	Harraz *et al*, 2008; Chiu et al, 2013

Table 3.2 Select genes upregulated in microarray analysis of the CBA-WPRE vector. Fold change is CBA-WPRE vector over PBS.

Therapeutic impact of different AAVrh8 vectors in GM1-gangliosidosis mice

From the studies performed in βgal$^{+/-}$ mice above, a correlation was determined that reduced protein expression from the transgene could reduce the pathological transcription level changes in the injected structure. We then sought to determine if the changes in AAV vector design translated into differences in therapeutic outcome in GM1-gangliosidosis mice (βgal$^{-/-}$). Six to eight week old βgal$^{-/-}$ mice received bilateral injections of AAV vector into thalamus (1 µl/side) and deep cerebellar nuclei (0.3 µl/side) and the outcomes measured at ~ 6 weeks post-injection. Study cohorts were βgal$^{-/-}$ mice injected with CBA-WPRE, CB6 (CB6-Low), and Transgene Empty vectors administered at a total dose of 4.4e9vg. In addition, CB6 was injected at a total dose of 2.6e10vg (CB6-High). Naïve untreated βgal$^{-/-}$ and βgal$^{+/+}$ animals were used as controls. Evaluation of βgal activity by 4-MU assay of the CNS (Fig. 3.14) showed that in the cerebrum CBA-WPRE was 45-fold higher than wild type level (Fig. 3.14, orange bar), where CB6 Low was 9-fold higher (Fig. 3.14, olive bars) and CB6 High was 30-fold higher (Fig. 3.14, green bar). As expected T.Empty and untreated cohorts of βgal$^{-/-}$ mice had no detectable βgal activity in any CNS region analyzed (Fig. 3.14, blue and purple bars, respectively). In the cerebellum + brainstem the trend was the same, with CBA-WPRE at 47-fold (Fig. 3.14, orange bar), CB6-Low at 6-fold (Fig. 3.14, olive bar), and CB6-High at 27-fold above wild type level (Fig. 3.14, green bar). Interestingly, in the spinal cord CBA-WPRE was only 50% of wild type level (Fig. 3.14, orange bar), CB6-High was 30% (Fig. 3.14, olive
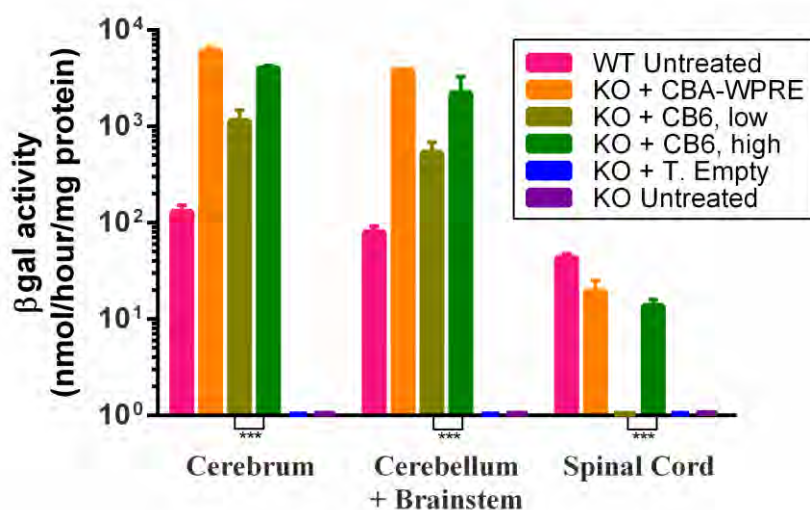
Figure 3.14 Varied anatomical distribution of βgal enzyme activity in the CNS of treated βgal$^{-/-}$ mice

βgal enzyme activity in cerebrum, cerebellum + brainstem or spinal cord of βgal$^{-/-}$ injected bilaterally 1µl into the thalamus and 0.3ul in the DCN of AAVrh8-vector (total dose 3.4e9vg, or 2.0e10vg, CBA High only) or untreated (KO Untreated) or βgal$^{+/+}$ mice untreated (WT Untreated), as determined by 4-MU assay at ~6 weeks post injections. Enzyme activity is normalized to protein concentration by Bradford, and is reported as nmol/hour/mg protein. Values represent mean + SD, N = 3/group, and * indicates significant difference of βgal$^{-/-}$ + AAVrh8-CB6 vector (total dose 3.4e9vg, KO + CB6 Low) vs. βgal$^{-/--}$ + AAVrh8-CB6 vector (total dose 2.0e10vg, KO + CB6 High). P value calculated using unpaired T tests (Holm-Sidak) where *** = p<0.001.

bar), and CB6-Low had no detectable activity (Fig. 3.14, green bar). In all CNS

tissues analyzed, CB6-High was significantly higher ($p < 0.001$) in βgal activity

than the same vector injected at the lower dose, CB6-Low.

The βgal distribution pattern in the brain as exemplified by histological

stain X-gal (Fig. 3.15) correlated with the activity levels in the cerebrum or

cerebellum + brainstem determined by the 4-Mu assay (Fig. 3.14). The CBA-

WPRE vector resulted in dark blue staining in thalamus and DCN and

widespread distribution of detectable enzyme activity throughout the brain (Fig.

3.15a). In contrast, in the CB6-Low cohort (Fig. 3.15b) there was intense

staining in thalamus and DCN but lower detectable levels throughout the

cerebrum, cerebellum or brainstem. In CB6-High animals, the βgal pattern of

distribution in brain appeared broader than in CB6-Low animals (Fig. 3.15c). As

anticipated, there was no evidence of increased βgal activity in T.Empty (Fig.

3.15d) and naïve βgal$^{-/-}$ mouse cohorts (Fig. 3.15e).

Results of histological analysis of lysosomal storage in brain and spinal

cord using Filipin staining (Fig. 3.16) paralleled the βgal activities (Fig. 3.14) and

distribution patterns (Fig. 3.15) described above. In CBA-WPRE injected

animals, there was nearly complete clearance of storage throughout the brain

(Fig. 3.16a-g), except at the injection site and track with Filipin-positive cells in

ventral hippocampus and throughout the thalamus (Fig. 3.16, d, respectively,

arrows). Storage clearance in the CB6-Low cohort appeared less efficient

| a KO + CBA-WPRE | b KO + CB6, low | c KO + CB6, high |
| d KO + T. Empty | e KO Untreated | f CA Untreated |
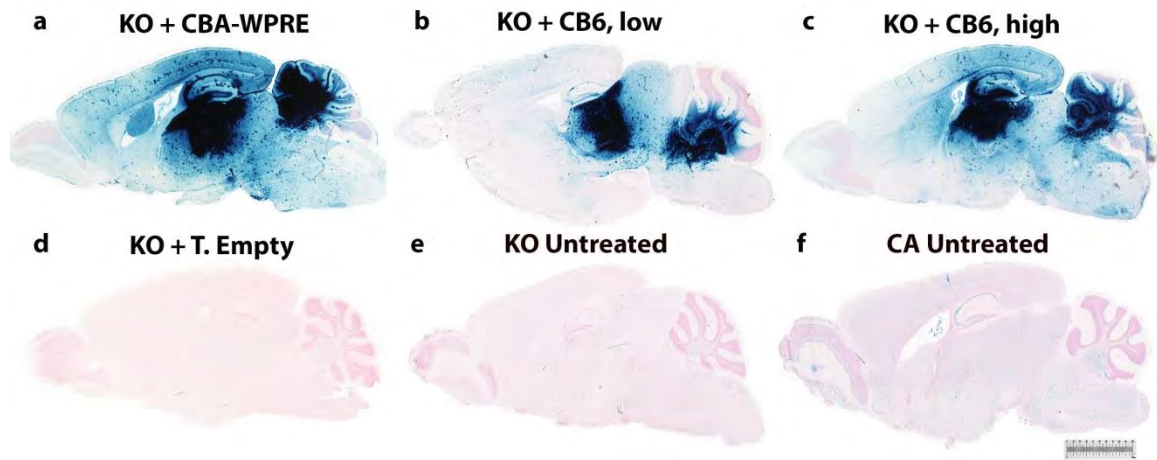
Fig 3.15 Xgal staining for βgal enzyme presence in βgal$^{-/-}$ mice demonstrates spread of enzyme throughout the brain in an expression and dose dependent manner

Sagittal sections of mouse brain stained with Xgal (blue) for βgal enzyme activity and counterstained with Nuclear Fast Red (red) at ~6 weeks post injection in a representative βgal$^{-/-}$ injected bilaterally with 1µl into the thalamus and 0.3ul in the DCN of AAVrh8-vector (total dose 3.4e9vg, or 2.0e10vg for the CBA High only), or untreated (KO Untreated) or βgal$^{+/-}$ mice untreated (CA Untreated). N = 2-3/group. Scale bar = 10mm.
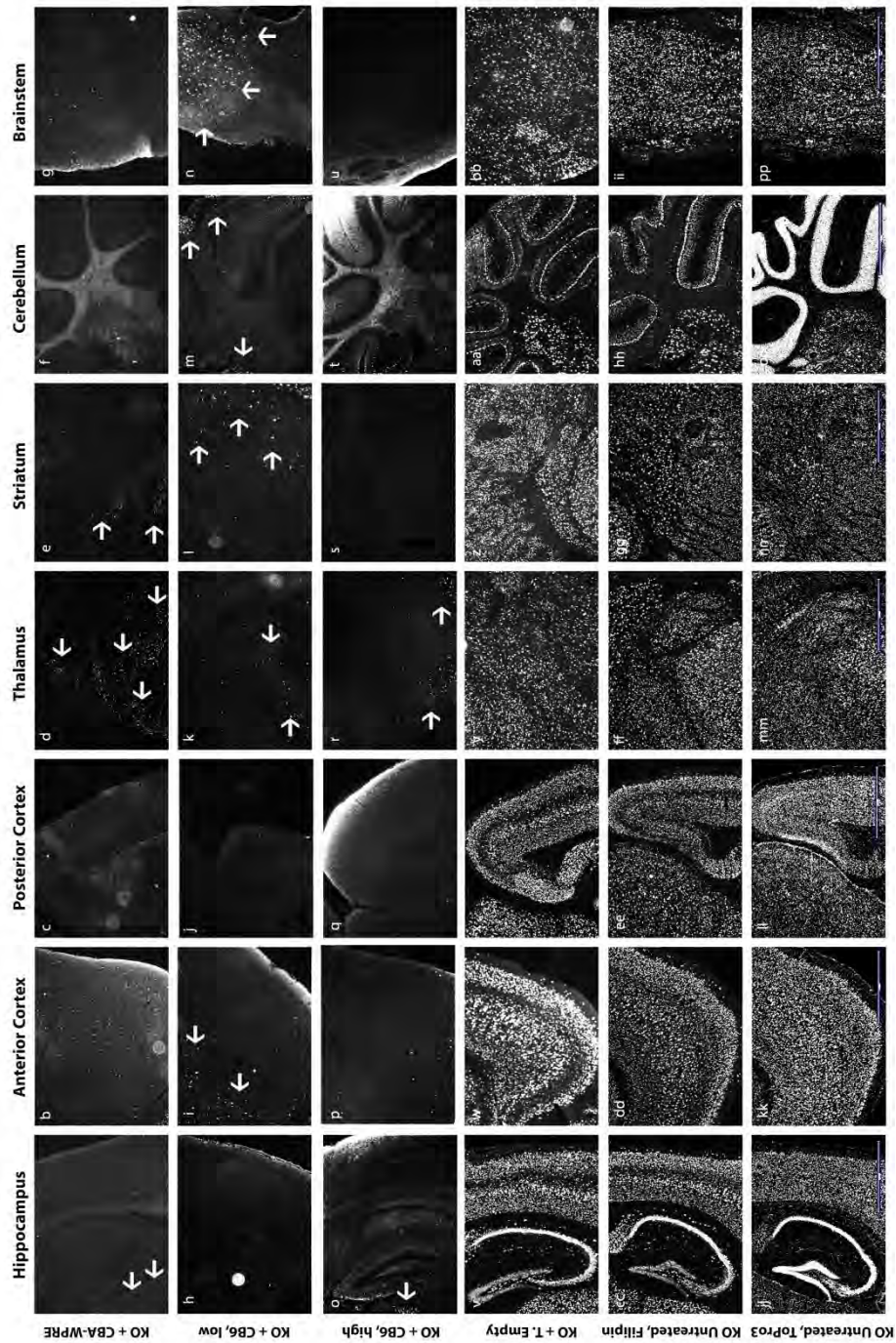
Figure 3.16 Filipin staining for GM1-ganglioside content in the brain of βgal^{-/-} mice after therapeutic AAVrh8 treatment

Figure 3.16 Filipin staining for GM1-ganglioside content in the brain of βgal^{-/-} mice after therapeutic AAVrh8 treatment

Sagittal sections of mouse brain stained with Filipin for GM1 content or nuclear stain ToPro3 (KO Untreated, ToPro3, bottom row) at 6 weeks post injection in a representative βgal$^{-/-}$ injected bilaterally with 1μl into the thalamus and 0.3ul in the DCN of AAVrh8-vector (total dose 3.4e9vg, or 2.0e10vg, CBA High only), or untreated (KO Untreated). N = 2-3/group. Images taken at 5X, scale = 100mm.
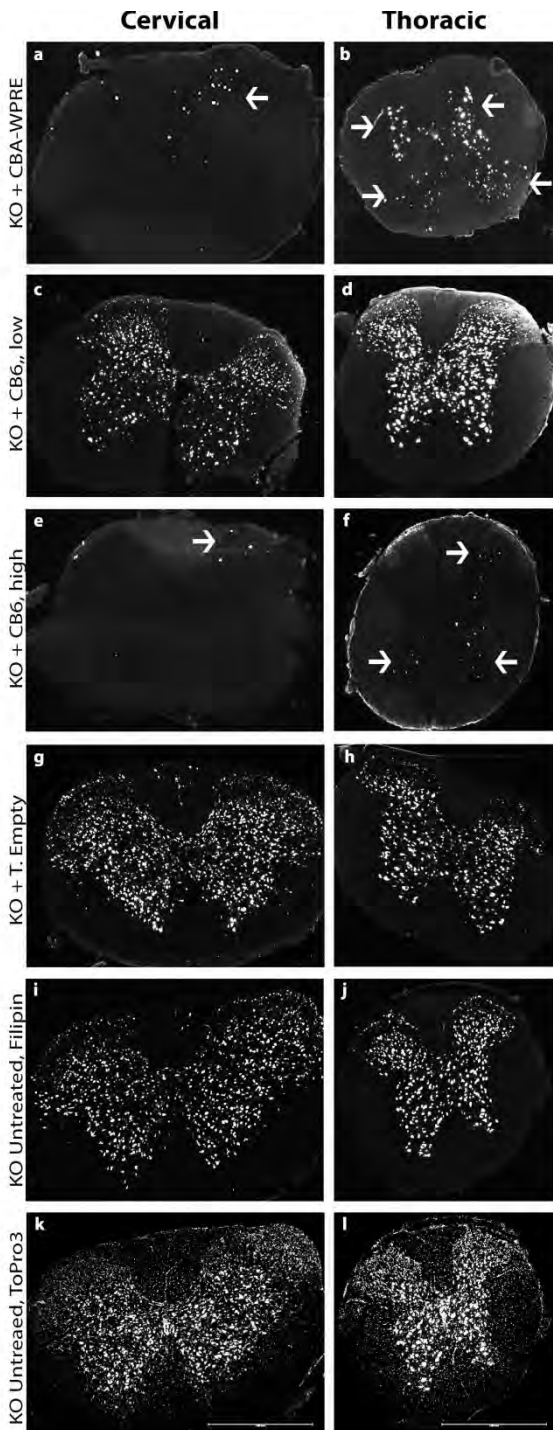
Figure 3.17 Filipin staining for GM1 content in spinal cords of βgal$^{-/-}$ mice after therapeutic treatment with AAVrh8 vectors

Figure 3.17 Filipin staining for GM1 content in spinal cords of βgal^{-/-} mice after therapeutic treatment with AAVrh8 vectors

Cervical and thoracic sections of spinal cord stained with Filipin for GM1 content or nuclear stain ToPro3 (KO Untreated, ToPro3, bottom row) at 6 weeks post injection in representative βgal^{-/-} injected bilaterally with 1µl into the thalamus and 0.3ul in the DCN of AAVrh8-vector (total dose 3.4e9vg, or 2.0e10vg, CBA High only), or untreated (KO Untreated). N = 2-3/group. Images taken at 5X, scale = 100mm.

(Fig. 3.16h-n) as Filipin-positive cells were still present in anterior cortex, striatum and brainstem (Fig. 3.16i, l, n, respectively, arrows). At the higher dose (CB6-High) the efficiency of CB6 vector was very high with resolution of lysosomal storage throughout the brain (Fig. 3.16o-u). As before, Filipin-positive cells were present in ventral hippocampus and dorsal thalamus, however less then in CBA-WPRE (Fig. 3.16o, r, respectively, arrows). The T.Empty cohort (Fig. 3.16v-bb) showed no change in lysosomal storage compared to βgal$^{-/-}$ untreated controls (Fig. 3.17cc-ii).

The spinal cords of AAV-treated animals were also evaluated for storage content by Filipin staining. Spinal cords in CBA-WPRE animals had almost no remaining storage in the cervical region however, the thoracic region only showed minimal reduction (Fig. 3.17a-b, respectively, arrows). Spinal cords in CB6-Low animals had almost no distinguishable reduction in storage compared to untreated controls (Fig. 3.17c-d). Spinal cords in CB6-High animals were nearly devoid of lysosomal storage in cervical and thoracic regions (Fig. 3.17e-f, arrows). As anticipated, the spinal cords of T.Empty animals showed no change in lysosomal storage compared to untreated βgal$^{-/-}$ control. (Fig. 3.17g-h and i-j, respectively).

GM1 ganglioside level in CNS was quantified by LC-MS/MS (Fig. 3.18). In CBA-WPRE and CB6-Low cohorts there was significant reduction in GM1 ganglioside content in comparison to untreated βgal$^{-/-}$ controls in cerebrum
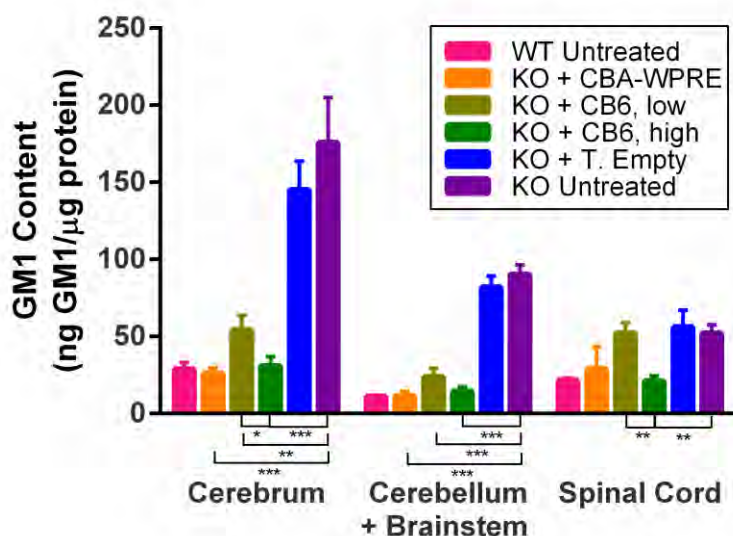
Figure 3.18 Therapeutic treatment using AAVrh8 in the CNS of βgal$^{-/-}$ mice result in normalization of GM1 content when treated with a lower expressing promoter at a higher dose.

GM1 content as quantitated by LC-MS/MS in cerebrum, cerebellum + brainstem or spinal cord of mice at. 6 weeks post injection in βgal$^{-/-}$ injected bilaterally with 1μl into the thalamus and 0.3ul in the DCN of AAVrh8-vector (total dose 3.4e9vg, or 2.0e10vg for the CBA High group only), untreated (KO Untreated), or βgal$^{+/-}$ untreated (WT Untreated). GM1 content represented as ng GM1/μg protein. Values represent mean + SD, N ≥ 3/group and * indicates significant difference of KO + AAVrh8 vs. KO + PBS, or as indicated by connecting line, using multiple T tests (Holm-Sidak) where * = $p < 0.05$, ** = $p < 0.01$, and *** = $p < 0.001$.

(p = 0.0009 and p = 0.002, respectively) and cerebellum + brainstem (p < 0.0001 and p = 0.0001, respectively). There was no significant change in GM1 ganglioside content in the spinal cord in either cohort. In the CB6-High cohort the GM1 ganglioside level was normalized in all CNS areas investigated cerebrum, cerebellum + brainstem, and spinal cord (Fig. 3.18, green bars, p = 0.64, p = 0.06 and p = 0.79 respectively). As anticipated, there was no change in GM1 ganglioside content anywhere in CNS in the T.Empty cohort compared to naïve βgal$^{-/-}$ controls (Fig. 3.18, blue and purple bars, respectively).

Discussion

Previous studies from our lab using intracranial injection of AAV gene therapy for GM1-gangliosidosis used an AAV1 vector delivered in neonates via the cerebral lateral ventricles (197) or injected bilaterally into thalamus and DCN in adult animals (198). These vectors were efficient at delivering high levels of active enzyme to the brain and provided a delay in disease onset (197), but were not effective at retaining motor function and only provided nominal increases in survival outcomes (198).

In this study we show that intracranial delivery of AAVrh8 into the thalamus and DCN of adult animals with total dose 4e10vg, 2.6e10vg, or 2.6e9vg successfully delivers enzyme to the brain (Fig 4.2), provides a significant but modest retention of motor function (Fig. 3.3) and significantly extends lifespan in

all groups (Fig 4.4) in a dose dependent manor. However, in the course of this work we also discovered an unusual occurrence where the histological stain indicating the storage of GM1 ganglioside, Filipin, was present at the areas of highest enzyme expression. In addition, this finding was consistent in both GM1 affected βgal$^{-/-}$ and non-disease carrying βgal$^{+/-}$ mice (Fig.4.5 and 4.9), which demonstrates that Filipin was responding in an abnormal manner and may be indicating a pathological finding. Further analysis of AAV treated βgal$^{-/-}$ mice showed that these animals displayed signs of neuropathology at the injection site of inflammation, vascular cuffing and apparent neuronal engulfment, which were lessened with decreasing vector, dose (Fig.4.7 and 4.8).

Dogma in the LSD field is to try and deliver the largest amount of transgene product to the CNS in order to obtain the best therapeutic outcome. . Utilizing the property of cross correction (85-88).and by injection of a viral vector into highly connected structures within the brain, it is believed that the largest therapeutic impact can be achieved. In addition, methods to enhance transgene output, vector spread throughout the tissue, and entry into the CNS are also employed. To this end, methods used include the application of ubiquitous promoters (199, 200, 233) (210) and post-translational elements (198-200, 228), capsid selection for tissue/cell tropism (231, 234), convection enhanced delivery (235, 236), injecting during the neonatal period when the blood-brain barrier (BBB) is not fully formed (197, 231), and blood-brain barrier disrupting agents such as mannitol (175, 235). In our current study we utilized many of these

parameters by injecting into the thalamus and DCN, using a broad transduction capsid and widely expressing promoter as well as a post transcriptional element. However, our results led to questioning the safety of such high expression in a sensitive tissue. The safety of overexpressing an LSD enzyme was previously evaluated by two papers from the Sly group investigating the transgenic overexpression of the enzyme β-glucuronidase (GUSB) in an animal model of the LSD mucopolysaccharidosis VII (MPS VII) in a mouse deficient of the active enzyme (237), and a following study with extreme overexpression in a non-diseasing carrying mouse model (238) . Interestingly, these studies indicated that no abnormal phenotypes were detected, the animals were fertile and mortality was not increased even in animals expressing 100-1000s fold increase of the enzyme (204).

Results from our current study suggest there may be an upper limit to tolerance of the CNS to enzyme expression levels as the neuropathological response at the injection site were dose-dependent. Gentner *et al.* support this hypothesis, as overexpression of a transgene product was detrimental in cultured cells of the lysosomal storage disorder, Globoid cell leukodystrophy (GLD) (179). In that study, a lentiviral infection of the missing galactocerebrosidase enzyme, but not a GFP expressing vector led to apoptosis (179). This work demonstrated that in particular cell populations, here hematopoietic stem and progenitor cells, over expression of the lysosomal enzyme led to deleterious effects. Salegio *et al.*, revealed a pathological response to enzyme over expression (239), A safety

study of the intracranially delivered AAV2 vector carrying the lysosomal enzyme

acid sphigomyelinase for the treatment of LDS Niemann-Pick disease in

nonhuman primates presented with dose related toxicity behavioral alterations,

histological alterations, and biochemical responses (239). Interestingly, this

effect was not found in AAV2-treated disease carrying rats. Also noteworthy is

that the primary substrate of this enzyme, sphingomyelin leads to further

breakdown products which are known signaling molecules in cell death and cell

survival pathways. Interestingly, in the safety study of the lysosomal enzyme β-

glucuronidase (GUSB), GUSB overexpression led to lysosomal storage of the

enzyme itself in peripheral tissues as well as the brain, but did not result in

neuropathology (237).

Using a series of AAVrh8 vectors that sequentially varied the amount of

protein and/or active enzyme in the system after intracranial injection we

evaluated the abnormal responses to mβgal overexpression (Table 3.1).

Modifications included removal of the post translational element, creation of an

inactive form of the mouse-β-galactosidase enzyme, a minimally expressing

promoter, and removal of the mβgal cDNA from the transgene. Analysis of direct

injection of these viral vectors into the thalami of βgal$^{+/-}$ mice determined a

protein expression dependent correlation to the abnormal Filipin. Abnormal

Filipin staining was detected from a highly expressed vector with an active

enzyme, CBA-mβgal-WPRE, as well as in a vector with the same backbone

carrying an inactive enzyme, CBA-E269Q-mβgal-WPRE, but was not seen in low expressing vector with active enzyme CB6-mβgal (Fig. 3.12).

Further elucidation of this process was provided by microarray analysis on punch biopsies from animals injected with vectors expressing mβgal at levels over βgal$^{+/-}$ levels of 686 fold (CBA-mβgal-WPRE), 54 fold (CB6-mβgal), no additional expression (CBA-transgene empty-WPRE), and mock-injected (PBS). Microarray results (Fig. 3.13a-b) showed that CBA-WPRE provided the biggest response with 232 genes upregulated and 7 downregulated. In comparison, CB6 had 20 genes up and 12 down and Transgene Empty with 18 genes up and 17 down. These resulted indicated that a large effect on transcription was occurring from the presence of a high expressing vector, and that this effect was mitigated by a low expressing vector or the AAVrh8 capsid alone. Interestingly, distinct upregulation of genes related to immune and astrogliosis responses were also determined from the CBA-WPRE vector, but not in the either the CB6 and CBA-T. Empty-WPRE (Figure 4.2). This type of upregulation was also seen in from a study investing the transcriptional profile of neurodegeneration in ALS effecting microglia (the immune cells of the brain) (240), and in another profile of reactive astrogliosis (241) (which responds to CNS insults). These results support our observations of neuropathological effects from our overexpressing insult to the brain. At least 3 genes from these studies were identified as transcriptionally responsive in our high expressing vector that were associated with reactive gliosis (241), a peptidase inhibitory and cytokine response, *Serpina3n* (242) or

responses to interferon β and γ, *Gbp3* (243, 244), and *B2m* related to antigen

processing (245) and cellular defense (246) (Table 3.2). In addition, the

microglia transcriptome also co-identified hits from our CBA-WPRE microarray of

the costimulatory ligand *Cd86* (240), the transmembrane protein which triggers

myeloid cells and increased phagocytic activity (247), and suppress cytokine

production and immune responses (248), *Trem2*, the complement activation

(249) *Clqa*, the proinflammatory oxidase (250), *Cybb* and, reactive gliosis marker

(251), *GFAP*. Taken together, these results indicate that some of the processes

occurring through the expression of a lysosomal enzyme in the CNS lead to a

course of inflammation and astrogliosis which is not detectable when expressed

by a lower expressing promoter or from the capsid alone.

The reason why this level of overexpression lead to an inflammatory

process can be addressed by the vector system. Importantly, the enzyme

introduced in our work is of mouse origin and is introduced into an animal which

is already expressing a functional copy of the mouse GLB1 gene. This removes

the possibility of an immune response to a non-self protein as seen in other

studies(155), however response to extreme overexpression regardless of origin

is still an outstanding question. The effect could be related to the burden of

individual cells to produce large amounts of protein product. This is supported by

the reduction of transcriptional changes seen with a lower producing vector. In

addition, injection into the thalami of βgal$^{+/-}$ mice with the CB6 vector with both

same viral particles as CBA-WPRE as well as CB6 with a log higher dosing

appeared to have reduced Filipin staining despite similar amounts of enzyme produced. In addition, dose dependent responses leading to neuropathology at the injection site was seen in both our study and with NHP and the lysosomal enzyme acid sphigomyelinase (239). Investigation into a per-cell response to the expression of the mβgal enzyme would further enlighten this hypothesis and will be studied in detail in future work.

These newly constructed, reduced expression, minimal transcriptional impact vectors were also shown effective as a therapeutic in disease containing βgal$^{-/-}$ mice, however this effect was dose dependent. CB6 at the low dose was able to deliver enzyme to the cerebrum and cerebellum, but had surprisingly no activity for CB6 low in the spinal cord. This lack of spinal cord expression may be due to minimal amount of enzyme in the cerebellum + brainstem which was ~7 fold wild type levels overall and had reduced spread as seen in Xgal staining (Fig. 3.15b). We hypothesize that this level was insufficient to spread thought the tissue through cross correction between neighboring cells. This theory was supported at the higher dose CB6 High which was able to successfully spread throughout the tissues and achieved a non-significant difference from the original vector in cerebellum + brainstem, but was still an average of 20 fold lower in enzyme expression than CBA-WPRE vector in that tissue. Excitingly, storage clearance and Filipin presence was the most telling result as the original vector CBA-WPRE still displayed abnormal Filipin presence at the injection site (Fig. 3.16a, d), but this was minimized to absent in the CB6 High vector (Fig. 3.16o, r)

which was able to clear GM1 from the spinal cord where CBA-WPRE was not (Fig. 3.17e-f versus a-b). This finding is revealing as in both this study and our lab's previous attempt at intracranial gene therapy as the extreme overexpression in the cerebellum may have been the culprit for the inability to reach the spinal cord (Fig. 3.6a, d, f and Fig. 3.17e, f) (198). As we show here, supraphysiological levels of enzyme has deleterious consequences in the surrounding cells and could lead to dysregulation of lysosomal function and initiate immune and astrogliosis responses (240, 241, 251). We hypothesize that cells in the DCN that overexpress βgal are taxed beyond ability to compensate and are unable to properly connect to the spinal cord either through dysfunction or cell death in the corresponding nuclei. Furthering testing of this theory could be achieved by a selective, targeted destruction of the DCN using methods such as in Parkinson's' studies where site specific neurodegeneration is accomplished by introduction of the neurotoxin 1-methyl-4-phenyl-1,2,3,6-tetrahydropyridine (252). In the current study we achieved therapeutic success by lowering the total output from each vector we reduce the strain on each cell to process protein loads, and by increasing vector dose an increased ability to spread throughout neuronal connections was possible.

Taken together this work demonstrates that lysosomal storage disorders treated with viral expressing transgenes do not have unlimited capacity to withstand protein expression and this effect occurs in both disease and non-diseased animals. Importantly, immune and astrogliosis related responses

occurred in response to high levels of protein within the brain, but not to the viral capsid alone. Finally, mitigating the amount of enzyme produced from a single vector we reduced the burden of a single cell, and by increasing the total viral load we were able to utilize the network of connections functioning throughout the CNS. This work reveals that using a lower expressing promoter offers a larger dynamic range then high expressing transgenes and allows for the fine control of therapeutic intervention necessary for a lysosomal storage disorder affecting the central nervous system.

CHAPTER V: Final Summary and Conclusions

The work in this thesis comprises the investigation into multiple aspects and practical considerations for the therapeutic treatment of the lysosomal storage disorder, GM1-gangliosidosis. In addition, the benefit of these studies will have far reaching implications to the field of lysosomal storage disorder research and the practice of intracranial gene therapy.

Chapter II and III investigated two therapeutic approaches for the treatment of GM1-gangliosidosis in a mouse model which both achieved unprecedented increases in survival. In Chapter II, the investigation of a systemic approach utilizing AAV9 was presented. Here, we found that in the GM1-ganglioside mouse model we could express enzyme in the CNS at low but efficient levels with therapeutic impact. This expression was move effective in females than males, as noted previously (190, 191), and this difference led to increased storage clearance of the GM1 ganglioside in the brain and spinal cord in female mice. Despite the overall reduced response in the brain of male mice, higher liver expression in those animals did result in a corresponding increase in serum levels of the mβgal enzyme and uptake of this enzyme from the serum is also an efficient method for delivering enzyme to the CNS. Similar work by Ruzo *et al* used an intravenous administration of AAV8 with a liver-directed promoter to deliver a sulfamidase enzyme for the LSD, MPS IIIA which lead to correction of

CNS pathology in diseased mice. Consistent with our data, the male response was more robust then females with 4 fold greater liver expression (253). Notably, in our studies dose delivered to each animal was not adjusted for weight and therefore the possibility of less total vector genomes(vg) per kg of weight could be a factor in the resulting overall success of this therapy. This could lead to animal or sex based variation as male animals were typically larger then females at time of injection. To further probe this hypothesis future experiments could include adjustment of vg to kg of each animal and using testosterone injection into female animals to see if the male vs. female difference are still present (191).

Interestingly, in our IV approach we saw that even minimal expression in the CNS led to unprecedented behavior correction in this model where normalization of most parameters were noted for female mice at 30 weeks of age. Eventually, these animals all developed tremor which may be related to the lack of enzyme in the deep brain structures (thalamus and striatum) as well as the purkinje and molecular layers of the cerebellum, while the mobility retention may be due to success in targeting the spinal cord. As mentioned earlier, the deep cerebellar nuclei has been shown to have connections to the spinal cord as determined in a series of experiment in a rat model using anterograde labeling with biotinylated dextran (254-258), and also with therapeutic gene in a mouse model (215). In turn, successful spinal cord and then DCN expression could be due to the innervating neuronal connections from muscle to spinal cord where movement of the viral vector/ secreted βgal enzyme could originate from the viral

transduced and high enzyme expressing skeletal muscle (259). Therefore, storage correction in DCN could be caused by enzyme uptake at axonal terminals the spinal cord and its retrograde transport to the cell body. This hypothesis could be tested by the intravenous injection of a vector expressing mβgal with muscle specific promoter muscle creatin kinase (MCK) (260) and/or with a muscle targeting capsid such as AAV1 or AAV6 (261), or with a direct muscle injection. Another approach for teasing out this effect would be to include a microRNA detargeting sequence for muscle, miR-1 (189).

In our IV study, hallmarks of the disease (6) were apparent in the poorly treated regions where astrogliosis occurred. Interestingly, previous studies in an LSD model using AAV9 IV also had a challenge in accessing these regions (187) and was consistent even when utilizing a self complimentary (sc) AAV vector (216). Importantly, significant extension in life span (p < 0.0001) was seen in all groups and genders. Together, this data raise the possibility that a higher dose, or more efficient promoter may be even more effective then 3e11vg, however caution regarding liver overexpression is justified and a liver detargeted vector suggested (183, 189).

Chapter III employed an intracranial approach for GM1-gangliosisdosis which was superior to previous approaches in lifespan and motor function (197, 198). However, in the course of this work we also noted abnormal findings from the GM1-ganglioside identifying staining, Filipin, which was dose dependent and correlated with neuropathological morphological changes at the injection site and

warranted further investigation. We confirmed this abnormal staining was not disease dependent by using normal animals and developed a vector series to probe the cause. In these experiments we found an association with protein presence, but not enzyme activity at injection site. Furthermore, using a microarray approach we were able to determine that astrogliosis and immune responses (240, 241, 251) occurred at the injection site when using a high expressing vector, but was mitigated or absent if the expression was low. Importantly, a vector containing only promoter and post-translational elements, but not a protein product had almost no effect on the system. Previous studies investigating immune responses to intracranial injection include AAV2 encoding thymidine kinase (TK) or human aromatic $_L$-ammino acid decarboxylase (hAADC) in NHP brains (236), AAV1 expressing a humanized green fluorescent protein from *Renilla reniformis* (hGFP) in NHP brains (156), and AAV9 expressing hAADC or GFP in rat brains (155). In these studies, a relation to transgene and immune response was made, but only when the capsid itself was found to transduce antigen presenting cells (APC) that then triggered a cellular immune response to the transgene in AAV1 (156) or AAV9 (155) and not AAV2 (236). In our study, immune responses were determined to be protein dependent due to the high expression of the enzyme in a CBA-mβgal-WPRE transgene, but not when a highly expressing promoter was replaced and post translational element was removed, CB6-mβgal. Both the high and low enzyme producing transgenes carried the species-specific mβgal cDNA which was not foreign to the βgal$^{+/-}$

mouse that carries one functional copy of that gene. The AAVrh8 capsid did not have a consistent response across all vectors indicating that the capsid was not responsible for the immune response. In addition, previous studies intracranial injected AAVrh8 capsid expressing various transgenes within neonatal mice with GFP (231), in cats with mβgal (200), and in cats with hexosaminidase α and β (199) no immune responses were seen.

To further understand the role of enzyme overexpression in a highly expressing transgene a single cell-based analysis would be appropriate. RNAscope (Advanced Cell Dynamics, Hayward, CA) is a multiplex colorimetric or fluorescent method to perform *in situ* hybridization which provides the ability to view up to three different targets at once, and at sensitivities as low as single RNA molecules. This analysis would allow for single cell confirmation of the microarray results in conjunction with the detection a number of mβgal transcripts present, allowing quantification of the number of transcripts needed for an immune or toxic responses to occur. Laser capture micro-dissection for transduced cells in each cohort and subsequent biochemical analysis would also be useful in isolating only the subset of cells most highly expressing the transgene. Finally, neuronal cell culture could be employed to assess the effects of extreme enzyme overexpression with and without a viral capsid, as well as temporal effects that are more difficult to perform when in the context of a mouse model.

Continuing the intracranial study, we then brought these findings back into diseased mice and were able to achieve a therapeutic benefit of storage clearance throughout the CNS when using the lower expressing vector CB6-mβgal with a log higher dose. Importantly, the spinal cord which was not targeted successfully in all previous attempts (197, 198) had unprecedented therapeutic impact with normalization of GM1 storage. As stated above, the DCN is employed as a conduit within the brain to access the spinal cord for delivery of a therapeutic transgene (215). Connections between the DCN and spinal cord have been traced in previous studies (254-258), however the disruption of the DCN leading to loss of these connection have not been demonstrated. Direct injection of the CBA-mβgal-WPRE vector into the DCN resulted in neuropathological effects and resulted in loss of enzyme expression and storage clearance in the spinal cord. Therefore, we hypothesized that the extreme over expression of these enzymes in the DCN were leading to these downstream consequences. To further test this hypothesis, track-tracing of the connections in the DCN after expression of CBA-mβgal-WPRE or other cell damaging methods could be employed such as radiation, ischemic insult or hypoxia, or known toxic agents.

This work indicates that gene therapy for LSD is a fragile system and despite the many benefits of secreted enzymes in this therapy, that caution must be employed toward the injection site. By reducing the burden through a low

expressing promoter and increasing viral spread through higher dose it is possible to avoid these adherent responses. .

This work provides vital insight into the treatment of lysosomal storage disorders affecting the central nervous system however, additional questions exist. Which population of cells is sensitive to this pathological effect within the brain and is there another cell type that could act as a safer enzyme-producing center. To understand these implications experiments could be performed on cell culture with specific populations of cells such as neurons, astrocytes or brain endothelia, or the generation of mice that express the mβgal enzyme in a cre dependent manner. Another question remains regarding the universality of these findings; is this specific to mβgal, all lysosomal enzymes, all secreted enzymes?. Richness to this work can be provided by the analysis of a variety of disorders affecting the central nervous system.

The next challenge for viral therapy approaches is the ability to have fine control over the transgene output. In this work, we have shown a method that creates a dynamic range of expression levels and therefore the capacity to provide variable treatment modalities which can be scaled for larger animals. Additional levels of transgene regulation can be obtained through TET promoters in which transgene expression is controlled ON or OFF with an inducible transcriptional activator by the addition or removal of tetracycline or derivatives (262, 263). However, these promoters can be leaky and the need for turning off

of the transgene may be too late to keep damage from occurring. A next generation of Tet-like regulation that was responsive to cell stress rather than provided by the user would be an advantage for researchers and patients alike. Cell type specific promoters for the CNS(264) and RNAi detargeting sites (189) can also be employed to restrict expression to certain cell populations or tissues providing further control over transgene expression.

Taken together these studies show that a balance of vector targeting, CNS accessibility, enzyme expression and cellular stress must be factored into therapeutic approaches for LSD's. These studies have implications for translation to human studies as the ability to have fine control over a viral transgene is paramount. Long term expression of a transgene in the CNS could both treat a devastating disorder and lead to additional issues within the system. In the future, a holistic approach may be the most beneficial where a low expressing, regulated, direct injection can access deep brain structures, and a liver detargeted systemic vector can treat the periphery for safe and effective therapeutic intervention.

BIBLIOGRAPHY

1   Vitner, E.B., Platt, F.M. and Futerman, A.H. (2010) Common and uncommon pathogenic cascades in lysosomal storage diseases. *The Journal of biological chemistry*, **285**, 20423-20427.

2   Norman, R.M., Urich, H., Tingey, A.H. and Goodbody, R.A. (1959) Tay-Sachs' disease with visceral involvement and its relationship to Niemann-Pick's disease. *J Pathol Bacteriol*, **78**, 409-421.

3   Okada, S. and O'Brien, J.S. (1968) Generalized gangliosidosis: beta-galactosidase deficiency. *Science*, **160**, 1002-1004.

4   Tessitore, A., del, P.M.M., Sano, R., Ma, Y., Mann, L., Ingrassia, A., Laywell, E.D., Steindler, D.A., Hendershot, L.M. and d'Azzo, A. (2004) GM1-ganglioside-mediated activation of the unfolded protein response causes neuronal death in a neurodegenerative gangliosidosis. *Mol Cell*, **15**, 753-766.

5   Sano, R. (2009) GM1-ganglioside accumulation at the mitochondria-associated ER membranes links ER stress to Ca(2+)-dependent mitochondrial apoptosis. *Mol Cell*, **36**, 500-511.

6   Jeyakumar, M., Thomas, R., Elliot-Smith, E., Smith, D.A., van der Spoel, A.C., d'Azzo, A., Perry, V.H., Butters, T.D., Dwek, R.A. and Platt, F.M. (2003) Central nervous system inflammation is a hallmark of pathogenesis in mouse models of GM1 and GM2 gangliosidosis. *Brain*, **126**, 974-987.

7   Suzuki, Y., Oshima, A. and Nanba, E. (2008), In *The Online Metabolic and Molecular Bases of Inherited Disease*. McGraw Hill, New York, in press., pp. 1-101.

8   Callahan, J.W. (1999) Molecular basis of GM1 gangliosidosis and Morquio disease, type B. Structure-function studies of lysosomal beta-galactosidase and the non-lysosomal beta-galactosidase-like protein. *Biochim Biophys Acta*, **1455**, 85-103.

9   Chamoles, N.A., Blanco, M.B., Iorcansky, S., Gaggioli, D., Specola, N. and Casentini, C. (2001) Retrospective diagnosis of GM1 gangliosidosis by use of a newborn-screening card. *Clin Chem*, **47**, 2068.

10   Uribe, A. and Giugliani, R. (2013) Selective screening for lysosomal storage diseases with dried blood spots collected on filter paper in 4,700 high-risk Colombian subjects. *JIMD Rep.*, **11**, 107-116.

11   Warner, T.G., Robertson, A.D., Mock, A.K., Johnson, W.G. and O'Brien, J.S. (1983) Prenatal diagnosis of GM1 gangliosidosis by detection of galactosyl-oligosaccharides in amniotic fluid with high-performance liquid chromatography. *American journal of human genetics*, **35**, 1034-1041.

12   Brunetti-Pierri, N. and Scaglia, F. (2008) GM1 gangliosidosis: review of clinical, molecular, and therapeutic aspects. *Mol Genet Metab*, **94**, 391-396.

13   Privitera, S., Prody, C.A., Callahan, J.W. and Hinek, A. (1998) The 67-kDa enzymatically inactive alternatively spliced variant of beta-galactosidase is identical to the elastin/laminin-binding protein. *The Journal of biological chemistry*, **273**, 6319-6326.

14   Mochizuki, S., Brassart, B. and Hinek, A. (2002) Signaling pathways transduced through the elastin receptor facilitate proliferation of arterial smooth muscle cells. *The Journal of biological chemistry*, **277**, 44854-44863.

15   Caciotti, A., Donati, M.A., Bardelli, T., d'Azzo, A., Massai, G., Luciani, L., Zammarchi, E. and Morrone, A. (2005) Primary and secondary elastin-binding protein defect leads to impaired elastogenesis in fibroblasts from GM1-gangliosidosis patients. *Am J Pathol*, **167**, 1689-1698.

16   van der Spoel, A., Bonten, E. and d'Azzo, A. (2000) Processing of lysosomal beta-galactosidase. The C-terminal precursor fragment is an essential domain of the mature enzyme. *The Journal of biological chemistry*, **275**, 10035-10040.

17   McCarter, J.D., Burgoyne, D.L., Miao, S.C., Zhang, S.Q., Callahan, J.W. and Withers, S.G. (1997) Identification of Glu-268 as the catalytic nucleophile of human lysosomal beta-galactosidase precursor by mass spectrometry. *Journal of Biological Chemistry*, **272**, 396-400.

18   Ohto, U., Usui, K., Ochi, T., Yuki, K., Satow, Y. and Shimizu, T. (2012) Cyrstal structure of human beta-galactosidase: structural basis of GM1 Gangliosidosis and Morquio B diseases. *Journal of Biological Chemistry*, **287**, 1801-1812.

19   Kolter, T., Proia, R.L. and Sandhoff, K. (2002) Combinatorial ganglioside biosynthesis. *The Journal of biological chemistry*, **277**, 25859-25862.

20   Hanada, K., Kumagai, K., Yasuda, S., Miura, Y., Kawano, M., Fukasawa, M. and Nishijima, M. (2003) Molecular machinery for non-vesicular trafficking of ceramide. *Nature*, **426**, 803-809.

21   Nomura, T., Takizawa, M., Aoki, J., Arai, H., Inoue, K., Wakisaka, E., Yoshizuka, N., Imokawa, G., Dohmae, N., Takio, K. *et al.* (1998) Purification, cDNA cloning, and expression of UDP-Gal: glucosylceramide beta-1,4-galactosyltransferase from rat brain. *The Journal of biological chemistry*, **273**, 13570-13577.

22   Pohlentz, G., Klein, D., Schwarzmann, G., Schmitz, D. and Sandhoff, K. (1988) Both Ga2, Gm2, and Gd2 synthases and Gm1b, Gd1a, and Gt1b synthases are single enzymes in golgi vesicles from rat-liver. *Proc Natl Acad Sci U S A*, **85**, 7044-7048.

23   Wilkening, G., Linke, T., Uhlhorn-Dierks, G. and Sandhoff, K. (2000) Degradation of membrane-bound ganglioside GM1. Stimulation by bis(monoacylglycero)phosphate and the activator proteins SAP-B and GM2-AP. *The Journal of biological chemistry*, **275**, 35814-35819.

24   Sandhoff, K. and Harzer, K. (2013) Gangliosides and gangliosidoses: principles of molecular and metabolic pathogenesis. *J Neurosci*, **33**, 10195-10208.

25   Ngamukote, S., Yanagisawa, M., Ariga, T., Ando, S. and Yu, R.K. (2007) Developmental changes of glycosphingolipids and expression of glycogenes in mouse brains. *J Neurochem*, **103**, 2327-2341.

26   Svennerholm, L., Bostrom, K., Fredman, P., Mansson, J.E., Rosengren, B. and Rynmark, B.M. (1989) Human brain gangliosides: developmental changes from early fetal stage to advanced age. *Biochim Biophys Acta*, **1005**, 109-117.

27   Sheikh, K.A., J., S., Liu, Y., Kawai, H., Crawford, T.O.P., R. L. , Griffin, J.W. and Schnaar, R.L. (1999) Mice lacking complex gangliosides develop Wallerian degeneration and myelination defects. *Proc Natl Acad Sci U S A*, **96**, 7532-7537.

28   Simons, K. and Toomre, D. (2000) Lipid rafts and signal transduction. *Nat Rev Mol Cell Biol*, **1**, 31-39.

29   Posse de Chaves, E. and Sipione, S. (2010) Sphingolipids and gangliosides of the nervous system in membrane function and dysfunction. *FEBS Lett.*, **584**, 1748-1759.

30   Sonnino, S., Mauri, L., Chigorno, V. and Prinetti, A. (2007) Gangliosides as components of lipid membrane domains. *Glycobiology*, **17**, 1R-13R.

31   Wu, G., Xie, X., Lu, Z.H. and Ledeen, R.W. (2009) Sodium-calcium exchanger complexed with GM1 ganglioside in nuclear membrane transfers calcium from nucleoplasm to endoplasmic reticulum. *Proc Natl Acad Sci U S A*, **106**, 10829-10834.

32   Ledeen, R.W. and Wu, G. (2002) Ganglioside function in calcium homeostasis and signaling. *Neurochem Res*, **27**, 637-647.

33   Denny, C.A., Desplats, P.A., Thomas, E.A. and Seyfried, T.N. (2010) Cerebellar lipid differences between R6/1 transgenic mice and humans with Huntington's disease. *J Neurochem*, **115**, 748-758.

34   Maglione, V., Marchi, P., Di Pardo, A., Lingrell, S., Horkey, M., Tidmarsh, E. and Sipione, S. (2010) Impaired ganglioside metabolism in Huntington's disease and neuroprotective role of GM1. *J Neurosci*, **30**, 4072-4080.

35   Di Pardo, A., Maglione, V., Alpaugh, M., Horkey, M., Stwal, R.S., Sassone, J., Ciammola, A., Steffan, J.S., Fouad, K., Truant, R. *et al.* (2012) Ganglioside GM1 induces phosphorylation of mutant huntingtin and restores normal motor behavior in Huntington disease mice. *Proc Natl Acad Sci U S A*, **109**, 3528-3533.

36   Wei, J., Fujita, M., Nakai, M., Waragai, M., Sekigawa, A., Sugama, S., Takenouchi, T., Masliah, E. and Hashimoto, M. (2009) Protective role of endogenous gangliosides for lysosomal pathology in a cellular model of synucleinopathies. *Am J Pathol*, **174**, 1891-1909.

37   Hadjiconstantinou, M., Rossetti, Z.L., Paxton, R.C. and Neff, N.H. (1986) Administration of GM1 ganglioside restores the dopamine content in striatum after chronic treatment with MPTP. *Neuropharmacology*, **25**, 1075-1077.

38   Pope-Coleman, A., Tinker, J.P. and Schneider, J.S. (2000) Effects of GM1 ganglioside treatment on pre- and postsynaptic dopaminergic markers in the striatum of parkinsonian monkeys. *Synapse (New York, N.Y.)*, **36**, 120-128.

39   Schneider, J.S., Gollomp, S.M., Senedek, S., Colcher, A. and Cambi, F.D., W. (2013) A randomized, controlled, delayed start trial of GM1 ganglioside in treated Parkinson's disease patients. *J Neurol Sci.*, **324**, 140-148.

40   Kakio, A., Nishimoto, S., Yanagisawa, K., Kozutsumi, Y. and Matsuzaki, K. (2002) Interactions of amyloid beta-protein with various gangliosides in raft-like membranes: importance of GM1 ganglioside-bound form as an endogenous seed for Alzheimer amyloid. *Biochemistry*, **41**, 7385-7390.

41   Molander-Melin, M., Blennow, K., Bogdanovic, N., Dellheden, B., Mansson, J.E. and Fredman, P. (2005) Structural membrane alterations in Alzheimer brains found to be associated with regional disease development; increased density of gangliosides GM1 and GM2 and loss of cholesterol in detergent-resistant membrane domains. *J Neurochem*, **92**, 171-182.

42   Barrier, L., Ingrand, S., Damjanac, M., Rioux Bilan, A., Hugon, J. and Page, G. (2007) Genotype-related changes of ganglioside composition in brain regions of transgenic mouse models of Alzheimer's disease. *Neurobiology of aging*, **28**, 1863-1872.

43   Kreutz, F., Frozza, R.L., Breier, A.C., de Oliveria, V.A., Horn, A.P., Pettenusso, L.F., Netto, C.A., Sabego, C.G. and Trindade, V.M. (2011) Amyloid-β induced toxicity involves ganglioside expression and is sensitive to GM1 neuroprotective action. *Neurochem Int.*, **59**, 648-655.

44   Kreutz, F., Scherer, E.B., Ferreira, A.G., Petry Fdos, S., Pereira, C.L., Santana, F., de Souza Wyse, A.T., Salbego, C.G. and Trindade, V.M. (2013) Alterations on Na^+,K^+-ATPase and acetylcholinesterase activities induced by amyloid-β peptide in rat brain and GM1 ganglioside neuroprotective action. *Neurochem Res*, **38**, 2342-2350.

45   Takamura, A., Higaki, K., Kajimaki, K., Otsuka, S., Ninomiya, H., Matsuda, J., Ohno, K., Suzuki, Y. and Nanba, E. (2008) Enhanced autophagy and mitochondrial aberrations in murine G(M1)-gangliosidosis. *Biochem Biophys Res Commun*, **367**, 616-622.

46   Sano, R., Tessitore, A., Ingrassia, A. and d'Azzo, A. (2005) Chemokine-induced recruitment of genetically modified bone marrow cells into the CNS of GM1-gangliosidosis mice corrects neuronal pathology. *Blood*, **106**, 2259-2268.

47   Dawson, V.L. and Dawson, T.M. (1998) R. Ranney Mize, T.M.D.V.L.D. and Michael, J.F. (eds.), In *Progress in Brain Research*. Elsevier, Vol. Volume 118, pp. 215-229.

48   Matsuda, J., Suzuki, O., Oshima, A., Ogura, A., Naiki, M. and Suzuki, Y. (1997) Neurological manifestations of knockout mice with beta-galactosidase deficiency. *Brain Dev*, **19**, 19-20.

49   Itoh, M., Matsuda, J., Suzuki, O., Ogura, A., Oshima, A., Tai, T., Suzuki, Y. and Takashima, S. (2001) Development of lysosomal storage in mice with targeted disruption of the beta-galactosidase gene: a model of human G(M1)-gangliosidosis. *Brain Dev*, **23**, 379-384.

50   Matsuda, J., Suzuki, O., Oshima, A., Oqura, A., Noguchi, Y., Yamamoto, Y., Asano, T., Takimoto, K., Sukegawa, K., Suzuki, Y. *et al.* (1997) Beta-galactosidase-deficient mouse as an animal model for GM1-gangliosidosis. *Glycoconj J.*, **14**, 729-736.

51   Hahn, C.N., del Pilar Martin, M., Schroder, M., Vanier, M.T., Hara, Y., Suzuki, K., Suzuki, K. and d'Azzo, A. (1997) Generalized CNS disease and massive GM1-ganglioside accumulation in mice defective in lysosomal acid beta-galactosidase. *Hum Mol Genet*, **6**, 205-211.

52   Tanaka, H. and Suzuki, K. (1977) Substrate specificities of the two genetically distinct human brain beta-galactosidases. *Brain Res*, **122**, 325-335.

53   Fingerhut, R., van der Horst, G.T., Verheijen, F.W. and Conzelmann, E. (1992) Degradation of gangliosides by the lysosomal sialidase requires an activator protein. *European journal of biochemistry / FEBS*, **208**, 623-629.

54   Li, S.C., Li, Y.T., Moriya, S. and Miyagi, T. (2001) Degradation of G(M1) and G(M2) by mammalian sialidases. *Biochem*, **360**, 233-237.

55   Suzuki, K. and Chen, G.C. (1967) Brain ceramide hexosides in Tay-Sachs disease and generalized gangliosidosis (GM1-gangliosidosis). *J Lipid Res*, **8**, 105-113.

56   Sano, R., Trindade, V.M., Tessitore, A., d'Azzo, A., Vieira, M.B., Giugliani, R. and Coelho, J.C. (2005) G(M1)-ganglioside degradation and biosynthesis in human and murine G(M1)-gangliosidosis. *Clin Chim Acta*, **354**, 131-139.

57   Baker, H.J. and Lindsey, J.R. (1974) Animal model: feline GM1 gangliosidosis. *Am J Pathol*, **74**, 649-652.

58   Baker, H.J.J., Lindsey, J.R., McKhann, G.M. and Farrell, D.F. (1971) Neuronal GM1 gangliosidosis in a Siamese cat with beta-galactosidase deficiency. *Science*, **174**, 838-839.

59   Baker, H.J., Reynolds, G.D., Walkley, S.U., Cox, N.R. and Baker, G.H. (1979) The gangliosidoses: comparative features and research applications. *Vet Pathol*, **16**, 635-649.

60   Read, D.H., Harrington, D.D., Keenana, T.W. and Hinsman, E.J. (1976) Neuronal-visceral GM1 gangliosidosis in a dog with beta-galactosidase deficiency. *Science*, **194**, 442-445.

61   Alroy, J., Orgad, U., DeGasperi, R., Richard, R., Warren, C.D., Knowles, K., Thalhammer, J.G. and Raghavan, S.S. (1992) Canine GM1-gangliosidosis: a clinical, morphologic, histochemical, and biochemical comparison of two different models. *Am J Pathol*, **140**, 675-689.

62   Wang, Z.H., Zeng, B., Shibuya, H., Johnson, G.S., Alroy, J., Pastores, G.M., Raghavan, S. and Kolodny, E.H. (2000) Isolation and characterization of the normal canine beta-galactosidase gene and its mutation in a dog model of GM1-gangliosidosis. *J Inherit Metab Dis*, **23**, 593-606.

63   Yamato, O., Masuoka, Y., Yonemura, M., Hatakeyama, A., Satoh, H., Kobayashi, A., Nakayama, M., Asano, T., Shoda, T., Yamasaki, M. *et al.* (2003) Clinical and clinico-pathologic characteristics of Shiba dogs with a deficiency of lysosomal acid beta-galactosidase: a canine model of human GM1 gangliosidosis. *J Vet Med Sci*, **65**, 213-217.

64   Yamato, O., Ochiai, K., Masuoka, Y., Hayashida, E., Tajima, M., Omae, S., Iijima, M., Umemura, T. and Maede, Y. (2000) GM1 gangliosidosis in shiba dogs. *Vet Rec*, **146**, 493-496.

65   Hasegawa, D., Yamato, O., Nakamoto, Y., Ozawa, T., Yabuki, A., Itamoto, K., Kuwabara, T., Fujita, M., Takahashi, K., Mizoguchi, S. *et al.* (2012) Serial MRI features of canine GM1 gangliosidosis: a possible imaging biomarker for diagnosis and progression of the disease. *TheScientificWorldJournal*, **2012**, 250197.

66   Satoh, H., Yamauchi, T., Yamasaki, M., Maede, Y., Yabuki, A., Chang, H.S., Asanuma, T. and Yamato, O. (2011) Rapid detection of GM1 ganglioside in cerebrospinal fluid in dogs with GM1 gangliosidosis using matrix-assisted laser desorption ionization time-of-flight mass spectrometry. *J Vet Diagn Invest.*, **23**, 1202-1207.

67   Satoh, H., Yamato, O., Asano, T., Yonemura, M., Yamauchi, T., Hasegawa, D., Orima, H., Arai, T., Yamasaki, M. and Maede, Y. (2007) Cerebrospinal fluid biomarkers showing neurodegeneration in dogs with GM1 gangliosidosis: possible use for assessment of a therapeutic regimen. *Brain Res*, **1133**, 200-208.

68   O'Neill, K., Chen, S. and Diaz Brinton, R. (2004) Impact of the selective estrogen receptor modulator, tamoxifen, on neuronal outgrowth and survival following toxic insults associated with aging and Alzheimer's disease. *Exp Neurol*, **188**, 268-278.

69   Orlino, E.N., Jr., Olmstead, C.E., Lazareff, J.A., Peacock, W.J., Fisher, R.S. and Fluharty, A.L. (1997) An enzyme immunoassay for neuron-specific enolase in cerebrospinal fluid. *Biochemical and molecular medicine*, **61**, 41-46.

70   Hatfield, R.H. and McKernan, R.M. (1992) CSF neuron-specific enolase as a quantitative marker of neuronal damage in a rat stroke model. *Brain Res*, **577**, 249-252.

71   Donnelly, W.J., Sheahan, B.J. and Rogers, T.A. (1973) GM1 gangliosidosis in Friesian calves. *J Pathol*, **111**, 173-179.

72   Ryder, S.J. and Simmons, M.M. (2001) A lysosomal storage disease of Romney sheep that resembles human type 3 GM1 gangliosidosis. *Acta Neuropathol*, **101**, 225-228.

73   Prieur, D.J., Ahern-Rindell, A.J. and Murnane, R.D. (1991) Ovine GM-1 gangliosidosis. *Am J Pathol*, **139**, 1511-1513.

74   Muthupalani, S., Torres, P.A., Wang, B.C., Zeng, B.J., Eaton, S., Erdelyi, I., Ducore, R., Maganti, R., Keating, J., Perry, B.J. *et al.* (2014) GM1-gangliosidosis in American black bears: Clinical, pathological, biochemical and molecular genetic characterization. *Mol Genet Metab*, **111**, 513-521.

75   Minet, J.C., Fowler, B. and Litschg, J. (2004) GM1 gangliosidosis therapeutical trial with Miglustat (Zavesca) a case report. *Neuropediatrics*, **35**, P85.

76   Caciotti, A.e.a. (2011) GM1 gangliosidosis and Morquio B disease: an update on genetic alterations and clinical findings. *Biochim Biophys Acta*, **7**, 782-790.

77   Garzone, A., Pompilio, A., Ciuccarelli, F., Andresciani, E., Ficcadenti, A., De Meo, M., Mannucci, A., Marzioni, P., Buccolini, M., Carloni, L. *et al.* (2013) CPC-086 Miglustat off-label in a

pediatric formulation for a rare metabolic disease: early infantile GM1 gangliosidosis. *European Journal of Hospital Pharmacy: Science and Practice*, **20**, A196.

78   Elliot-Smith, E., Speak, A.O., Lloyd-Evans, E., Smith, D.A., van der Spoel, A.C., Jeyakumar, M., Butters, T.D., Dwek, R.A., d'Azzo, A. and Platt, F.M. (2008) Beneficial effects of substrate reduction therapy in a mouse model of GM1 gangliosidosis. *Mol Genet Metab*, **94**, 204-211.

79   Matsuda, J., Suzuki, O., Oshima, A., Yamamoto, Y., Noguchi, A., Takimoto, K., Itoh, M., Matsuzaki, Y., Yasuda, Y., Ogawa, S. *et al.* (2003) Chemical chaperone therapy for brain pathology in G(M1)-gangliosidosis. *Proc Natl Acad Sci U S A*, **100**, 15912-15917.

80   Kasperzyk, J.L., El-Abbadi, M.M., Hauser, E.C., D'Azzo, A., Platt, F.M. and Seyfried, T.N. (2004) N-butyldeoxygalactonojirimycin reduces neonatal brain ganglioside content in a mouse model of GM1 gangliosidosis. *J Neurochem*, **89**, 645-653.

81   Aguilar-Moncayo, M., Takai, T., Higaki, K., Mena-Barragan, T., Hirano, Y., Yura, K., Li, L., Yu, Y., Ninomiya, H., Garcia-Moreno, M.I. *et al.* (2012) Tuning glycosidase inhibition through aglycone interactions: pharmacological chaperones for Fabry disease and GM1 gangliosidosis. *Chemical communications*, **48**, 6514-6516.

82   O'Brien, J.S., Storb, R., Raff, R.F., Harding, J., Appelbaum, F., Morimoto, S., Kishimoto, Y., Graham, T., Ahern-Rindell, A. and O'Brien, S.L. (1990) Bone marrow transplantation in canine GM1 gangliosidosis. *Clinical genetics*, **38**, 274-280.

83   Shield, J.P., Stone, J. and Steward, C.G. (2005) Bone marrow transplantation correcting beta-galactosidase activity does not influence neurological outcome in juvenile GM1-gangliosidosis. *J Inherit Metab Dis*, **28**, 797-798.

84   Sawada, T., Tanaka, A., Higaki, K., Takamura, A., Nanba, E., Seto, T., Maeda, M., Yamaguchi, E., Matsuda, J. and Yamano, T. (2009) Intracerebral cell transplantation therapy for murine GM1 gangliosidosis. *Brain Dev*, **31**, 717-724.

85   Hickman, S., Shapiro, L.J. and Neufeld, E.F. (1974) A recognition marker required for uptake of a lysosomal enzyme by cultured fibroblasts. *Biochem Biophys Res Commun*, **57**, 55-61.

86   Jessup, W. and Dean, R.T. (1982) Secretion by mononuclear phagocytes of lysosomal hydrolases bearing ligands for the mannose-6-phosphate receptor system of fibroblasts: evidence for a second mechanism of spontaneous secretion? *Biochem Biophys Res Commun*, **105**, 922-927.

87   Klumperman, J., Hille, A., Veenendaal, T., Oorschot, V., Stoorvogel, W., von Figura, K. and Geuze, H.J. (1993) Differences in the endosomal distributions of the two mannose 6-phosphate receptors. *J Cell Biol*, **121**, 997-1010.

88   Fratantoni, J.C., Hall, C.W. and Neufeld, E.F. (1968) Hurler and Hunter syndromes: mutual correction of the defect in cultured fibroblasts. *Science*, **162**, 570-572.

89   Samoylova, T.I., Martin, D.R., Morrison, N.E., Hwang, M., Cochran, A.M., Samoylov, A.M., Baker, H.J. and Cox, N.R. (2008) Generation and characterization of recombinant feline beta-galactosidase for preclinical enzyme replacement therapy studies in GM1 gangliosidosis. *Metab Brain Dis*, **23**, 161-173.

90   Reynolds, G.D., Baker, H.J. and Reynolds, R.H. (1978) Enzyme replacement using liposome carriers in feline GM1 gangliosidosis fibroblasts. *Nature*, **275**, 754-755.

91   Obermeier, B., Daneman, R. and Ransohoff, R.M. (2013) Development, maintenance and disruption of the blood-brain barrier. *Nat Med*, **19**, 1584-1596.

92   Cardone, M., Porto, C., Tarallo, A., Vicinanza, M., Rossi, B., Polishchuk, E., Donaudy, F., Andria, G., De Matteis, M.A. and Parenti, G. (2008) Abnormal mannose-6-phosphate receptor

trafficking impairs recombinant alpha-glucosidase uptake in Pompe disease fibroblasts. *Pathogenetics*, **1**, 6.

93   Sun, B., Li, S., Bird, A., Yi, H., Kemper, A., Thurberg, B.L. and Koeberl, D.D. Antibody formation and mannose-6-phosphate receptor expression impact the efficacy of muscle-specific transgene expression in murine Pompe disease. *J Gene Med*, **12**, 881-891.

94   Koeberl, D.D., Luo, X., Sun, B., McVie-Wylie, A., Dai, J., Li, S., Banugaria, S.G., Chen, Y.T. and Bali, D.S. Enhanced efficacy of enzyme replacement therapy in Pompe disease through mannose-6-phosphate receptor expression in skeletal muscle. *Mol Genet Metab*, **103**, 107-112.

95   Dickson, P.I. and Chen, A.H. Intrathecal enzyme replacement therapy for mucopolysaccharidosis I: translating success in animal models to patients. *Curr Pharm Biotechnol*, **12**, 946-955.

96   Dickson, P.I., Hanson, S., McEntee, M.F., Vite, C.H., Vogler, C.A., Mlikotic, A., Chen, A.H., Ponder, K.P., Haskins, M.E., Tippin, B.L. *et al.* Early versus late treatment of spinal cord compression with long-term intrathecal enzyme replacement therapy in canine mucopolysaccharidosis type I. *Mol Genet Metab*, **101**, 115-122.

97   Dierenfeld, A.D., McEntee, M.F., Vogler, C.A., Vite, C.H., Chen, A.H., Passage, M., Le, S., Shah, S., Jens, J.K., Snella, E.M. *et al.* (2010) Replacing the enzyme alpha-L-iduronidase at birth ameliorates symptoms in the brain and periphery of dogs with mucopolysaccharidosis type I. *Sci Transl Med*, **2**, 60ra89.

98   Chen, A., Volgler, C., McEntee, M., Hanson, S., Ellinwood, N.M., Jens, J., Snella, E., Passage, M., Le, S., Guerra, C. *et al.* (2011) Glycosaminoglycan storage in neuroanatomical regions of mucopolysaccharidosis I dogs following intrathecal recombinant human iduronidase. *APMIS*, **119**, 513-521.

99   Vite, C.H., Wang, P., Patel, R.T., Walton, R.M., Walkley, S.U., Sellers, R.S., Ellinwood, N.M., Cheng, A.S., White, J.T., O'Neill, C.A. *et al.* (2011) Biodistribution and pharmacodynamics of recombinant human alpha-L-iduronidase (rhIDU) in mucopolysaccharidosis type I-affected cats following multiple intrathecal administrations. *Mol Genet Metab*, **103**, 268-274.

100   Chang, M., Cooper, J.D., Sleat, D.E., Cheng, S.H., Dodge, J.C., Passini, M.A., Lobel, P. and Davidson, B.L. (2008) Intraventricular enzyme replacement improves disease phenotypes in a mouse model of late infantile neuronal ceroid lipofuscinosis. *Mol Ther*, **16**, 649-656.

101   Ziegler, R.J., Salegio, E.A., Dodge, J.C., Bringas, J., Treleaven, C.M., Bercury, S.D., Tamsett, T.J., Shihabuddin, L., Hadaczek, P., Fiandaca, M. *et al.* Distribution of acid sphingomyelinase in rodent and non-human primate brain after intracerebroventricular infusion. *Exp Neurol*, **231**, 261-271.

102   Sly, W.S., Vogler, C., Grubb, J.H., Levy, B., Galvin, N., Tan, Y., Nishioka, T. and Tomatsu, S. (2006) Enzyme therapy in mannose receptor-null mucopolysaccharidosis VII mice defines roles for the mannose 6-phosphate and mannose receptors. *Proc Natl Acad Sci U S A*, **103**, 15172-15177.

103   Grubb, J.H., Vogler, C., Tan, Y., Shah, G.N., MacRae, A.F. and Sly, W.S. (2008) Infused Fc-tagged beta-glucuronidase crosses the placenta and produces clearance of storage in utero in mucopolysaccharidosis VII mice. *Proc Natl Acad Sci U S A*, **105**, 8375-8380.

104   O'Mahony, A.M., Godinho, B.M.D.C., Cryan, J.F. and O'Driscoll, C.M. (2013) Non-viral nanosystems for gene and small interfering RNA delivery to the central nervous system: formulating the solution. *J Pharm Sci*, **102**, 3469-3484.

105   Giacca, M. and Zacchigna, S. (2012) Virus-mediated gene delivery for human gene therapy. *Journal of Controlled Release*, **161**, 377-388.

106   Bryne, B.J., Falk, D.J., Clement, N. and Mah, C.S. (2012) Gene therapy approaches for lysosomal storage disease: next-generation treatment. *Hum Gene Ther*, **23**, 808-815.

107   Atchison, R.W., C., C.B. and Hammon, W.M. (1965) Adenovirus-assocaited defective virus particles. *Science*, **149**, 754-756.

108   Gerry, H.W., Kelly, T.J.J. and Berns, K.I. (1973) Arrangement of nucleotide sequences in adeno-associated virus DNA. *J Mol Biol*, **79**, 207-225.

109   Lusby, E., Fife, K.H. and Berns, K.I. (1980) Nucleotide sequence of the inverted terminal repetition in adeno-associated virus DNA. *J Virol*, **34**, 402-409.

110   Srivastava, A., Lusby, E.W. and Berns, K.I. (1983) Nucleotide sequence and organization of the adeno-associated virus 2 genome. *J Virol*, **45**, 555-564.

111   Wistuba, A., Weger, S., Kern, A. and Kleinschmidt, J.A. (1995) Intermediates of adeno-associated virus type 2 assembly: identification of soluble complexes containing Rep and Cap proteins. *J Virol*, **1995**, 9.

112   Sonntag, F., Schmidt, K. and Kleinschmidt, J.A. (2010) A viral assembly factor promotes AAV2 capsid formation in the nucleolus. *Proc Natl Acad Sci U S A*, **107**, 10220-10225.

113   Sonntag, F., Kother, K., Schmidt, K., Weghofer, M., Raupp, C., Nieto, K., Kuck, A., BGerlach, B., Bottcher, B., Muller, O.J. *et al.* (2011) The assembly-activating protein promotes capsid assembly of different adeno-associated virus serotypes. *J Virol*, **85**, 12686-12697.

114   Naumer, M., Sonntag, F., Schmidt, K., Nieto, K., Panke, C., Davey, N.E., Popa-Wagner, R. and Kleinschmidt, J.A. (2012) Properties of the adeno-associated virus assembly-activating protein. *J Virol*, **86**, 13038-13048.

115   Duan, D., Yan, Z., Yue, Y. and Engelhardt, J.F. (1999) Structural analysis of adeno-associated virus transduction circular intermediates. *Virology*, **261**, 8-14.

116   Bartlett, J.S., Wilcher, R. and Samulski, R.J. (2000) Infectious entry pathway of adeno-associated virus and adeno-associated virus vectors. *J Virol*, **74**, 2777-2785.

117   Duan, D., Li, Q., Kao, A.W., Yue, Y., Pessin, J.E. and Engelhardt, J.F. (1999) Dynamin is required for recombinant adeno-associated virus type 2 infection. *J Virol*, **73**, 10371-10376.

118   Nonnenmacher, M. and Weber, T. (2011) Adeno-Associated Virus 2 Infection Requires Endocytosis through the CLIC/GEEC Pathway. *Cell Host & Microbe*, **10**, 563-576.

119   Gao, G., Alvira, M.R., Somanathan, S., Lu, Y., Vandenberghe, L.H., Rux, J.J., Calcedo, R., Sanmiguel, J., Abbas, Z. and Wilson, J.M. (2003) Adeno-associated viruses undergo substantial evolution in primates during natural infections. *Proceedings of the National Academy of Sciences*, **100**, 6081-6086.

120   Gao, G., Vandenberghe, L.H. and Wilson, J.M. (2005) New recombinant serotypes of AAV vectors. *Curr Gene Ther*, **5**, 285-297.

121   Gao, G.P., Alvira, M.R., Wang, L.L., Calcedo, R., Johnston, J. and Wilson, J.M. (2002) Novel adeno-associated viruses from rhesus monkeys as vectors for human gene therapy. *P Natl Acad Sci USA*, **99**, 11854-11859.

122   Wu, Z., Miller, E., Agbandje-McKenna, M. and Samulski, R.J. (2006) Alpha2,3 and alpha2,6 N-linked sialic acids facilitate efficient binding and transduction by adeno-associated virus types 1 and 6. *J Virol*, **80**, 9093-9103.

123   Ng, R., Govindasamy, L., Gurda, B.L., McKenna, R., Kozyreva, O.G. and Samulski, R.J. (2010) Structural characterization of the dual glycan binding adeno-associated virus serotype 6. *J Virol*, **84**, 12945-12957.

124   Weller, M.L., Amornphimoltham, P., Schmidt, M., Wilson, P.A., Gutkind, J.S. and Chiorini, J.A. (2010) Epidermal growth factor receptor is a co-receptor for adeno-associated virus serotype 6. *Nat Med*, **16**, 662-664.

125   Summerford, C. and Samulski, R.J. (1998) Membrane-associated heparan sulfate proteoglycan is a receptor for adeno-associated virus type 2 virions. *J Virol*, **72**, 1438-1445.

126   Akache, B., Grimm, D., Pandey, K., Yant, S., Xu, H. and Kay, M.A. (2006) The 37/67-kilodalton laminin receptor is a receptor for adeno-associated virus serotypes 8, 2, 3, and 9. *J Virol*, **80**, 9831-9836.

127   Qing, K., Mah, C., Hansen, J., Zhou, S., Dwarki, V. and Srivastava, A. (1999) Human fibroblast growth factor receptor 1 is a co-receptor for infection by adeno-associated virus 2. *Nat Med*, **5**, 71-77.

128   Kashiwakura, Y., Tamayose, K., Iwabuchi, K., Hira, Y., Shimada, T., Matsomoto, K., Nakamura, T., Watanabe, M., Oshima, K. and Daida, H. (2005) Hepatocyte growth factor receptor is a coreceptor for adeno-associated virus type 2 infection. *J Virol*, **79**, 609-614.

129   Asokan, A., Hamra, J.B., Govindasamy, L., Agbandje-McKenna, M. and Samulski, R.J. (2006) Adeno-associated virus type 2 contains an integrin alpha5beta1 binding domain essential for viral cell entry. *J Virol*, **80**, 8961-8969.

130   Kaludov, N., Brown, K.E., Walters, R.W., Zabner, J. and Chiorini, J.A. (2001) Adeno-associated virus serotype 4 (AAV4) and AAV5 both require sialic acid binding for hemagglutination and efficient transduction but differ in sialic acid linkage specificity. *J Virol*, **75**, 6884-6893.

131   Walters, R.W., Yi, S.M., Keshavjee, S., Brown, K.E., Welsh, M.J., Chiorini, J.A. and Zabner, J. (2001) Binding of adeno-associated virus type 5 to 2,3-linked sialic acid is required for gene transfer. *The Journal of biological chemistry*, **276**, 20610-20616.

132   Di Pasquale, G., Davidson, B.L., Stein, C.S., Martins, I., Scudiero, D., Monks, A. and Chiorini, J.A. (2003) Identification of PDGFR as a receptor for AAV-5 transduction. *Nat Med*, **9**, 1306-1312.

133   Shen, S., Bryant, K.D., Brown, S.M., Randell, S.H. and Asokan, A. (2011) TerminalN-Linked Galactose Is the Primary Receptor for Adeno-associated Virus 9. *The Journal of biological chemistry*, **286**, 13532-13540.

134   Zinn, E. and Vandenberghe, L.H. (2014) Adeno-associated virus: fit to serve. *Current opinion in virology*, **8c**, 90-97.

135   Bantel-Schaal, U., Hub, B. and Kartenbeck, J. (2002) Endocytosis of adeno-associated virus type 5 leads to accumulation of virus particles in the Golgi compartment. *J Virol*, **76**, 2340-2349.

136   Xiao, P.J. and Samulski, R.J. (2012) Cytoplasmic trafficking, endosomal escape, and perinuclear accumulation of adeno-associated virus type 2 particles are facilitated by microtubule network. *J Virol*, **86**, 10462-10473.

137   Kelkar, S., De, B.P., Gao, G., Wilson, J.M., Crystal, R.G. and Leopold, P.L. (2006) A common mechanism for cytoplasmic dynein-dependent microtubule binding shared among adeno-associated virus and adenovirus serotypes. *J Virol*, **80**, 7781-7785.

138   Kronenberg, S., Bottcher, B., von der Lieth, C.W., Bleker, S. and Kleinschmidt, J.A. (2005) A conformational change in the adeno-associated virus type 2 capsid leads to the exposure of hidden VP1 N termini. *J Virol*, **79**, 5296-5303.

139   Sonntag, F., Bleker, S., Leuchs, B., Fischer, R. and Kleinschmidt, J.A. (2006) Adeno-associated virus type 2 capsids with externalized VP1/VP2 trafficking domains are generated prior to passage through the cytoplasm and are maintained until uncoating occurs in the nucleus. *J Virol*, **80**, 11040-11054.

140   Cotmore, S.F., D'Abramo A, M., Jr., Ticknor, C.M. and Tattersall, P. (1999) Controlled conformational transitions in the MVM virion expose the VP1 N-terminus and viral genome without particle disassembly. *Virology*, **254**, 169-181.

141   Girod, A., Wobus, C.E., Zadori, Z., Ried, M., Leike, K., Tijssen, P., Kleinschmidt, J.A. and Hallek, M. (2002) The VP1 capsid protein of adeno-associated virus type 2 is carrying a phospholipase A2 domain required for virus infectivity. *The Journal of general virology*, **83**, 973-978.

142   Grieger, J.C., Snowdy, S. and Samulski, R.J. (2006) Separate basic region motifs within the adeno-associated virus capsid proteins are essential for infectivity and assembly. *J Virol*, **80**, 5199-5210.

143   Johnson, J.S., Li, C., DiPrimio, N., Weinberg, M.S., McCown, T.J. and Samulski, R.J. (2010) Mutagenesis of adeno-associated virus type 2 capsid protein VP1 uncovers new roles for basic amino acids in trafficking and cell-specific transduction. *J Virol*, **84**, 8888-8902.

144   Nicolson, S.C. and Samulski, R.J. (2014) Recombinant adeno-associated virus utilizes host cell nuclear import machinery to enter the nucleus. *J Virol*, **88**, 4132-4144.

145   Thomas, C.E., Storm, T.A., Huang, Z. and Kay, M.A. (2004) Rapid uncoating of vector genomes is the key to efficient liver transduction with pseudotyped adeno-associated virus vectors. *J Virol*, **78**, 3110-3122.

146   Stieger, K., Schroeder, J., Provost, N., Mendes-Madeira, A., Belbellaa, B., Le Meur, G., Weber, M., Deschamps, J.Y., Lorenz, B., Moullier, P. *et al.* (2009) Detection of intact rAAV particles up to 6 years after successful gene transfer in the retina of dogs and primates. *Mol Ther*, **17**, 516-523.

147   Zhong, L., Li, W., Yang, Z., Qing, K., Tan, M., Hansen, J., Li, Y., Chen, L., Chan, R.J., Bischof, D. *et al.* (2004) Impaired nuclear transport and uncoating limit recombinant adeno-associated virus 2 vector-mediated transduction of primary murine hematopoietic cells. *Hum Gene Ther*, **15**, 1207-1218.

148   Ferrari, F.K., Samulski, T., Shenk, T. and Samulski, R.J. (1996) Second-strand synthesis is a rate-limiting step for efficient transduction by recombinant adeno-associated virus vectors. *J Virol*, **70**, 3227-3234.

149   Fisher, K.J., Gao, G.P., Weitzman, M.D., DeMatteo, R., Burda, J.F. and Wilson, J.M. (1996) Transduction with recombinant adeno-associated virus for gene therapy is limited by leading-strand synthesis. *J Virol*, **70**, 520-532.

150   Nakai, H., Storm, T.A. and Kay, M.A. (2000) Recruitment of single-stranded recombinant adeno-associated virus vector genomes and intermolecular recombination are responsible for stable transduction of liver in vivo. *J Virol*, **74**, 9451-9463.

151   Lusby, E., Bohenzky, R. and Berns, K.I. (1981) Inverted terminal repetition in adeno-associated virus DNA: independence of the orientation at either end of the genome. *J Virol*, **37**, 1083-1086.

152   Yang, J.S., Zhou, W.H., Zhang, Y.L., Zidon, T., Ritchie, T. and Engelhardt, J.F. (1999) Concatamerization of adeno-associated virus circular genomes occurs through intermolecular recombination. *Journal of Virology*, **73**, 9468-9477.

153   Miao, C.H., Snyder, R.O., Schowalter, D.B., Patijn, G.A., Donahue, B., Winther, B. and Kay, M.A. (1998) The kinetics of rAAV integration in the liver. *Nat Genet*, **19**, 13-15.

154   Gao, G., Wang, Q., Calcedo, R., Mays, L., Bell, P., Wang, L., Vandenberghe, L.H., Grant, R., Sanmiguel, J., Furth, E.E. *et al.* (2009) Adeno-associated virus-mediated gene transfer to nonhuman primate liver can elicit destructive transgene-specific T cell responses. *Hum Gene Ther*, **20**, 930-942.

155   Ciesielska, A., Hadaczek, P., Mittermeyer, G., Zhou, S., Wright, J.F., Bankiewicz, K.S. and Forsayeth, J. (2013) Cerebral infusion of AAV9 vector-encoding non-self proteins can elicit cell-mediated immune responses. *Mol Ther*, **21**, 158-166.

156   Hadaczek, P., Forsayeth, J., Mirek, H., Munson, K., Bringas, J., Pivirotto, P., McBride, J.L., Davidson, B.L. and Bankiewicz, K.S. (2009) Transduction of nonhuman primate brain with adeno-associated virus serotype 1: vector trafficking and immune response. *Hum Gene Ther*, **20**, 225-237.

157   Kotin, R.M., Sinsicalco, M., Samulski, R.J., Zhu, X.D., Hunter, L., Laughlin, C.A., MCLaughlin, S., Muzycka, N., Rocchi, M. and Berns, K.I. (1990) Site-specific integration by adeno-associated virus. *Proc Natl Acad Sci U S A*, **87**, 2211-2215.

158   Kotin, R.M., Menninger, J.C., Ward, D.C. and Berns, K.I. (1991) Mapping and direct visualization of a region-specific viral DNA integration site on chromosome 19q13-qter. *Genomics*, **10**, 831-834.

159   McCarty, D.M., Young, S.M., Jr. and Samulski, R.J. (2004) Integration of adeno-associated virus (AAV) and recombinant AAV vectors. *Annual review of genetics*, **38**, 819-845.

160   Flotte, T.R. and Berns, K.I. (2005) *Adeno-associated virus vectors for gene therapy*. Elsevier.

161   Samulski, R.J., Berns, K.I., Tan, M. and Muzyczka, N. (1982) Cloning of adeno-associated virus into pBR322: rescue of intact virus from the recombinant plasmid in human cells. *Proc Natl Acad Sci U S A*, **79**, 2077-2081.

162   Duan, D., Yue, Y., Yan, Z. and Engelhardt, J.F. (2000) A new dual-vector approach to enhance recombinant adeno-associated virus-mediated gene expression through intermolecular cis activation. *Nat Med*, **6**, 595-598.

163   McCarty, D.M., Monahan, P.E. and Samulski, R.J. (2001) Self-complementary recombinant adeno-associated virus (scAAV) vectors promote efficient transduction independently of DNA synthesis. *Gene Ther*, **8**, 1248-1254.

164   McCarty, D.M. (2008) Self-complementary AAV vectors; advances and applications. *Mol Ther*, **16**, 1648-1656.

165   Passini, M.A., Lee, E.B., Heuer, G.G. and Wolfe, J.H. (2002) Distribution of a lysosomal enzyme in the adult brain by axonal transport and by cells of the rostral migratory stream. *J Neurosci*, **22**, 6437-6446.

166   Liu, G., Martins, I., Wemmie, J.A., Chiorini, J.A. and Davidson, B.L. (2005) Functional correction of CNS phenotypes in a lysosomal storage disease model using adeno-associated virus type 4 vectors. *J Neurosci*, **25**, 9321-9327.

167   Broekman, M.L., Tierney, L.A., Benn, C., Chawla, P., Cha, J.H. and Sena-Esteves, M. (2009) Mechanisms of distribution of mouse beta-galactosidase in the adult GM1-gangliosidosis brain. *Gene Ther*, **16**, 303-308.

168   Cearley, C.N. and Wolfe, J.H. (2006) Transduction characteristics of adeno-associated virus vectors expressing cap serotypes 7, 8, 9, and Rh10 in the mouse brain. *Mol Ther*, **13**, 528-537.

169   Cearley, C.N., Vandenberghe, L.H., Parente, M.K., Carnish, E.R., Wilson, J.M. and Wolfe, J.H. (2008) Expanded repertoire of AAV vector serotypes mediate unique patterns of transduction in mouse brain. *Mol Ther*, **16**, 1710-1718.

170   Cearley, C.N. and Wolfe, J.H. (2007) A single injection of an adeno-associated virus vector into nuclei with divergent connections results in widespread vector distribution in the brain and global correction of a neurogenetic disease. *J Neurosci*, **27**, 9928-9940.

171   Salegio, E.A., Samaranch, L., Kells, A.P., Mittermeyer, G., San Sebastian, W., Zhou, S., Beyer, J., Forsayeth, J. and Bankiewicz, K.S. (2013) Axonal transport of adeno-associated viral vectors is serotype-dependent. *Gene Ther*, **20**, 348-352.

172   Kells, A.P., Hadaczek, P., Yin, D., Bringas, J., Varenika, V., Forsayeth, J. and Bankiewicz, K.S. (2009) Efficient gene therapy-based method for the delivery of therapeutics to primate cortex. *Proc Natl Acad Sci U S A*, **106**, 2407-2411.

173   Castle, M.J., Gershenson, Z.T., Giles, A.R., Holzbaur, E.L. and Wolfe, J.H. (2014) Adeno-associated virus serotypes 1, 8, and 9 share conserved mechanisms for anterograde and retrograde axonal transport. *Hum Gene Ther*, **25**, 705-720.

174   Dodge, J.C., Clarke, J., Song, A., Bu, J., Yang, W., Taksir, T.V., Griffiths, D., Zhao, M.A., Schuchman, E.H., Cheng, S.H. *et al.* (2005) Gene transfer of human acid sphingomyelinase corrects neuropathology and motor deficits in a mouse model of Niemann-Pick type A disease. *Proc Natl Acad Sci U S A*, **102**, 17822-17827.

175   Cachon-Gonzalez, M.B., Wang, S.Z., McNair, R., Bradley, J., Lunn, D., Ziegler, R., Cheng, S.H. and Cox, T.M. (2012) Gene Transfer Corrects Acute GM2 Gangliosidosis-Potential Therapeutic Contribution of Perivascular Enzyme Flow. *Mol Ther*, **20**, 1489-1500.

176   Priller, J., Flugel, A., Wehner, T., Boentert, M., Haas, C.A., Prinz, M., Fernandez-Klett, F., Prass, K., Bechmann, I., de Boer, B.A. *et al.* (2001) Targeting gene-modified hematopoietic cells to the central nervous system: use of green fluorescent protein uncovers microglial engraftment. *Nat Med*, **7**, 1356-1361.

177   Biffi, A., De Palma, M., Quattrini, A., Del Carro, U., Amadio, S., Visigalli, I., Sessa, M., Fasano, S., Brambilla, R., Marchesini, S. *et al.* (2004) Correction of metachromatic leukodystrophy in the mouse model by transplantation of genetically modified hematopoietic stem cells. *J Clin Invest*, **113**, 1118-1129.

178   Visigalli, I., Delai, S., Politi, L.S., Di Domenico, C., Cerri, F., Mrak, E., D'Isa, R., Ungaro, D., Stok, M., Sanvito, F. *et al.* Gene therapy augments the efficacy of hematopoietic cell transplantation and fully corrects mucopolysaccharidosis type I phenotype in the mouse model. *Blood*, **116**, 5130-5139.

179   Gentner, B., Visigalli, I., Hiramatsu, H., Lechman, E., Ungari, S., Giustacchini, A., Schira, G., Amendola, M., Quattrini, A., Martino, S. *et al.* Identification of hematopoietic stem cell-specific miRNAs enables gene therapy of globoid cell leukodystrophy. *Sci Transl Med*, **2**, 58ra84.

180   Biffi, A., Aubourg, P. and Cartier, N. Gene therapy for leukodystrophies. *Hum Mol Genet*, **20**, R42-53.

181   Foust, K.D., Nurre, E., Montgomery, C.L., Hernandez, A., Chan, C.M. and Kaspar, B.K. (2009) Intravascular AAV9 preferentially targets neonatal neurons and adult astrocytes. *Nat Biotechnol*, **27**, 59-65.

182   Zhang, H., Yang, B., Mu, X., Ahmed, S.S., Su, Q., He, R., Wang, H., Mueller, C., Sena-Esteves, M., Brown, R. *et al.* (2011) Several rAAV vectors efficiently cross the blood-brain barrier and transduce neurons and astrocytes in the neonatal mouse central nervous system. *Mol Ther*, **19**, 1440-1448.

183   Yang, B., Li, S., Wang, H., Guo, Y., Gessler, D.J., Cao, C., Su, Q., Kramer, J., Zhong, L., Ahmed, S.S. *et al.* (2014) Global CNS transduction of adult mice by intravenously delivered rAAVrh.8 and rAAVrh.10 and nonhuman primates by rAAVrh.10. *Mol Ther*, **22**, 1299-1309.

184   Bevan, A.K., Duque, S., Foust, K.D., Morales, P.R., Braun, L., Schmelzer, L., Chan, C.M., McCrate, M., Chicoine, L.G., Coley, B.D. *et al.* (2011) Systemic gene delivery in large species for targeting spinal cord, brain, and peripheral tissues for pediatric disorders. *Mol Ther*, **19**, 1971-1980.

185   Duque, S., Joussemet, B., Riviere, C., Marais, T., Dubreil, L., Douar, A.M., Fyfe, J., Moullier, P., Colle, M.A. and Barkats, M. (2009) Intravenous administration of self-complementary AAV9 enables transgene delivery to adult motor neurons. *Mol Ther*, **17**, 1187-1196.

186   Foust, K.D., Wang, X., McGovern, V.L., Braun, L., Bevan, A.K., Haidet, A.M., Le, T.T., Morales, P.R., Rich, M.M., Burghes, A.H. *et al.* (2010) Rescue of the spinal muscular atrophy phenotype in a mouse model by early postnatal delivery of SMN. *Nat Biotechnol*, **28**, 271-274.

187   Fu, H., Dirosario, J., Killedar, S., Zaraspe, K. and McCarty, D.M. (2011) Correction of neurological disease of mucopolysaccharidosis IIIB in adult mice by rAAV9 trans-blood-brain barrier gene delivery. *Mol Ther*, **19**, 1025-1033.

188   Ruzo, A., Marco, S., Garcia, M., Villacampa, P., Ribera, A., Ayuso, E., Maggioni, L., Mingozzi, F., Haurigot, V. and Bosch, F. (2012) Correction of pathological accumulation of glycosaminoglycans in central nervous system and peripheral tissues of MPSIIIA mice through systemic AAV9 gene transfer. *Hum Gene Ther*, **23**, 1237-1246.

189   Xie, J., Xie, Q., Zhang, H., Ameres, S.L., Hung, J.H., Su, Q., He, R., Mu, X., Seher Ahmed, S., Park, S. *et al.* (2011) MicroRNA-regulated, systemically delivered rAAV9: a step closer to CNS-restricted transgene expression. *Mol Ther*, **19**, 526-535.

190   Ruzo, A., Garcia, M., Ribera, A., Villacampa, P., Haurigot, V., Marco, S., Ayuso, E.A., X. M., Roca, C., Agudo, J., Ramos, D. *et al.* (2012) Liver production of sulfamidase reverses peripheral and ameliorates CNS pathology in mucopolysaccharidosis IIIA mice. *Mol Ther*, **20**, 254-266.

191   Davidoff, A.M., Ng, C.Y.C., Zhou, J.F., Spence, Y. and Nathwani, A.C. (2003) Sex significantly influences transduction of murine liver by recombinant adeno-associated viral vectors through an androgen-dependent pathway. *Blood*, **102**, 480-488.

192   Maguire, C.A., Crommentyijn, M.H., Mu, D., Hudry, E., Serrano-Pozo, A., Hyman, B.T. and Tannos, B.A. (2013) Mouse gender influences brain transduction by intravascularly administered AAV9. *Mol Ther*, **21**, 1470-1471.

193   Chen, Y.H., Chang, M. and Davidson, B.L. (2009) Molecular signatures of disease brain endothelia provide new sites for CNS-directed enzyme therapy. *Nat Med*, **15**, 1215-1218.

194   Chen, Y.H., Clafin, K., Geoghegan, J.C. and Davidson, B.L. (2012) Sialic acid deposition impairs the utility of AAV9, but not peptide-modified AAVs for brain gene therapy in a mouse model of lysosomal storage disease. *Mol Ther*, **7**, 1393-1399.

195   Oehmig, A., Cortes, M.L., Perry, K.F., Sena-Esteves, M., Fraefel, C. and Breakefield, X.O. (2007) Integration of active human beta-galactosidase gene (100 kb) into genome using HSV/AAV amplicon vector. *Gene Ther*, **14**, 1078-1091.

196   Takaura, N., Yagi, T., Maeda, M., Nanba, E., Oshima, A., Suzuki, Y., Yamano, T. and Tanaka, A. (2003) Attenuation of ganglioside GM1 accumulation in the brain of GM1 gangliosidosis mice by neonatal intravenous gene transfer. *Gene Ther*, **10**, 1487-1493.

197   Broekman, M.L., Baek, R.C., Comer, L.A., Fernandez, J.L., Seyfried, T.N. and Sena-Esteves, M. (2007) Complete correction of enzymatic deficiency and neurochemistry in the GM1-gangliosidosis mouse brain by neonatal adeno-associated virus–mediated gene delivery. *Molecular Therapy*, **15**, 30-37.

198   Baek, R.C., Broekman, M.L., Leroy, S.G., Tierney, L.A., Sandberg, M.A., d'Azzo, A., Seyfried, T.N. and Sena-Esteves, M. (2010) AAV-mediated gene delivery in adult GM1-gangliosidosis mice corrects lysosomal storage in CNS and improves survival. *PLoS One*, **5**, e13468.

199   Bradbury, A.M., Cochran, J.N., McCurdy, V.J., Johnson, A.K., Brunson, B.L., Gray-Edwards, H., Leroy, S.G., Hwang, M., Randle, A.N., Jackson, L.S. *et al.* (2013) Therapeutic response in feline sandhoff disease despite immunity to intracranial gene therapy. *Mol Ther*, **21**, 1306-1315.

200   McCurdy, V.J., Johnson, A.K., Gray-Edwards, H.L., Randle, A.N., Brunson, B.L., Morrison, N.E., Salibi, N., Johnson, J.A., Hwang, M., Beyers, R.J. *et al.* (2014) Sustained normalization of neurological disease after intracranial gene therapy in a feline model. *Sci Transl Med*, **6**, 231ra248.

201   O'Brien, J.S., Stern, M.B., Landing, B.H., O'Brien, J.K. and Donnell, G.N. (1965) Generalized Gangliosidosis: another inborn error of ganglioside metabolism? *American journal of diseases of children (1960)*, **109**, 338-346.

202   Suzuki, K. (1968) Cerebral GM1-gangliosidosis: chemical pathology of visceral organs. *Science*, **159**, 1471-1472.

203   Dickson, P.I. and Chen, A.H. (2011) Intrathecal enzyme replacement therapy for mucopolysaccharidosis I: translating success in animal models to patients. *Curr Pharm Biotechnol*, **12**, 946-955.

204   Dickson, P.I., Hanson, S., McEntee, M.F., Vite, C.H., Vogler, C.A., Mlikotic, A., Chen, A.H., Ponder, K.P., Haskins, M.E., Tippin, B.L. *et al.* (2010) Early versus late treatment of spinal cord compression with long-term intrathecal enzyme replacement therapy in canine mucopolysaccharidosis type I. *Mol Genet Metab*, **101**, 115-122.

205   Bosch, A., Perret, E., Desmaris, N. and Heard, J.M. (2000) Long-term and significant correction of brain lesions in adult mucopolysaccharidosis type VII mice using recombinant AAV vectors. *Mol Ther*, **1**, 63-70.

206   Skorupa, A.F., Fisher, K.J., Wilson, J.M., Parente, M.K. and Wolfe, J.H. (1999) Sustained production of beta-glucuronidase from localized sites after AAV vector gene transfer results in widespread distribution of enzyme and reversal of lysosomal storage lesions in a large volume of brain in mucopolysaccharidosis VII mice. *Exp Neurol*, **160**, 17-27.

207   Kaplitt, M.G., Feigin, A., Tang, C., Fitzsimons, H.L., Mattis, P., Lawlor, P.A., Bland, R.J., Young, D., Strybing, K., Eidelberg, D. *et al.* (2007) Safety and tolerability of gene therapy with an adeno-associated virus (AAV) borne GAD gene for Parkinson's disease: an open label, phase I trial. *Lancet*, **369**, 2097-2105.

208   Worgall, S., Sondhi, D., Hackett, N.R., Kosofsky, B., Kekatpure, M.V., Neyzi, N., Dyke, J.P., Ballon, D., Heier, L., Greenwald, B.M. *et al.* (2008) Treatment of late infantile neuronal ceroid lipofuscinosis by CNS administration of a serotype 2 adeno-associated virus expressing CLN2 cDNA. *Hum Gene Ther*, **19**, 463-474.

209   Tardieu, M., Zerah, M., Husson, B., de Bournonville, S., Deiva, K., Adamsbaum, C., Vincent, F., Hocquemiller, M., Broissand, C., Furlan, V. *et al.* (2014) Intracerebral administration of adeno-associated viral vector serotype rh.10 carrying human SGSH and SUMF1 cDNAs in children with mucopolysaccharidosis type IIIA disease: results of a phase I/II trial. *Hum Gene Ther*, **25**, 506-516.

210   Xu, L.F., Daly, T., Gao, C.H., Flotte, T.R., Song, S.H., Byrne, B.J., Sands, M.S. and Ponder, K.P. (2001) CMV-beta-actin promoter directs higher expression from an adeno-associated viral vector in the liver than the cytomegalovirus or elongation factor 1 alpha promoter and results in therapeutic levels of human factor X in mice. *Human Gene Therapy*, **12**, 563-573.

211   Folch, J., Lees, M. and Sloane Stanley, G.H. (1957) A simple method for the isolation and purification of total lipides from animal tissues. *The Journal of biological chemistry*, **226**, 497-509.

212   Jeyakumar, M., Butters, T.D., Cortina-Borja, M., Hunnam, V., Proia, R.L., Perry, V.H., Dwek, R.A. and Platt, F.M. (1999) Delayed symptom onset and increased life expectancy in Sandhoff disease mice treated with N-butyldeoxynojirimycin. *Proc. Natl. Acad. Sci. USA*, **96**, 6388-6393.

213   Steele, A.D., Jackson, W.S., King, O.D. and Lindquist, S. (2007) The power of automated high-resolution behavior analysis revealed by its application to mouse models of Huntington's and prion diseases. *Proc Natl Acad Sci U S A*, **104**, 1983-1988.

214   Arthur, J.R., Heinecke, K.A. and Seyfried, T.N. (2011) Filipin recognizes both GM1 and cholesterol in GM1 gangliosidosis mouse brain. *Journal of Lipid Research*, **52**, 1345-1351.

215   Dodge, J.C., Haidet, A.M., Yang, W., Passini, M.A., Hester, M., Clarke, J., Roskelley, E.M., Treleaven, C.M., Rizo, L., Martin, H. *et al.* (2008) Delivery of AAV-IGF-1 to the CNS extends survival in ALS mice through modification of aberrant glial cell activity. *Mol Ther*, **16**, 1056-1064.

216   Gray, S.J., Matagne, V., Bachaboina, L., Yadav, S., Ojeda, S.R. and Samulski, R.J. (2011) Preclinical differences of intravascular AAV9 delivery to neurons and glia: a comparative study of adult mice and nonhuman primates. *Mol Ther*, **19**, 1058-1069.

217   Bonten, E.J., Annunziata, I. and d'Azzo, A. (2014) Lysosomal multienzyme complex: pros and cons of working together. *Cellular and molecular life sciences : CMLS*, **71**, 2017-2032.

218   Cotugno, G., Annunziata, P., Tessitore, A., O'Malley, T., Capalbo, A., Faella, A., Bartolomeo, R., O'Donnell, P., Wang, P., Russo, F. *et al.* (2011) Long-term amelioration of feline Mucopolysaccharidosis VI after AAV-mediated liver gene transfer. *Mol Ther*, **19**, 461-469.

219   Pulicherla, N., Shen, S., Yadav, S., Debbink, K., Govindasamy, L., Agbandje-McKenna, M. and Asokan, A. (2011) Engineering liver-detargeted AAV9 vectors for cardiac and musculoskeletal gene transfer. *Mol Ther*, **19**, 1070-1078.

220   Karageorgos, L.E., Isaac, E.L., Brooks, D.A., Ravenscroft, E.M., Davey, R., Hopwood, J.J. and Meikle, P.J. (1997) Lysosomal biogenesis in lysosomal storage disorders. *Exp Cell Res*, **234**, 85-97.

221   Helip-Wooley, A. and Thoene, J.G. (2004) Sucrose-induced vacuolation results in increased expression of cholesterol biosynthesis and lysosomal genes. *Exp Cell Res*, **292**, 89-100.

222   Sardiello, M., Palmieri, M., di Ronza, A., Medina, D.L., Valenza, M., Gennarino, V.A., Di Malta, C., Donaudy, F., Embrione, V., Polishchuk, R.S. *et al.* (2009) A gene network regulating lysosomal biogenesis and function. *Science*, **325**, 473-477.

223   Medina, D.L., Fraldi, A., Bouche, V., Annunziata, F., Mansueto, G., Spampanato, C., Puri, C., Pignata, A., Martina, J.A., Sardiello, M. *et al.* (2011) Transcriptional activation of lysosomal exocytosis promotes cellular clearance. *Dev Cell*, **21**, 421-430.

224   Li, Z.J., Sun, P., Zhang, H.D., Li, S.F., Liu, X. and Wang, R.Z. (2010) Corpus callosum: a favorable target for rSFV-mediated gene transfer to rat brain with broad and efficient expression. *J Mol Neurosci*, **42**, 255-260.

225   Ziegler, R.J., Salegio, E.A., Dodge, J.C., Bringas, J., Treleaven, C.M., Bercury, S.D., Tamsett, T.J., Shihabuddin, L., Hadaczek, P., Fiandaca, M. *et al.* (2011) Distribution of acid sphingomyelinase in rodent and non-human primate brain after intracerebroventricular infusion. *Exp Neurol*, **231**, 261-271.

226   Magnusson, T., Haase, R., Schleef, M., Wagner, E. and Ogris, M. (2011) Sustained, high transgene expression in liver with plasmid vectors using optimized promoter-enhancer combinations. *Journal of Gene Medicine*, **13**, 382-391.

227   Virella-Lowell, I., Zusman, B., Foust, K., Loiler, S., Conlon, T., Song, S., Chesnut, K.A., Ferkol, T. and Flotte, T.R. (2005) Enhancing rAAV vector expression in the lung. *J Gene Med*, **7**, 842-850.

228   Loeb, J.E., Cordier, W.S., Harris, M.E., Weitzman, M.D. and Hope, T.J. (1999) Enhanced expression of transgenes from adeno-associated virus vectors with the woodchuck hepatitis virus posttranscriptional regulatory element: implications for gene therapy. *Hum Gene Ther*, **10**, 2295-2305.

229   Mastroyiannopoulos, N.P., Feldman, M.L., Uney, J.F., Mahadevan, M.S. and Phylactou, L.A. (2005) Woodchuck post-transcriptional element induces nuclear export of myotonic dystrophy 3' untranslated region transcripts. *EMBO Rep*, **6**, 458-463.

230   Suzuki, Y. (2013) Chaperone therapy update: Fabry disease, GM1-gangliosidosis and Gaucher disease. *Brain Dev*, **35**, 515-523.

231   Broekman, M.L.D., Comer, L.A., Hyman, B.T. and Siena-Esteves, M. (2006) Adeno-associated virus vectors serotyped with AAV8 capsid are more efficient than AAV-1 or-2 serotypes for widespread gene delivery to the neonatal mouse brain. *Neuroscience*, **138**, 501-510.

232   Whitfield, G.B., Brock, T.D., Ammann, A., Gottlieb, D. and Carter, H.E. (1955) Filipin, an Antifungal Antibiotic: Isolation and Properties. *Journal of the American Chemical Society*, **77**, 4799-4801.

233   Fu, H., Samulski, R.J., McCown, T.J., Picornell, Y.J., Fletcher, D. and Muenzer, J. (2002) Neurological correction of lysosomal storage in a mucopolysaccharidosis IIIB mouse model by adeno-associated virus-mediated gene delivery. *Mol Ther*, **5**, 42-49.

234   Van Vliet, K.M., Blouin, V., Brument, N., Agbandje-McKenna, M. and Snyder, R.O. (2008) The role of the adeno-associated virus capsid in gene transfer. *Methods in molecular biology (Clifton, N.J.)*, **437**, 51-91.

235   Carty, N., Lee, D., Dickey, C., Ceballos-Diaz, C., Jansen-West, K., Golde, T.E., Gordon, M.N., Morgan, D. and Nash, K. (2010) Convection-enhanced delivery and systemic mannitol increase gene product distribution of AAV vectors 5, 8, and 9 and increase gene product in the adult mouse brain. *Journal of neuroscience methods*, **194**, 144-153.

236   Hadaczek, P., Kohutnicka, M., Krauze, M.T., Bringas, J., Pivirotto, P., Cunningham, J. and Bankiewicz, K. (2006) Convection-enhanced delivery of adeno-associated virus type 2 (AAV2) into the striatum and transport of AAV2 within monkey brain. *Hum Gene Ther*, **17**, 291-302.

237   Kyle, J.W., Birkenmeier, E.H., Gwynn, B., Vogler, C., Hoppe, P.C., Hoffmann, J.W. and Sly, W.S. (1990) Correction of murine mucopolysaccharidosis VII by a human beta-glucuronidase transgene. *Proc Natl Acad Sci U S A*, **87**, 3914-3918.

238   Vogler, C., Galvin, N., Levy, B., Grubb, J., Jiang, J., Zhou, X.Y. and Sly, W.S. (2003) Transgene produces massive overexpression of human beta -glucuronidase in mice, lysosomal storage of enzyme, and strain-dependent tumors. *Proc Natl Acad Sci U S A*, **100**, 2669-2673.

239   Salegio, E.A., Samaranch, L., Jenkins, R.W., Clarke, C.J., Lamarre, C., Beyer, J., Kells, A.P., Bringas, J., Sebastian, W.S., Richardson, R.M. *et al.* (2012) Safety study of adeno-associated virus serotype 2-mediated human acid sphingomyelinase expression in the nonhuman primate brain. *Hum Gene Ther*, **23**, 891-902.

240   Chiu, I.M., Morimoto, E.T., Goodarzi, H., Liao, J.T., O'Keeffe, S., Phatnani, H.P., Muratet, M., Carroll, M.C., Levy, S., Tavazoie, S. *et al.* (2013) A neurodegeneration-specific gene-expression signature of acutely isolated microglia from an amyotrophic lateral sclerosis mouse model. *Cell reports*, **4**, 385-401.

241   Zamanian, J.L., Xu, L., Foo, L.C., Nouri, N., Zhou, L., Giffard, R.G. and Barres, B.A. (2012) Genomic analysis of reactive astrogliosis. *J Neurosci*, **32**, 6391-6410.

242   Winkler, I.G., Hendy, J., Coughlin, P., Horvath, A. and Lévesque, J.-P. (2005) Serine protease inhibitors serpina1 and serpina3 are down-regulated in bone marrow during hematopoietic progenitor mobilization. *The Journal of Experimental Medicine*, **201**, 1077-1088.

243   Burckstummer, T., Baumann, C., Bluml, S., Dixit, E., Durnberger, G., Jahn, H., Planyavsky, M., Bilban, M., Colinge, J., Bennett, K.L. *et al.* (2009) An orthogonal proteomic-genomic screen identifies AIM2 as a cytoplasmic DNA sensor for the inflammasome. *Nat Immunol*, **10**, 266-272.

244   Degrandi, D., Konermann, C., Beuter-Gunia, C., Kresse, A., Wurthner, J., Kurig, S., Beer, S. and Pfeffer, K. (2007) Extensive characterization of IFN-induced GTPases mGBP1 to mGBP10 involved in host defense. *Journal of immunology (Baltimore, Md. : 1950)*, **179**, 7729-7740.

245   Ugrinovic, S., Brooks, C.G., Robson, J., Blacklaws, B.A., Hormaeche, C.E. and Robinson, J.H. (2005) H2-M3 major histocompatibility complex class Ib-restricted CD8 T cells induced by Salmonella enterica serovar Typhimurium infection recognize proteins released by Salmonella serovar Typhimurium. *Infection and immunity*, **73**, 8002-8008.

246   Zijlstra, M., Li, E., Sajjadi, F., Subramani, S. and Jaenisch, R. (1989) Germ-line transmission of a disrupted [beta]2microglobulin gene produced by homologous recombination in embryonic stem cells. *Nature*, **342**, 435-438.

247   Bouchon, A., Dietrich, J. and Colonna, M. (2000) Cutting edge: inflammatory responses can be triggered by TREM-1, a novel receptor expressed on neutrophils and monocytes. *Journal of immunology (Baltimore, Md. : 1950)*, **164**, 4991-4995.

248   Melchior, B., Garcia, A.E., Hsiung, B.K., Lo, K.M., Doose, J.M., Thrash, J.C., Stalder, A.K., Staufenbiel, M., Neumann, H. and Carson, M.J. (2010) Dual induction of TREM2 and tolerance-related transcript, Tmem176b, in amyloid transgenic mice: implications for vaccine-based therapies for Alzheimer's disease. *ASN neuro*, **2**, e00037.

249   Azeredo da Silveira, S., Kikuchi, S., Fossati-Jimack, L., Moll, T., Saito, T., Verbeek, J.S., Botto, M., Walport, M.J., Carroll, M. and Izui, S. (2002) Complement activation selectively

potentiates the pathogenicity of the IgG2b and IgG3 isotypes of a high affinity anti-erythrocyte autoantibody. *J Exp Med*, **195**, 665-672.

250   Harraz, M.M., Marden, J.J., Zhou, W., Zhang, Y., Williams, A., Sharov, V.S., Nelson, K., Luo, M., Paulson, H., Schoneich, C. *et al.* (2008) SOD1 mutations disrupt redox-sensitive Rac regulation of NADPH oxidase in a familial ALS model. *J Clin Invest*, **118**, 659-670.

251   Jessen, K.R. and Mirsky, R. (1980) Glial cells in the enteric nervous system contain glial fibrillary acidic protein. *Nature*, **286**, 736-737.

252   Dauer, W. and Predborski, S. (2003) Parkinson's disease: mechanisms and models. *Neuron*, **39**, 889-909.

253   Ruzo, A., Garcia, M., Ribera, A., Villacampa, P., Haurigot, V., Marco, S., Ayuso, E., Anguela, X.M., Roca, C., Agudo, J. *et al.* (2012) Liver production of sulfamidase reverses peripheral and ameliorates CNS pathology in mucopolysaccharidosis IIIA mice. *Mol Ther*, **20**, 254-266.

254   Matsushita, M. (1999) Projections from the lowest lumbar and sacral-caudal segments to the cerebellar nuclei in the rat, studied by anterograde axonal tracing. *The Journal of comparative neurology*, **404**, 21-32.

255   Matsushita, M. (1999) Projections from the upper lumbar cord to the cerebellar nuclei in the rat, studied by anterograde axonal tracing. *The Journal of comparative neurology*, **412**, 633-648.

256   Matsushita, M. and Gao, X. (1997) Projections from the thoracic cord to the cerebellar nuclei in the rat, studied by anterograde axonal tracing. *The Journal of comparative neurology*, **386**, 409-421.

257   Matsushita, M. and Xiong, G. (1997) Projections from the cervical enlargement to the cerebellar nuclei in the rat, studied by anterograde axonal tracing. *The Journal of comparative neurology*, **377**, 251-261.

258   Matsushita, M. and Yaginuma, H. (1995) Projections from the central cervical nucleus to the cerebellar nuclei in the rat, studied by anterograde axonal tracing. *The Journal of comparative neurology*, **353**, 234-246.

259   Kaspar, B.K., et al. (2003) Retrograde Viral Delivery of IGF-1Prolongs Survival in a Mouse ALS Model. *Science*, **301**, 839-842.

260   Wang, B., Li, J., Fu, F.H., Chen, C., Zhu, X., Zhou, L., Jiang, X. and Xiao, X. (2008) Construction and analysis of compact muscle-specific promoters for AAV vectors. *Gene Ther*, **15**, 1489-1499.

261   Arnett, A.L., Beutler, L.R., Quintana, A., Allen, J., Finn, E., Palmiter, R.D. and Chamberlain, J.S. (2013) Heparin-binding correlates with increased efficiency of AAV1- and AAV6-mediated transduction of striated muscle, but negatively impacts CNS transduction. *Gene Ther*, **20**, 497-503.

262   Baron, U. and Bujard, H. (2000) Tet repressor-based system for regulated gene expression in eukaryotic cells: principles and advances. *Methods in enzymology*, **327**, 401-421.

263   Furth, P.A., St Onge, L., Boger, H., Gruss, P., Gossen, M., Kistner, A., Bujard, H. and Hennighausen, L. (1994) Temporal control of gene expression in transgenic mice by a tetracycline-responsive promoter. *Proc Natl Acad Sci U S A*, **91**, 9302-9306.

264   Gray, S.J., Foti, S.B., Schwartz, J.W., Bachaboina, L., Taylor-Blake, B., Coleman, J., Ehlers, M.D., Zylka, M.J., McCown, T.J. and Samulski, R.J. (2011) Optimizing promoters for recombinant

adeno-associated virus-mediated gene expression in the peripheral and central nervous system using self-complementary vectors. *Hum Gene Ther*, **22**, 1143-1153.